Evaluating the Performance of Inverted Pavements in Tennessee

Research Final Report from the University of Tennessee, Knoxville | Xi Jiang, Baoshan Huang, Hani Titi, Pawel Polaczyk | May 30, 2022

Sponsored by Tennessee Department of Transportation Long Range Planning
Research Office & Federal Highway Administration

DISCLAIMER

This research was funded through the State Planning and Research (SPR) Program by the Tennessee Department of Transportation and the Federal Highway Administration under ***RES2020-12: Research Project Title: Evaluating the Performance of Inverted Pavements in Tennessee.***

Technical Report Documentation Page

1. Report No. RES 2020-12	2. Government Accession No.	3. Recipient's Catalog No.
4. Title and Subtitle *Evaluating the Performance of Inverted Pavements in Tennessee*		5. Report Date May 2022 6. Performing Organization Code
7. Author(s) Xi Jiang, Baoshan Huang, Hani Titi, Pawel Polaczyk		8. Performing Organization Report No.
9. Performing Organization Name and Address Department of Civil and Environmental Engineering The University of Tennessee, Knoxville 851 Neyland Drive Knoxville, TN, 37996		10. Work Unit No. (TRAIS) 11. Contract or Grant No. RES 2020-12
12. Sponsoring Agency Name and Address Tennessee Department of Transportation 505 Deaderick Street, Suite 900 Nashville, TN 37243		13. Type of Report and Period Covered Final report January 2019 – May 2022 14. Sponsoring Agency Code
15. Supplementary Notes Conducted in cooperation with the U.S. Department of Transportation, Federal Highway Administration.		

16. Abstract

Inverted pavement is an unconventional type of flexible pavement structure. In this pavement structure, an unbound aggregate base (UAB) with a low initial modulus is sandwiched (layered) between two stiffer layers, a thinner asphalt concrete layer (AC) and a cement-treated base layer (CTB). This type of pavement structure has been a potential alternative to the conventional flexible pavement structure due to its cost-efficient usage of asphalt, comparable performance and durability based on past studies. However, field investigations of inverted pavement have not been widely conducted and are very limited in the USA. Therefore, the objective of this study is to present a comprehensive investigation of the inverted pavement system including field and laboratory works. In this study, the effect of nonlinear stress-dependent property of unbound aggregates on both the inverted and conventional flexible pavement structures was first investigated. Second, through field investigation in Vulcan pavement, a comparison study between the inverted and conventional pavements was conducted under the same traffic level and environmental conditions. In addition, the nondestructive pavement testing method – falling weight deflectometer (FWD) was applied to evaluate the structural conditions of the inverted pavement, contributing to the effective maintenance and preservation of pavements. Finally, the accelerated pavement testing (APT) method was used to evaluate the rutting performance of a full-scale inverted pavement constructed on the UT (University of Tennessee) campus. Based on the results of the comprehensive investigation of both field (full-scale) and numerical simulations, the inverted pavement structure can be regarded as an alternative to the conventional flexible pavement.

17. Key Words **Inverted pavement; Accelerated pavement test; Pavement evaluation; Unbound aggregate base**	18. Distribution Statement No restriction. This document is available to the public from the sponsoring agency at the website http://www.tn.gov/.		
19. Security Classif. (of this report) Unclassified	20. Security Classif. (of this page) Unclassified	21. No. of Pages	22. Price

Acknowledgement

We would like to thank the Tennessee Department of Transportation (TDOT) for funding this research project. We have continued to collaborate closely with regional engineers and local technicians. They have provided valuable support towards the fulfillment of the research objectives. Without their support, it would be impossible to finish this research project. We would also like to thank the administrative staff from the TDOT Research Office who have worked very closely with our research team and kept the whole project on the proposed schedule.

This project also partially supported the publication of two journal papers:

(1) Jiang, Xi, Jay Gabrielson, Baoshan Huang, Yun Bai, Pawel Polaczyk, Miaomiao Zhang, Wei Hu, and Rui Xiao. "Evaluation of inverted pavement by structural condition indicators from falling weight deflectometer." Construction and Building Materials 319 (2022): 125991.

(2) Jiang, Xi, Miaomiao Zhang, Rui Xiao, Pawel Polaczyk, Yun Bai, and Baoshan Huang. "An investigation of structural responses of inverted pavements by numerical approaches considering nonlinear stress-dependent properties of unbound aggregate layer." Construction and Building Materials 303 (2021): 124505.

(3) Jiang, Xi, Jay Gabrielson, Hani Titi, Baoshan Huang, Yun Bai, Pawel Polaczyk, Wei Hu, Miaomiao Zhang, and Rui Xiao. "Field investigation and numerical analysis of an inverted pavement system in Tennessee, USA." Transportation Geotechnics 35 (2022): 100759.

Executive Summary

The purpose of this study was to conduct an evaluation of the performance of inverted pavement as an alternative pavement structure in the state of Tennessee for State Industrial Access (SIA) projects. The evaluation was performed in comparison to flexible pavements with the same traffic level and environment conditions. The concept of inverted pavement was developed in South Africa in the 1950s, and many applications have been reported in Georgia, Louisiana, and Mississippi, among others. With inverted pavement, an unbound aggregate base layer, which is usually used as a subbase beneath the stabilized base, is sandwiched between the asphalt surface layer and the cement-treated base layer. The reason for the unique location of the unbound base in an inverted pavement structure is that unbound aggregate is a highly stress-dependent material. When placed between two stiffer layers, commonly an asphalt concrete layer and cement-treated base, the unbound aggregates will be subjected to a higher stress state, resulting in a higher stiffness of the unbound aggregate layer. Tennessee Department of Transportation (TDOT) has long been trying to evaluate and adopt this pavement structure due to its significant cost benefits. In the past several years, TDOT wanted to use the inverted pavement on more than three projects. However, each time the push has not gone beyond the letting stage due to lack of confidence. This research continued TDOT's effort to apply inverted pavement in Tennessee. At the current stage, there is limited field and full-scale investigations of inverted pavement in the state. Therefore, more practical studies on inverted pavement were conducted in this project.

To accelerate the application of inverted pavement in Tennessee, three research objectives were pursued. The first objective was to evaluate the usage and spread of inverted pavements in the USA using a survey. The second objective was to monitor the performance of inverted pavements built in Tennessee. The third objective was to provide TDOT with recommendations and experience on inverted pavements. To achieve this, a comprehensive field investigation was conducted on Vulcan inverted pavement in Knoxville, TN. Non-destructive testing methods such as ground penetration radar (GPR), Benkelman beam test, falling weight deflectometer (FWD), and 3D road profiling tests were used to assess the actual thickness, structural capacity and surface conditions of the pavement structures. In addition, a comparison study between the inverted and conventional pavements in Vulcan was conducted by field data and numerical analysis. The accelerated pavement testing (APT) method was also applied to the full-scale inverted pavement built on-campus at the University of Tennessee, Knoxville. The key findings and recommendations derived from this study present a better understanding of the inverted pavement structure. Furthermore, this project will be able to strengthen the confidence of TDOT to build inverted pavement and have it be considered as an alternative with good performance compared to conventional flexible pavement.

Key Findings

The key findings based on this project can be concluded as follows:

- Based on the numerical simulations, the nonlinear stress-dependent characteristic of unbound aggregates is significant in the inverted pavement but little effect can be found in the conventional flexible pavement. In addition, the stress-dependent property of the

unbound aggregate base layer results in the different stiffness (modulus) distribution in this layer under the same loading and boundary conditions. Furthermore, less tension stress is found at the bottom of surface asphalt layer, and less deflection is found at the surface of asphalt concrete layer and subgrade, which leads to longer service life of inverted pavement.

- Based on the field investigation of Vulcan inverted pavement, the deformation of the inverted pavement surface detected by the Benkelman beam test was less than that of conventional pavement. According to the road surface profile data measured by the (LCMS) system, the inverted pavement structure showed better performance in roughness, cracking condition and rutting depth. The better cracking condition in the inverted pavement section indicates that the inverted pavement can be effectively constructed to prevent the onset and propagation of reflective cracks. Inverted pavements have larger SCI values but smaller BDI, BCI and W_7 values when compared with the conventional pavement.
- Based on the FWD data, using the deflection basin parameters (DBPs)-based method with the FWD test can evaluate the structural conditions of the individual layer in the inverted pavement in a shorter time and without any damage to the pavement structure. In addition, the DBPs data show that the inverted pavement outperformed the conventional pavement structures. These advantages of DBPs-based method accelerate the development of the inverted pavement and contributes to the rehabilitation of inverted pavement.
- Based on the APT test results, the inverted pavement structure differed from the conventional pavement structure in the accumulating permanent surface deformation with APT's passes. The inverted pavement has a better or comparable performance on the surface's permanent deformation compared with conventional pavement. More deformation was observed at the top of the UAB layer in the conventional pavement, which meant less tension was generated at the bottom of the AC layer. In addition, the stiffer UAB layer in the inverted pavement contributed to the rutting performance and reduction of reflective cracks.

Key Recommendations

The key recommendations based on this project can be concluded as follows:

- The numerical differences between the linear and nonlinear models were much smaller in the conventional pavement. Thus, the structural response of the inverted pavement was much more sensitive to the nonlinear stress-dependent characteristic of the UAB layer due to the compaction effect from two stiffer layers of an upper thin AC layer and a lower CTB layer. Therefore, it is necessary to apply a nonlinear stress-dependent resilient modulus for the UAB layer during numerical analyses of inverted pavements.
- Ground-coupled GPR is a reliable approach to estimate thicknesses of pavement structures. Using a combination of GPR thickness data and designed thickness values can determine the high-accuracy thickness of different pavement layers without structure destruction, with time savings and without traffic disruption. Meanwhile, the accurate characterization of pavement layer thicknesses contributes to better analysis of pavement structures and the reliability of numerical simulation work.

- Using the DBP-based method by way of the FWD test can evaluate the structural conditions of the individual layer in the inverted pavement, which accelerates the development of inverted pavement and contributes to the rehabilitation of inverted pavement.
- Based on the overall rutting performance, the inverted pavement structure had a comparable (inverted pavement Ⅰ) or better performance (inverted pavement Ⅱ) compared with the conventional flexible pavement structure under the same loading and environmental conditions. Thus, the inverted pavement can be regarded as an alternative to the traditional flexible pavement.

Table of Contents

List of Tables

List of Figures

Chapter 1 Introduction

1.1 Problem Statement

Reflective cracking is a primary issue on composite pavements with a cement-treated base (CTB) and an asphalt surface layer. Numerous studies have indicated that the CTB is prone to shrinkage cracking, which often propagates upwards into the asphalt surface layer and causes the reflective cracking [1]. The maintenance of reflective cracking is very difficult, as it is related both to material defects and structural deficiency [2,3]. A demonstrated effective approach for addressing the reflective cracking is using inverted pavements. An inverted pavement, opposite to the conventional flexible pavement with CTB overlaying the unbound aggregate base, is constructed with a cement-treated sub-base underlying an unbound aggregate base [4–6].

The concept of inverted pavement was developed in South Africa in the 1950s, and many effective applications have been reported in Georgia [7], Louisiana [1], and Mississippi [8], among others. In the inverted pavement design, an unbound aggregate layer, which is usually used as a subbase beneath the stabilized base, is sandwiched between the asphalt surface layer and the cement stabilized base. The reason for the unique location of the unbound base in an inverted pavement is that unbound aggregate is a highly stress-dependent material. When placed closer to the pavement surface, the unbound aggregates will be subjected to a higher stress state, resulting in a higher stiffness of the unbound aggregate layer and, thus, better pavement performance. Compared to conventional flexible pavements, an inverted pavement has the following benefits:

- Significant cost savings due to a relatively thin asphalt surface layer;
- High rut resistance;
- Reduced transverse cracking;
- High traffic volume capacity;
- Reduced energy consumption;
- Longer service life.

TDOT has long been trying to evaluate and adopt this technology due to its significant cost benefits. In the past several years, TDOT wanted to use the inverted pavement on at least three projects. However, each time the push has not gone beyond the letting stage due to lack of confidence. This research project has continued TDOT's effort to apply this technology in Tennessee. Once successful, the research will bring/build the confidence that TDOT needs to implement this innovative technology.

1.2 Objectives

The primary objective of this proposed research was to conduct a long term evaluation of the performance, longevity and cost-effectiveness of inverted pavements as an alternative pavement structure in the state of Tennessee for State Industrial Access projects. The evaluation was performed in comparison to flexible and rigid pavements with the same traffic level. The findings weree used to validate the method, construction and maintenance procedures that work for TDOT.

The objectives of the proposed research were to:

1. Evaluate the usage and spread of inverted pavements in the USA using a survey;

2. Monitor the short- and long-term performance of inverted pavements in Tennessee;

3. Provide TDOT recommendations on inverted pavements best practices and life-cycle cost analysis.

1.3 Scope of Work

- Completed a synthesis of literature review and state DOT survey on the design, construction, and rehabilitation methods of inverted pavements in the US, especially in the Southeastern region;
- Identified the potential and economic feasibility of inverted pavement projects in Tennessee;
- Conducted field testing and long-term field performance monitoring of the inverted pavement project.
- Performed a cost-benefit analysis of inverted pavements in comparison to conventional flexible pavements under the same traffic level.

1.4 Methods Overview

In this project, several numerical analysis approach and testing methods were applied to evaluate the performance of the inverted pavement. The main methods are summarized as follows:

- The finite element method (FEM) was used in this study to simulate the nonlinear stress-dependent property of unbound aggregate materials in the inverted pavement. A commonly used stress-dependent resilient modulus model was programmed into user-defined material subroutine (UMAT) of the ABAQUS FEM to investigate the influence of UAB on the inverted pavement structural responses.
- The falling weight deflectometer (FWD) method was used in this study to evaluate the inverted pavement structure through the deflection basin parameters (DBPs). FWD is a type of nondestructive road testing device for pavement structural analysis. FWD is widely used to evaluate the conventional flexible pavement structure through deflection basin parameters (DBPs). DBPs serve as indicators of the pavement basin shape, which can assess the structural condition of in-service pavements.
- Ground-coupled antenna-based ground penetration radar (GPR) was used in this study to validate the thickness of inverted pavement. GPR is a good non-destructive method to measure and assess the thickness of pavement layers. The test data can be compared with the designed values to evaluate the construction quality.
- The accelerated pavement testing (APT) method was applied to a full-scale inverted pavement at UT campus. APT is defined as the controlled application of a prototype wheel loading at the appropriate load to the full-scale pavement structure, which is used to determine the structural responses and performance of the pavement over a short period. In this project, the APT method was used to investigate the structural responses of the inverted pavement.

1.5 Report Overview

The organization of this report is as follows. Chapter 2 introduces the inverted pavement and its application in the USA and worldwide. Relevant literature is also reviewed and summarized. In Chapter 3, the inverted pavement related studies are presented and discussed. In this chapter, the preliminary numerical simulations were presented to highlight the function of stress-dependence of UAB in the inverted pavement. Field investigation in the Vulcan inverted pavement is also presented and the corresponding numerical analysis was verified by the field testing data. In addition, the DBP-based evaluation approach by FWD was applied to the inverted pavement. Furthermore, the performance of a full-scale inverted pavement at UT's campus was tested by APT method. In Chapter 4, the methods for investigating inverted pavement structure are presented. Chapter 5 provides a summary of this project and discusses future work for inverted pavement structure.

Chapter 2 Literature Review

2.1 Inverted Pavement

Flexible pavement has been developed for many years, and it is the most common pavement type which can be used for high-volume interstate highways, airport runways and aprons subjected to heavy aircraft wheel loads [9]. The construction of a flexible pavement structure usually includes the paving of a bituminous surface over the unbound aggregate base and a layer of subgrade at the bottom. However, with the ever-growing traffic volume and budget constraints from departments of transportation (DOTs), more energy-efficient pavement structures with better performance are urgently needed [7,10,11]. Many agencies have been actively exploring new pavement structures that provide satisfactory performance and cost-efficient maintenance [12,13]. Inverted pavement is an emerging pavement structure that can deal with the aforementioned problems, and the less usage of asphalt in the inverted pavement makes it a sustainable and energy-efficient pavement structure. The concept of inverted pavement was firstly introduced in South Africa, and many practical applications have been regarded as competent pavement structures and a cost-effective alternative to conventional pavements since the 1950s [14]. The improvements of inverted pavement in service performance compared to the conventional pavement make it a practical design for heavy traffic loads in South Africa.

The inverted pavement is a type of flexible pavement that consists of a well compacted UAB layer sandwiched between two stiffer layers of upper thin asphalt concrete (AC) layer and a lower cement-treated base (CTB). Its structure is contrary to the conventional pavement. The schematic diagram in **Figure 2-1** makes a comparison to show the difference between the inverted pavement and conventional pavement structures. From **Figure 2-1**, it can be found that the main difference between them in the design aspect is the sequence of the layers. For the traditional pavement structure, the stiffer layers are usually constructed at the top. The stiffness of the layer decreases with the increasing depth of pavement. The first inverted pavement in the USA was built in New Mexico in 1954 [15]. However, the large-scale utilization of inverted pavement was hindered due to the lack of full-scale or field experiments concerning the structural response of inverted pavement.

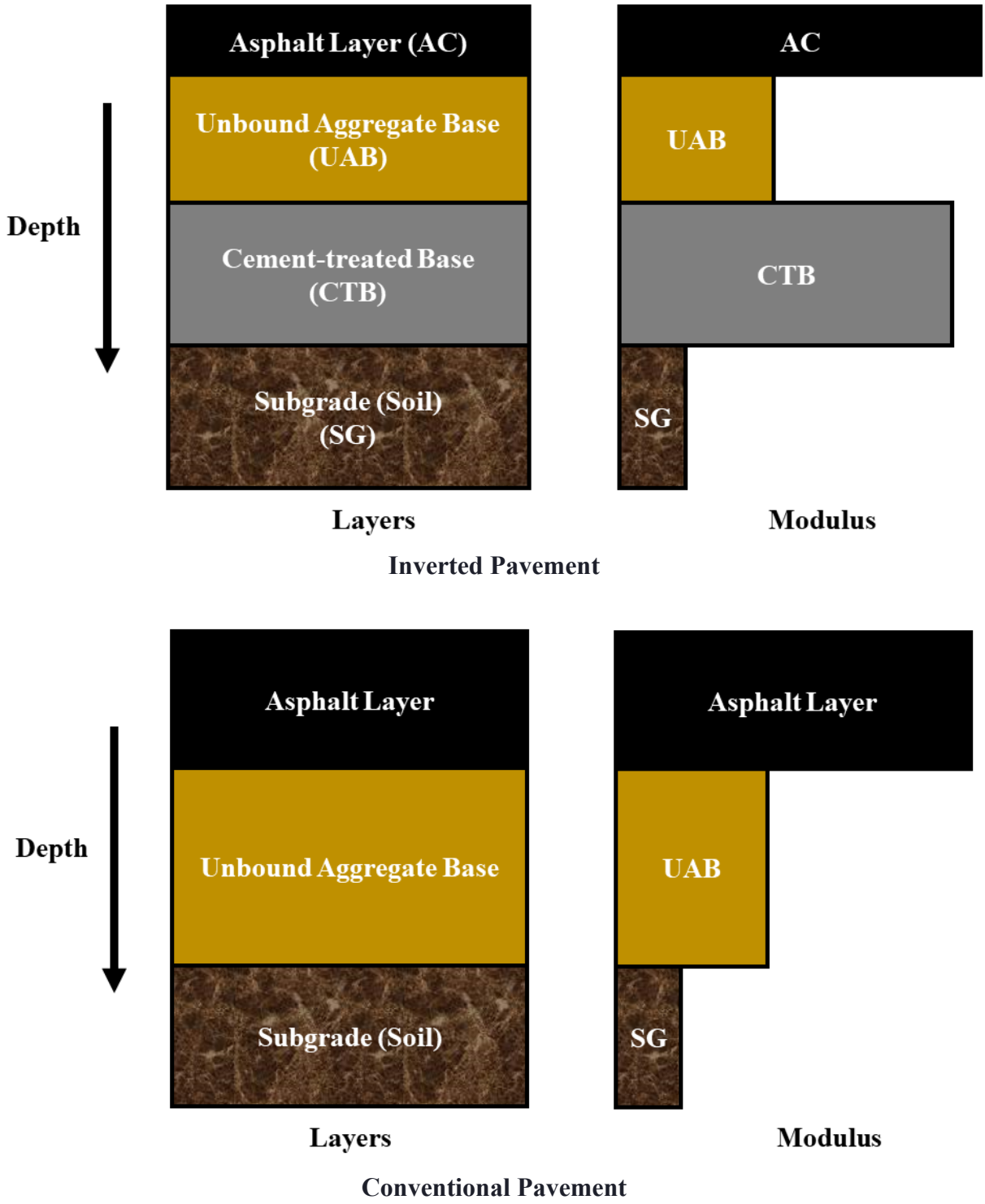

Figure 2-1. Comparison of inverted pavement and conventional pavement structures.

2.2 Numerical Simulations of Inverted Pavement

The design and construction of conventional pavement structures were mainly based on the empirical method in the past several decades. Nowadays, more mechanistic designs are being considered as the primary design approach, which is able to take the impacts of load and environment into consideration. The finite element method (FEM), based on commercial software such as ABAQUS and ANSYS, has attracted more and more interest from engineers and scholars in their analysis of pavement structures [16]. The structural responses induced by the wheel load can be predicted more accurately by finite element (FE) program due to its ability to incorporate realistic material properties. In the past, structures of flexible pavements were mostly designed and analyzed based on the layered elastic approach. These numerical cases made predictions of pavement structures by considering linear elastic material properties and models. However, the structural response in an inverted pavement structure is dominated by the mechanical properties or resilient characteristics of the UAB layer. UAB is a special material due to its dilatancy. This property contributes to the movement of aggregate particles and the particles tend to roll over one another under shear stress induced by the applied load. A self-induced confining pressure is produced, which will increase the stiffness of the UAB. Lytton et al [2] also investigated the stiffness of the granular layer of pavements. The experimental results show that the increased resilient volumetric strain resulted in the increasing mean normal effective stress in the UAB, which accounted for reduced tensile stress and higher stiffness. Furthermore, a UAB layer is not a continuous medium, and its mechanical response depends on the stress history and current stress state [17]. A nonlinear stress-dependent response was presented when the unbound aggregates were under cyclic loading [18]. Thus, the traditional linear elastic FE program is not able to meet the requirement of analysis in an inverted pavement. It is crucial for the nonlinear stress-dependent characteristic of UAB to be taken into consideration.

In previous studies, two popular methods were applied during the analysis of the UAB layer. The first was to analyze the variations of the resilient modulus by dividing the UAB into sublayers [17]. The change of resilient modulus was adjusted by an iteration program until the moduli were compatible with the stress calculation. However, the stress variation in the horizontal direction was not explained. To solve the problem, Tutumluer [4] investigated the influence of nonlinear properties on stress distribution in the pavement by using the GTPAVE FE program, which gave a more realistic simulation. Al-Qadi [19] made an analysis of the stress-dependent properties for the granular layer using a three-dimensional (3D) FE model by ABAQUS. Furthermore, the cross-anisotropic characterization of unbound granular materials was investigated in the conventional flexible pavements [20,21]. The tensile stress was eliminated by using cross-anisotropic model based on the simulation results. Papadopoulos and Santamarina [22] studied the structural response of inverted base pavements with thin-asphalt layers. The nonlinear constitutive model was used to investigate the function and characteristics of unbound aggregate base in the inverted structures.

2.3 Field Investigation of Inverted Pavement

Laboratory studies and numerical simulations were conducted to investigate the characteristics of UAB in the inverted pavements in the past thirty years. However, there were limited studies

with full scale field tests and evaluation of constructed inverted pavement structures in the USA. Li et al. [18] investigated the performance and failure modes of an inverted pavement with soil-cement bases under accelerated loading conditions in Louisiana, USA. Titi et al. [1] presented the results of long-term performance testing and evaluation of an alternative flexible pavement design referred to as the stone interlayer pavement. For a period of 10 years, Titi et al. [1] monitored the performance of both the conventional and the stone interlayer pavements constructed on highway LA-97 in Louisiana by measuring pavement distresses and evaluating pavement conditions including pavement structural capacity and roughness (ride quality). They compared the field results with the results of full-scale accelerated loading experiments conducted at the Pavement Research Facility (PRF) site in Louisiana. The long-term pavement monitoring and accelerated load testing of the stone interlayer pavement both demonstrated the inverted pavement's outstanding performance. Terrell et al. [7] evaluated the stiffness distribution of unbound aggregate base in different sections of a haul road in Morgan County, Georgia. The measurements consisted of horizontally propagating compression (P) and shear (S) waves. Cortes et al. [23] conducted a full-scale study with the Georgia Department of Transportation (GDOT) on the LaGrange inverted pavement, Georgia, USA. In their study, both laboratory and field tests were developed to characterize the nonlinear stiffness-stress relationship of the unbound aggregate layer in the inverted pavement system. In addition, the results from both the field investigation and numerical simulations bridge the gaps between the practical inverted pavement construction and numerical simulation analysis, which provides construction and research experiences for future inverted pavement projects.

Chapter 3 Methodology

3.1 Stress-Dependent Model

The stress-dependent stiffness property of UAB is the critical point in this study due to its contribution to the structure of an inverted pavement. In previous studies, the resilient modulus calculated by a secant stiffness formulation was used to predict the stiffness of the UAB in numerical simulations. Yoo et al. [24] investigated viscoelastic pavement structures considering the secant stiffness during the model development. Al-Qadi et al. [19] also considered the secant stiffness in a 3-D finite element model. The dynamic responses of flexible pavement under impulsive loading, similar to a falling weight deflectometer test (FWD), was investigated in the research. However, the process of incremental response in materials is not included in this method. Therefore, a tangent formulation was utilized in this study to model the nonlinear stress-dependent stiffness of UAB. In addition, any arbitrary stress path could be captured in this method.

The resilient modulus of UAB is defined as the ratio of the repeated deviatoric stress to the recoverable part of the axial strain [19]. Among the proposed nonlinear models for the resilient modulus in past studies, the k-θ model or the two-parameter bulk stress model was the most popular model to predict stiffening and hardening characteristics of UAB [25]. The M_r is calculated by **Equation (3-1)**:

$$M_r = k_1 \theta^{k_2} \tag{3-1}$$

Where M_r represents the resilient modulus; θ represents the bulk stress or sum of principal stresses ($\sigma_1 + \sigma_2 + \sigma_3$); k_1 and k_2 represent the regression constants from the triaxial test.

The softening characteristic of finer aggregate can be calculated by **Equation (3-2)**:

$$M_r = k_3 \sigma_d^{k_4} \tag{3-2}$$

Where σ_d represents deviatoric stress; k_3 and k_4 represent the regression constants.

The above models in **Equations (3-1)** & **(3-2)** were widely used in the past due to their easy implementation in FE programs for flexible pavements. However, the shear-stress component for the dimensional change is not considered, which is not suitable for accurate prediction of thin flexible pavements [17]. Therefore, the octahedral shear-stress term should be added to the model. The stress-dependent behavior of an inverted pavement can be predicted by Uzan's resilient modulus model. This model considers the dilation effect induced by the large principal stress ratio. As shown in **Equation (3-3)**, a fixed point iteration algorithm is used to implement this model into FE software.

$$M_r = k \theta^n \tau_{oct}^m \tag{3-3}$$

Where τ_{oct} represents the octahedral shear stress $(\sqrt{\frac{1}{3}[(\sigma_1 - \sigma_2)^2 + (\sigma_2 - \sigma_3)^2 + (\sigma_3 - \sigma_1)^2]}$; and k, n, and m represent the material constants.

However, the fixed-point iteration does not tend to converge when the loads are too large. Thus, a modification was made to predict the resilient modulus based on the strains of the last iteration

rather than the previous stresses in the formerly fixed-point iteration algorithm [26]. **Equation (3-4)** shows the modified model. The nonlinear stress-dependent model in this study was implemented as fixed-point iterations wherein an initial resilient modulus was assumed (fixed) for UAB. A linear analysis of the modulus of UAB was performed using the current value of the resilient modulus. Then, the resulting displacements were used to calculate strains, subsequent stresses, and a new resilient modulus. The process was repeated until the new modulus of the UAB was equal to the value of last iteration, and the process of the analysis from stress to strain could be considered as a strain-based method.

$$M_r = (1+\nu)[\frac{K}{1+\nu}(\frac{\nu}{1-2\nu}+\frac{1}{3})^n]^{\mu}\rho^{\mu n}\gamma^{\mu m} \quad (3\text{-}4)$$

Where ν represents Poisson's ratio; $\mu = \frac{1}{1-n-m}$; ρ represents the bulk strain or sum of principal strains $=|\varepsilon_1+\varepsilon_2+\varepsilon_3|$; γ represents octahedral shear strain $=\sqrt{\frac{1}{3}[(\varepsilon_1-\varepsilon_2)^2+(\varepsilon_2-\varepsilon_3)^2+(\varepsilon_3-\varepsilon_1)^2]}$; K, n, and m represent the material constants.

Before applying the model in software, a lower limit of the octahedral strain in the user subroutine was used to prevent the overflow induced by low computed strains with small loading steps.

3.2 Ground Penetration Radar (GPR)

The as-built pavement layer thicknesses generally deviate from the design values due to construction variabilities resulting from the equipment of construction crews. Inaccuracies in assessing pavement layer thicknesses lead to erroneous structural response analysis studies and could impact the pavement maintenance in real life application. To achieve accurate pavement modeling and simulation, verification of the pavement layer thicknesses is usually conducted by coring or excavating test pits in pavements as reported in the past studies [27,28]. However, the use of these traditional methods is limited by their characteristics such as their destructive nature, being time-consuming, the need for traffic control and requiring detailed location information [29]. Therefore, Non-Destructive Testing systems are used because of their versatility for non-intrusive nature of obtaining detailed thickness data without traffic disruptions and lane closure. GPR is a popular and advanced system used to measure and assess the thickness of pavement layers. In this study, a ground-coupled antenna-based GPR, as shown in **Figure 3-1 (a)**, was used to determine whether the pavement construction quality (thickness) met the design requirements. **Figure 3-1 (b)** shows that the research team conducted detection processing using a GSSI SIR 4000 GPR antenna (900 MHz) along with a three-wheel cart.

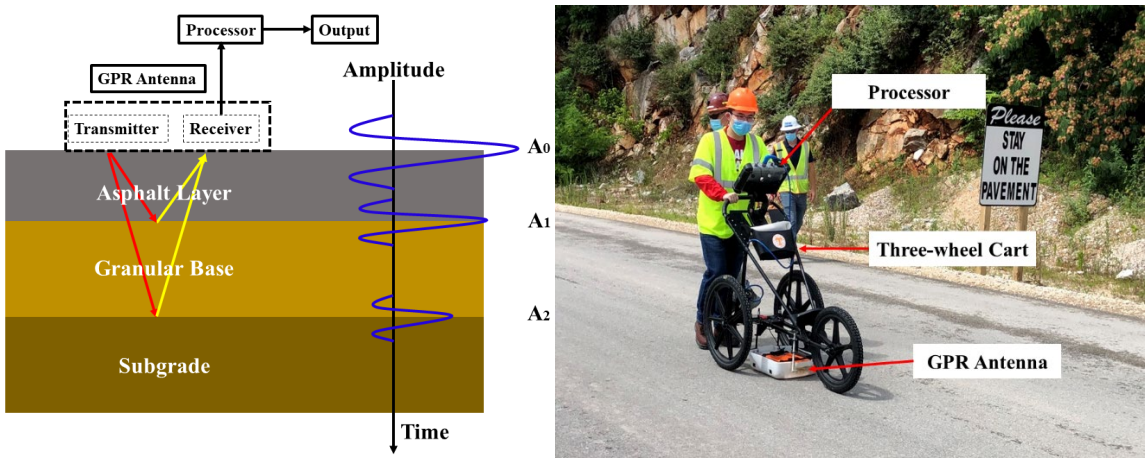

(a) (b)

Figure 3-1. (a) Ground-coupled antennas-based GPR; (b) Pavement thickness detection process using GPR used on the investigated pavement section in Knoxville, TN

As shown in **Figure 3-1 (a)**, a short electromagnetic pulse is transmitted and received by the GPR mechanism. The penetration depth of the signals from GPR depends on the central antenna frequency [30]. Lower resolution leads to a larger penetration depth. Before the thickness evaluation, the approximate thickness of the entire pavements' structure should be assessed, and the GPR with the most suitable frequency is used for the target pavement structure. The local calibration of GPR should be conducted by professionals. In this study, a 900 MHz ground-coupled antenna was used for pavement thickness assessment due to its penetration of around 1.5 m. The thickness $\mathbf{h_{AC}}$ can be obtained by:

$$h_{AC} = \frac{c \times t_{AC}}{2\sqrt{\varepsilon_{AC}}} \quad (3\text{-}5)$$

Where **c** represents the speed of light in free space; $\mathbf{t_{AC}}$ is the time difference between the reflected pulses in interfaces of mediums; $\boldsymbol{\varepsilon}_{\mathbf{AC}}$ is the dielectric constant of AC layer; and $\frac{c}{\sqrt{\varepsilon_{AC}}}$ is the electromagnetic wave velocity.

$\boldsymbol{\varepsilon}_{\mathbf{AC}}$ is an important parameter that is usually found in the Dielectric Constant Table or estimated by surface reflection method [31,32]. The following equation can be used to calculate the dielectric constant of the asphalt layer:

$$\varepsilon_{AC} = \left(\frac{1+\frac{A_0}{A_m}}{1-\frac{A_0}{A_m}}\right) \quad (3\text{-}6)$$

Where A_0 represents the amplitude of the AC layer reflection and A_m is the amplitude reflected by a flat metallic plate for calibration purposes [33].

3.3 Falling Weight Deflectometer (FWD) Method

An FWD is a type of nondestructive road testing device for pavement structural analysis. FWDs are widely used to evaluate the conventional flexible pavement structure through deflection basin parameters (DBPs). DBPs serve as indicators of the pavement basin shape, which can assess the structural condition of in-service pavements. The DBPs' evaluation system was first introduced and utilized in South Africa [34,35], and then the DBPs were further developed and used in the United States. **Table 1** shows the details of DBPs in South Africa and the USA based on the summary of literature and reports [35,36]. Definitions of parameters SCI, BDI, and BCI in the USA system are similar to those in the South Africa system. SCI or BLI represents the difference of deflections measured with load geophones located at the center of the loading plate (D_0) and 300 mm (12 inches) from the center. BDI or MLI represents the difference of deflections measured with load geophones located at a distance of 300 mm (12 inches) and 600 mm (24 inches). BCI or LLI represents the difference of deflections measured with load geophones located at 600 mm (24 inches) and 900 mm (36 inches). W_7 represents the deflection at the 7th sensor (1500 mm or 60 inches) of FWD. **Figure 3-2** shows the schematic of the FWD deflection basin curve.

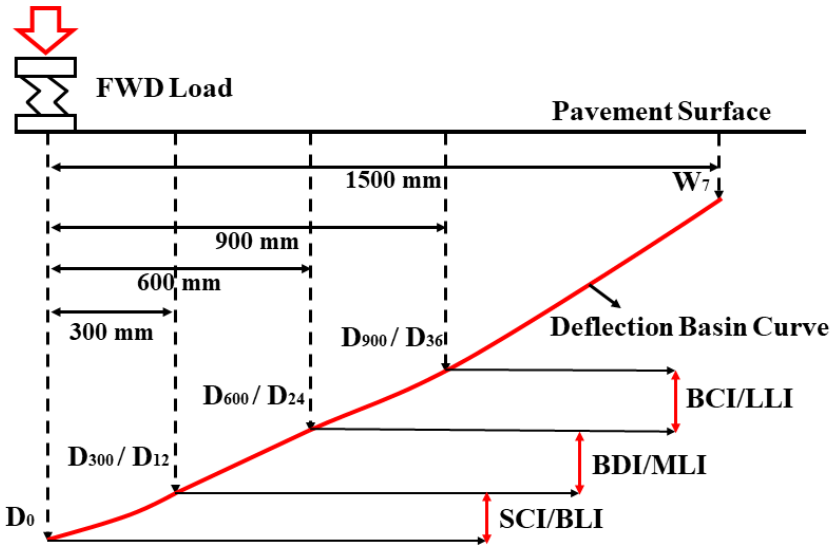

Figure 3-2**.** Schematic of FWD deflection basin curve

3.4 Accelerated Pavement Testing (APT) Method

An accelerated pavement test (APT) is defined as the controlled application of a prototype wheel loading at the appropriate load to the full-scale pavement structure, which is used to determine the structural responses and performance of the pavement in a short period [37]. The APT facilities used on the public roads have been developed in the United States since 1924 [37,38]. Compared with the traditional field investigations, a full-scale test using an APT facility has many advantages, such as controlled loading and environmental conditions. In addition, APT has the capacity to perform the full-scale test in a shorter testing time. Therefore, APT facility has been used a lot to conduct the pavement-related experimental work in the previous studies. In this

project, a full-scale accelerated pavement testing (APT) system simulated the wheel loads on the test sections. The equipment had the dimension of 8.5 m length × 2.5 m width × 2.5 m height (see **Figure 3-3**). **Figure 3-3** (a) and (b) show the external and internal frameworks of the testing machine, respectively. A dual-wheel loading system with a bi-directional moving mode was applied in this study. The size of each loading wheel was 110 cm in diameter and 25 cm in width. And the length of the wheel motion trajectory on the testing pavement was 5.5 m based on the measured tire marks. To ensure the smooth operation of the APT equipment, the running speed of the dual-wheel system was set at 3.6s/pass (1,000 passes/hour). A load of 80 kN (kilonewtons), which was twice the standard axle load, was applied and the contact pressure between the wheel and pavement surface was 1.4 MPa in this study. In addition, the temperature of the APT indoor lab was set at 20 ℃ to avoid the influence of temperature on the pavement performance.

(a) (b)

Figure 3-3. The accelerated pavement testing (APT) facility

Chapter 4 Results and Discussion

4.1 Preliminary Numerical Simulations of Inverted Pavement Considering the Nonlinear Stress-dependent Property of Unbound Aggregates

4.1.1 Finite-element model

The FE method has been widely used in analyzing the structural response of flexible pavements due to its accurate prediction for construction design. The inverted pavement model in this study consists of a surface AC layer, a UAB layer, a CTB layer, and a subgrade (SG). The conventional pavement model has an AC layer, UAB layer, and SG layer. The schematic design of the pavement structures in the model is shown in **Figure 4-1**. The left lane pavement is the typical design of an inverted pavement. The middle lane is also an inverted pavement with a different thickness of UAB and CTB for comparison with the left. These two inverted pavement structures were designed to compare the effect of the thickness of the UAB layer and CTB layer. The right lane as the benchmark is a conventional pavement structure used to compare the structural responses to that of the inverted pavements. A quarter of the whole geometry, as shown in **Figure 4-3**, is modeled to simulate the pavement structure in this study due to the double symmetry of the dimensions of the structures. The length and width of the quarter domain were modeled to be 1.0 m and 1.0 m respectively.

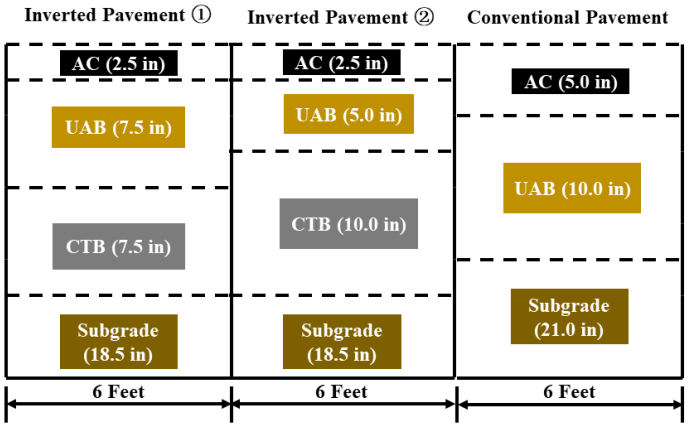

Figure 4-1. Pavement structures in models (1 inch = 2.54 cm; 1 foot = 30.48 cm).

4.1.2 Material properties

The material properties of all the pavement structures in this study for the structural response study are summarized in **Table 4-1**. These parameters of materials are collected from other verified literature [17,39,40]. The model in this study considered the UAB as a type of elastic material, and its initial elastic modulus of UAB was set at 100 MPa. The modulus of UAB changed with the iteration process in the simulation.

Table 4-1 MATERIALS PROPERTIES USED IN THE NUMERICAL MODEL.

Layer (Inverted)	***Thickness (m)***	***Elastic Modulus (MPa)***	***Poisson's ratio***	***Density (kg/m^3)***
AC	0.07/0.07	1700	0.35	2400
UAB	0.21/0.14	100	0.25	2000
CTB	0.21/0.28	10000	0.25	2200
SG	0.51/0.51	50	0.45	1800
Layer (Conventional)	***Thickness (m)***	***Elastic Modulus (MPa)***	***Poisson's ratio***	***Density (kg/m^3)***
AC	0.14	1700	0.35	2400
UAB	0.28	100	0.25	2000
SG	0.58	50	0.45	1800

4.1.3 Boundary condition

Proper boundary constraints contribute to the accuracy of the calculation. In this study, the bottom of the SG was constrained, and all types of movements were constrained (ENCASTRE). Roller support was used to simulate the inside vertical surfaces. This support allows translational movement in the vertical direction while restricting the movement in the horizontal plane in respective directions [9,39,41–43]. The outside vertical surfaces were modeled as free of movements. The top of the model was also free of the boundary. In this model, the interaction between layers was not taken into consideration to simplify the calculation.

4.1.4 Loading condition

In previous studies, the equivalent contact area was used to simulate the actual tire contact area as rectangular or circular [42,43]. The vehicle load in this study adopted the standard single axle with double wheels. And the size of the actual tire marks on the calculation paper is closer to the area of the rectangular area. Thus, as shown in **Figure 4-2**, the loading area was simplified as a uniformly distributed load on a rectangle area with a length of 10 inches which equaled the actual contact area. The tire pressure was set at 1.36 MPa based on actual tire pressure on the pavement. The objective of simplifying the load pattern was to improve the calculation efficiency of the model.

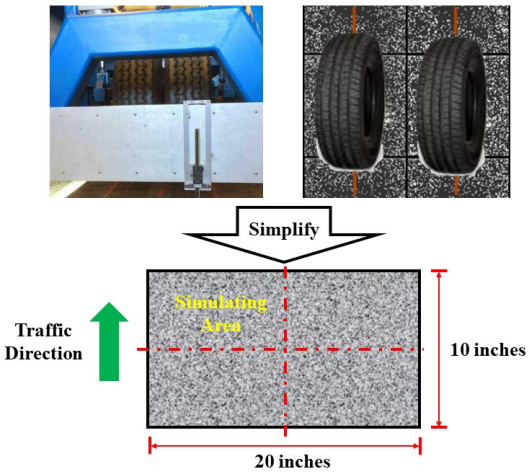

Figure 4-2.The simplified contact area of dual wheels.

4.1.5 Mesh generation

The mesh size contributes to the accuracy of the simulation in FEM [39]. The C3D8 type mesh was applied in this research to minimize the calculation time and improve accuracy. A varying mesh can improve the calculation results. The approximate element size is 0.05, and the deviation factor of curvature control is 0.1. Meanwhile, finer mesh refinement was set for upper layers due to the loading area at the top. The meshed models for inverted and conventional structures are displayed in **Figure 3 (a) & (b)**.

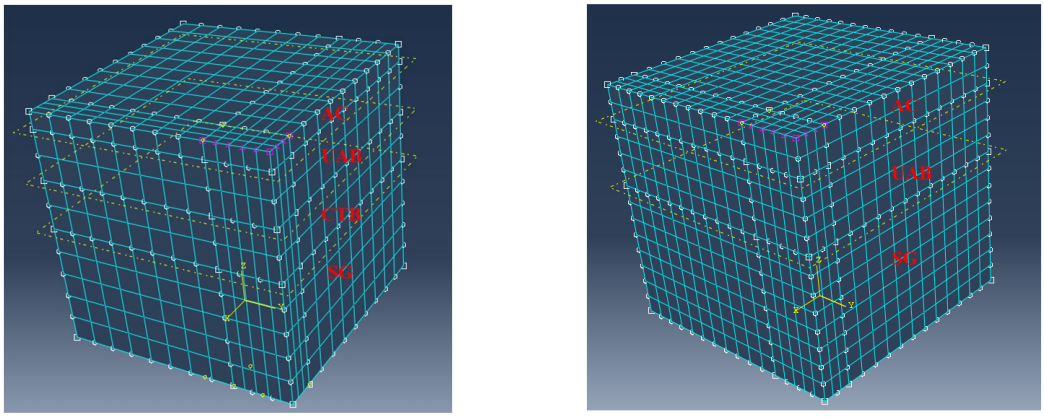

(a) (b)

Figure 4-3. Meshed models for (a) inverted pavement and (b) conventional pavement.

4.1.6 Verification of the numerical model

In order to verify the feasibility of the constitutive model in the UMAT program, the GT-PAVE model was utilized to validate the numerical model. The current nonlinear stress-dependent model used in this study was validated by the field data. As shown in **Figure 4-4**, the detailed pavement design and materials properties for validation were from Tutumluer [44]. The comparison results are presented in **Table 4-2**. The predicted stress in the vertical direction was just 4.41% higher than the field data. For the predicted deflection at the surface of the AC layer,

only the maximum deflection at the load center was 12.67% higher than the measured data. Therefore, the numerical model can be verified based on the comparison results.

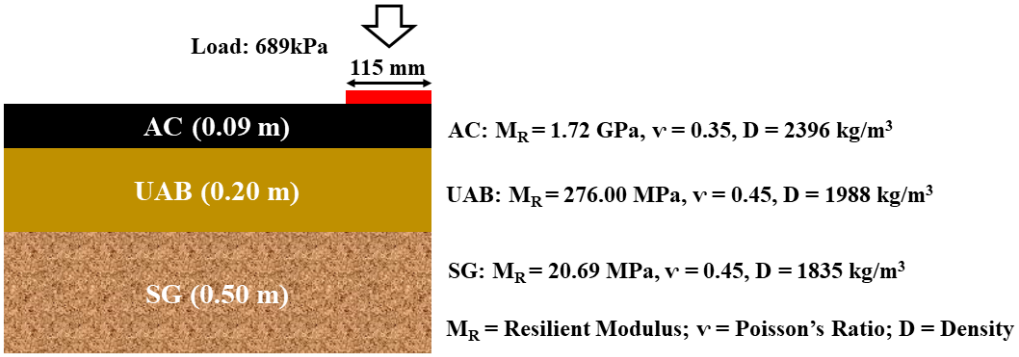

Figure 4-4. GTPAVE conventional pavement structure for model verification [44]

Table 4-2 COMPARISON OF THE PAVEMENT RESPONSES

	Stress (vertical direction) at the top of the SG layer	***Deflection in the AC layer Radial distance (mm)***		
Response	**σ_z (kPa)**	**0**	**254**	**368**
Section 8	82		0.51	0.33
Section 9	77		0.56	0.33
Section 10	47		0.43	0.25
Average (measured)	68	0.71	0.43	0.33
Current research (Prediction)	71	0.80	0.44	0.34
Error % (Compared to average)	4.41	12.67	0.02	0.03

4.1.7 Comparison with the linear model

A linear elastic system was also applied in this study to compare it with the nonlinear stress-dependent system to confirm the reliability of the nonlinear system. The same material properties with the nonlinear system were used in the linear elastic system. **Figure 4-5** (a) & (b) present the comparison of the predicted X-direction stress distribution in the conventional pavement and inverted pavement (1) between these two systems. It can be seen that the two systems have almost the same value of compressive stress at the surface of the AC layer for the conventional pavement. The maximum tensile stress also appeared at the same position (the bottom of the AC layer). The value gap between them was just 28 % which was acceptable based on the study by Kim et al. [9]. For the inverted pavement structure, the maximum tensile stress appeared at the same positions: the bottom of the AC layer and the bottom of the CTB layer in the two systems. However, the value gap was much higher than that of the conventional pavement. The tensile stress at the bottom of the AC layer in the linear system was much higher compared to the nonlinear system. The maximum tensile stress at the bottom of the CTB layer in the linear system was 80% more than that in the nonlinear system, which was not acceptable.

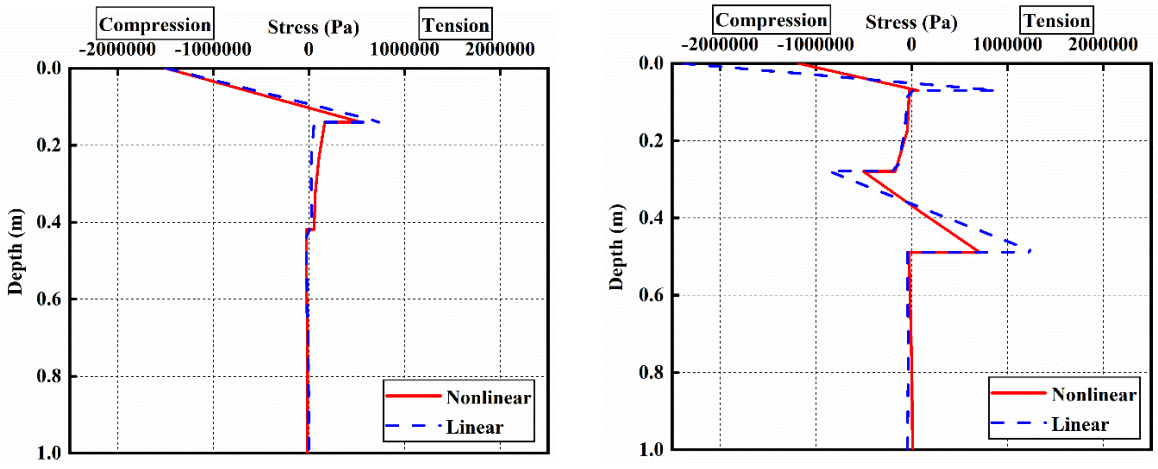

Figure 4-5. Comparison of stress (X direction) in (a) conventional pavement structure; (b) inverted pavement (1)

Figure 4- 6 (a) & (b) show the comparison of the predicted X-direction strain distribution in the conventional pavement and inverted pavement (1) between these two systems. The comparison also indicated that the nonlinear stress-dependent model had a more significant influence on the inverted model, and the continuous distribution of the strain verified the reliability of the comparison in the stress.

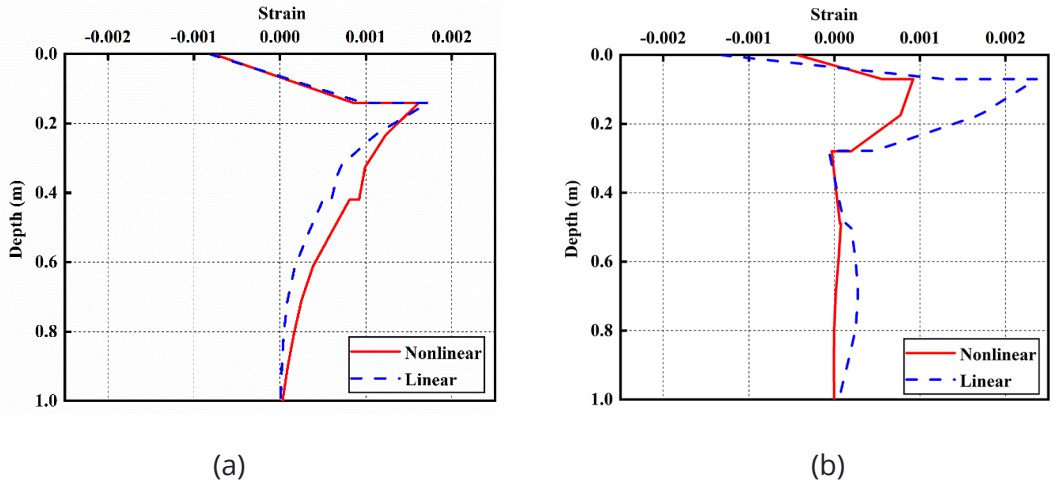

Figure 4-6. Comparison of strain in X direction (E11) in (a) conventional pavement structure; (b) inverted pavement (1)

Figure 4-7 (a) & (b) present the comparison of the predicted deflection in the conventional pavement and inverted pavement (1) between these two systems. The maximum deflection in the two systems occurred at the centerline of the wheel load, and the value gap was just 13%. For the inverted pavement, although the maximum deflection appeared at the same position of the pavement, the value gap is too large to be explained. Based on the comparison results, the structural response of the inverted pavement is more sensitive to the effect of the UAB layer than the conventional pavement due to the compaction effect from two stiffer layers of an upper thin

AC layer and a lower CTB layer. The nonlinear stress-dependent characteristic of the UAB layer has a more extensive influence on the structural response of an inverted pavement due to the compaction effect from two stiffer layers of an upper thin AC layer and a lower CTB layer. Therefore, the nonlinear property must be taken into consideration during the structural analysis of the inverted pavement.

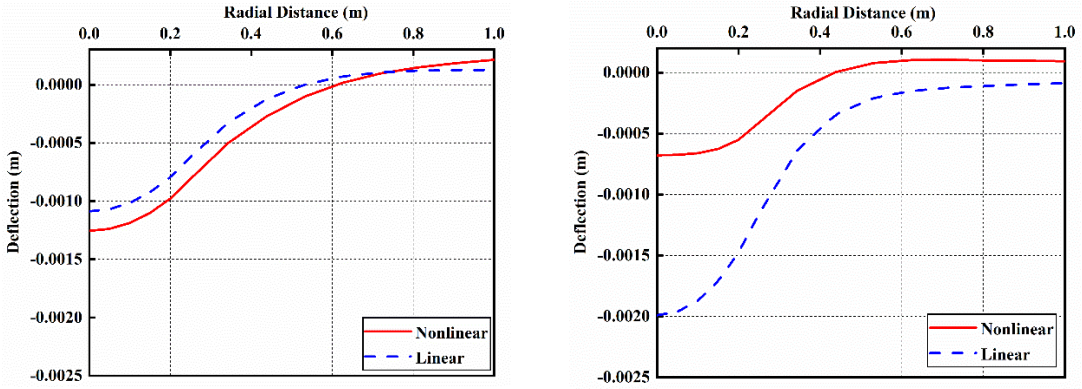

Figure 4-7. Comparison of deflection in (a) conventional pavement structure; (b) inverted pavement (1)

To investigate the feasibility of the inverted pavement structure, the conventional pavement structure was set as a benchmark for comparison. The thickness of AC, UAB, and SG was designed as 0.14 m, 0.28 m, and 0.58 m, respectively. **Figure 4-8** shows the stress distribution (s11) along the load centerline in the X-direction, which is used to comparison study with inverted pavement stress distribution, as shown in **Figure 4-11**. The compressive stress at the surface of the AC layer was 1501 kPa in **Figure 4-8**, which was higher than that of the inverted pavement structures, as shown in **Figure 4-11**. The tensile stress at the bottom of the AC layer was 542 kPa, which was much higher than 69 kPa and 43 kPa in the inverted pavement structures (1) and (2). The cracks could be induced by the severe tension of the AC layer, which led to the damage of the pavement structure. The stress distribution in the UAB layer was also totally different from that of the inverted pavement. The compressive stress was distributed in the UAB layer of the inverted pavement because of the stress-dependent property in the UAB. However, in the conventional pavement structure, only the tensile stress was distributed within the UAB layer due to the assumption that the particles in the UAB are elastic. The lack of confinement of the CTB layer led to the loose condition of the UAB compared to that of the inverted pavement. The loose UAB is not able to provide a rigid base for the AC layer, which resulted in the higher tension and more cracks at the bottom of the AC layer in the conventional pavement. The UAB in the inverted pavement acted as a cushion layer to support the AC layer [22]. Moreover, the tension from the CTB was relieved due to its compression condition. Thus, the inverted pavement structure is able to reduce the tension stress at the bottom of the AC layer and improve the stress distribution in the pavement structure, which contributes to the service performance of the pavement. The stress at the top of the SG is also important to the pavement structure. The tensile stress at the top of SG in the conventional pavement is 119.72 kPa which is contrary to the stress state of compression stress in inverted pavements. The compression stress at the top of SG in the

inverted pavement (1) & (2) is 37.09 kPa and 31.44 kPa, respectively. The state of compression stress in the inverted pavement indicated that the UAB layer could also protect the SG to reduce the deformation of the pavement structure and improve its bearing capacity.

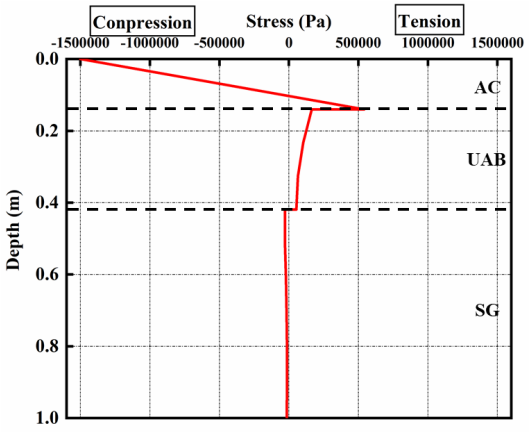

Figure 4-8. Stress distribution in X direction (s11) for conventional pavement (nonlinear model)

Figure 4-9 shows the deflection distribution of the conventional pavement from the load centerline to the boundary of the lane. The maximum deflection was also located in the vertical direction of the loading area compared to that of the inverted pavement. The deflection value of 0.00125 m in the conventional pavement was almost twice to three times that in the inverted pavement. The radial distance that the deflection changed from settlement to uplift was around 0.62 m, which showed that there was a more substantial settlement area in the conventional pavement when the load was the same. The broader settlement area could lead to severe damage to the pavement structure. Therefore, the inverted pavement structure is better than the conventional pavement in the aspect of surface deflection.

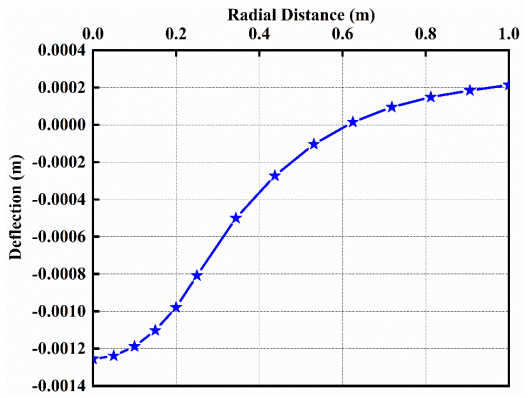

Figure 4-9. Deflection response of conventional pavement

Figure 4-10 shows the distribution of stiffness contours within the UAB layer in the conventional pavement. It can be found that the contours were a little denser compared to that of the inverted pavement. In addition, the values of stiffness were much lower than that of the inverted pavement. The maximum stiffness was 178 MPa, as shown in **Figure 4-10**. The lower stiffness in the UAB could not provide the rigid base for the AC layer and, thus, greater tension occurred at

the bottom of the AC layer. Therefore, the UAB obtained a much higher stiffness in the inverted pavement structure compared to the conventional pavement.

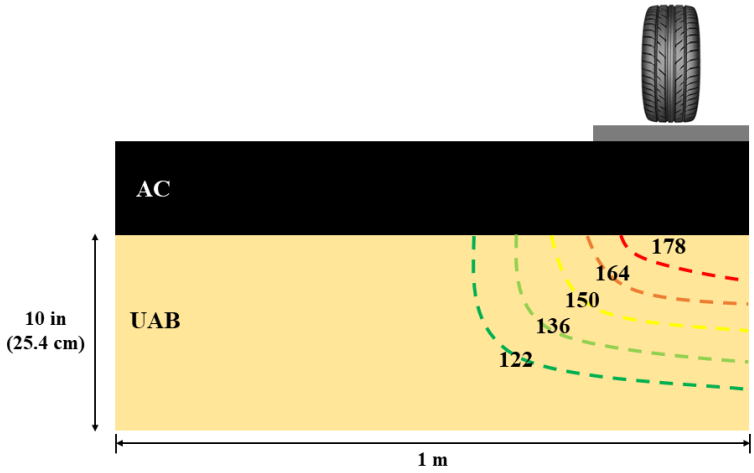

Figure 4-10. Stiffness (MPa) distribution within the unbound aggregate layer under the load (conventional pavement)

4.1.8 Results of the structural response in the inverted pavement

The structural response of both the inverted pavements and the conventional pavement is presented in the following part. The inverted pavements with different thicknesses of UAB were compared in terms of stress, strain, and deflection. In addition, the conventional pavement structure was also compared with the inverted pavements.

The horizontal stress distribution at the bottom of the AC and CTB plays an essential role in the structural safety of the pavement structures. **Figure 4-11** shows the stress distribution along the load centerline for inverted pavement structures (1) and (2). The thickness of the AC layer is 2.5 inches in both cases. The difference between these two is the thickness of the unbound aggregate base layer and the cement-treated base layer. **Figure 4-11** shows that the value of the maximum compression stress that occurred at the surface of the AC layer is 1182 kPa. However, the stress changed into tensile stress at the bottom of the AC layer. The compressive stress was distributed along with the whole UAB layer. Then, the compressive stress increased to 505 kPa at the top of the CTB layer and changed into tensile stress again at the bottom of the CTB layer. It is easily found that the maximum tensile stress along the load centerline was located at the CTB layer. It is known that tensile stress is bad for the service life of a pavement structure due to the cracks induced by the unbearable tension. For comparison, the inverted pavement (2) under the same loading condition was also simulated using the same model. The compressive stress at the surface of the AC was 966 kPa, which was smaller than that of inverted pavement (1). The tensile stress at the bottom of the AC layer was 43 kPa which was also lower than that of inverted pavement (1). The thicker CTB developed a lower tension state to reduce fatigue cracking. In addition, the thicker UAB layer could increase the bending of the AC layer, which was consistent with the research conducted by Papadopoulos and Santamarina [22]. The tensile stress at the bottom of the CTB layer was 341 kPa which was larger than 256 kPa in inverted pavement (1). Thus, the bending stress could be reduced under the influence of the thicker UAB layer. The compressive stress at the bottom of the UAB layer was 270 kPa which was larger than 172 kPa in

inverted pavement (1). Although the thickness of CTB layers in these two inverted pavements was different, there was little difference in the tendency of stress change. The thickness of the CTB layer had little influence on the structural responses of the AC layer and UAB layer. The SG of the inverted pavement was slightly affected by the load at the surface.

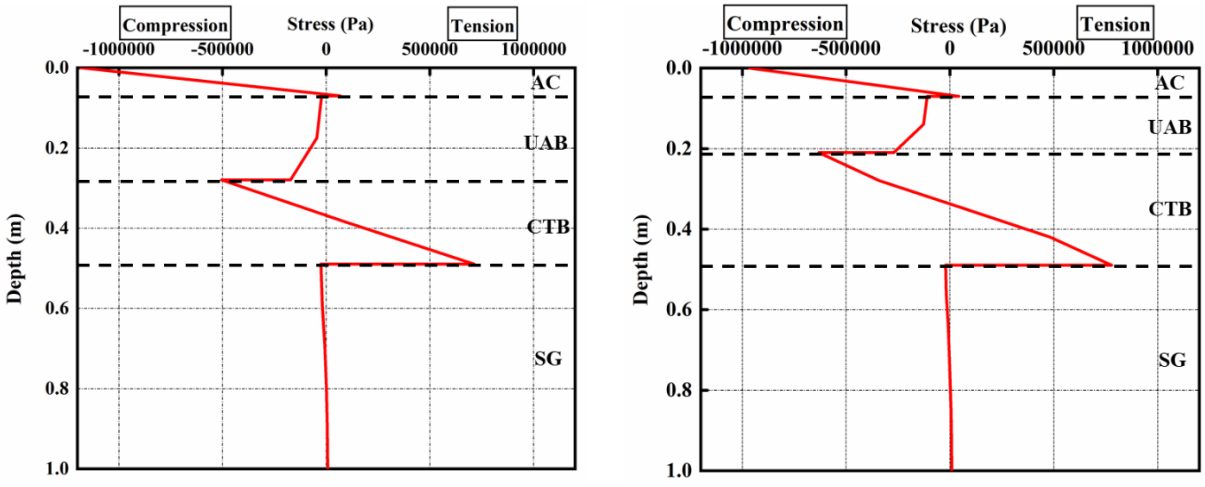

Figure 4-11. Stress distribution in the X direction (s11) for inverted pavement (a) (1) & (b) (2)

The deformation in the asphalt layer is critical distress, which will compromise the service performance of the pavement and requires higher budgets for rehabilitation [45]. Surface deflection is an essential indicator in estimating the quality of the pavement structure. **Figure 4-12** illustrates the surface deflection responses of the inverted pavements in the vertical direction. The measured area was from the load center to the boundary of the testing lane. As shown in **Figure 4-12**, the maximum deflection occurred at the load center, consistent with the results from Sahoo et al. [42] and Biswal et al. [39]. The maximum deflection of inverted pavement (1) was 0.000679 m. With the increase of radial distance from the load center, the deflection gradually decreased. The deflection response turned into uplift from the settlement when the radial distance reached around 0.43 m. As for the inverted pavement (2), the maximum deflection was 0.000486 m. Furthermore, the deflection status change occurred when the radial distance was 0.42 m. Thus, the uplift appeared at almost the same location in these two structures.

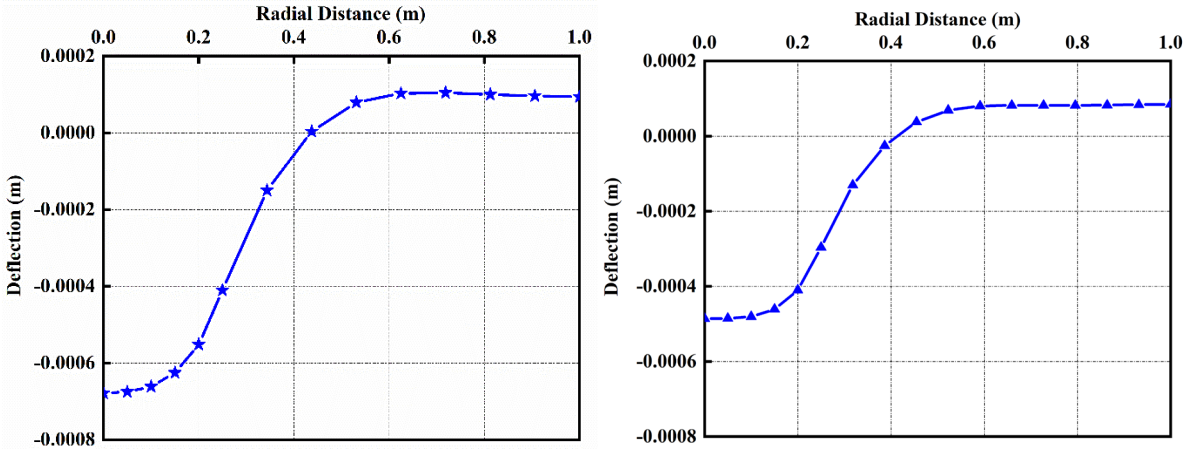

(a) (b)

Figure 4-12. Deflection response of inverted pavement (a) (1) & (b) (2)

As discussed above, the UAB layer is critical to the inverted pavement structure. The stiffness of the unbound aggregate base is sensitive to the dynamic load [46]. The stiffness of the UAB layer was calculated by the mentioned constitutive model and equations. To investigate the stiffness property within the UAB layer more intuitively, the stiffness contours are presented in **Figure 4-13**. It can be seen that the maximum stiffness of inverted pavement (1) at 337 MPa is lower than 371 MPa in inverted pavement (2). In addition, it can be seen that the stiffness of the UAB decreased with the increasing distance from the wheel load. The confinement provided by the CTB contributes to the increase of stiffness within the UAB. Moreover, the thicker UAB under the same load results in a lower level of stiffness.

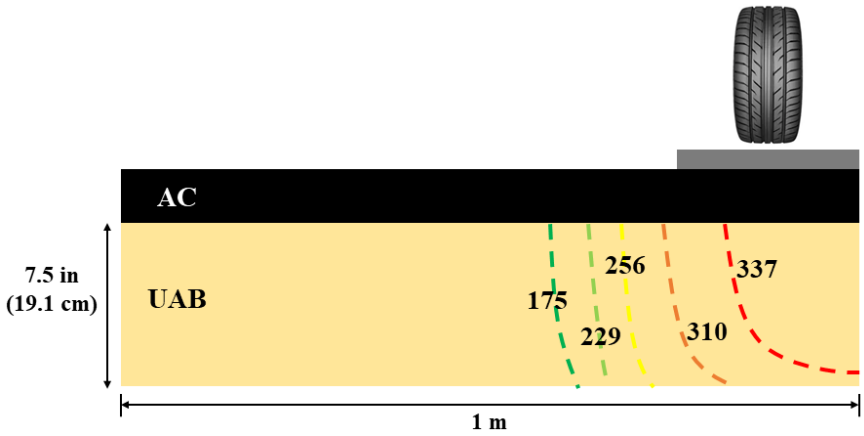

(a)

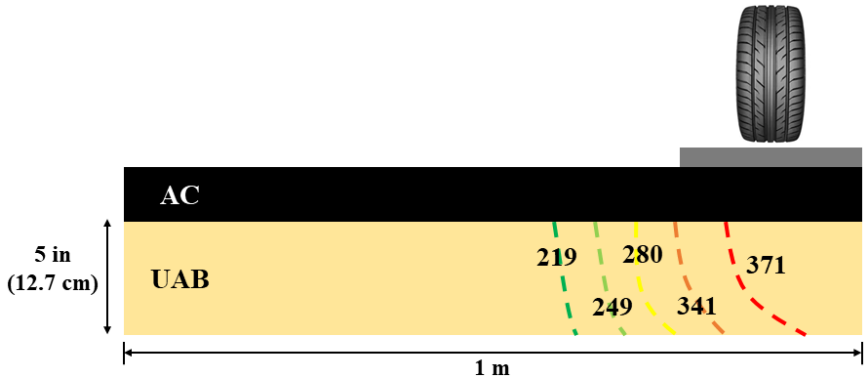

(b)

Figure 4-13. Stiffness (MPa) distribution within the unbound aggregate layer under the load (a) inverted pavement (1); (b) inverted pavement (2)

4.2 Field Investigation and Numerical Analysis of Inverted Pavement in Tennessee, USA

4.2.1 Project description – inverted and conventional pavements

The construction of the inverted and conventional pavement test sections was started in November 2018 and was completed in April 2019. The pavement test sections are part of the truck road entrance from Riverside Drive to Vulcan Materials quarry in Knoxville, Tennessee. The preparation work and construction of the subgrade (SG) was conducted between December 2018 and March 2019. Compaction and placement work of TDOT Grade D base materials [47] on subgrade was performed in March 2019. Then 4% (by weight) ordinary Portland cement (type Ⅰ) was mixed by a soil stabilizer machine and added to the inverted pavement section for a seven-day curing started from March 22, 2019, and resulted in forming the CTB layer. The unbound granular base material was placed at the top of the CTB layer and was compacted on April 11, 2019 (part of the inverted pavement section). To meet the specification of G1 crushed stone for base course in South Africa, there is some difference in unbound aggregates for the inverted and conventional pavement sections [48]. Lower quantities of small particle aggregates were used in the UAB of the inverted pavement section. An asphalt concrete layer was paved on both the conventional and the inverted pavement sections on April 15 and 16, 2019. As shown in **Figure 4-14**, both the inverted and the conventional pavement sections are part of a two-lane road, and each pavement section is 122 m long and 9 m wide. **Figure 4-15** shows the designed profile of the conventional and the inverted pavements. The inverted pavement section consists of an asphalt layer, unbound aggregate base, cement-treated base on subgrade, whereas the conventional section does not contain the CTB layer. The road with both pavement types was open to traffic including heavy truck traffic from the quarry on April 17, 2019. In addition, the estimated annual traffic load for this pavement was approximately 330,000 equivalent single-axle loads (ESALs).

Figure 4-14**.** The conventional and inverted pavement test sections constructed at the entrance of the Vulcan Materials Quarry in Knoxville, TN

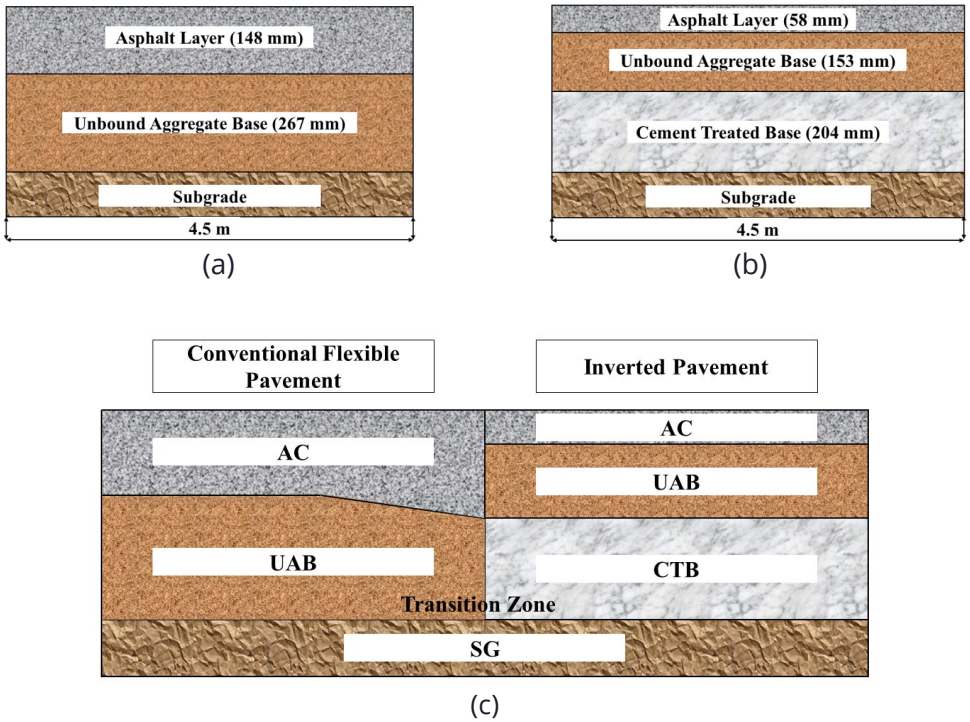

Figure 4 15. Designed profiles of pavement structures: (a) Conventional section; (b) Inverted section; (c) Transition zone between the conventional and inverted pavements

Figure 4-16 shows profiles of pavement layer thicknesses obtained by the GPR after processing, filtering, interfacing and demonstrating the pavement layers for conventional, inverted and transition section. The depth measuring range in the vertical axis is from the ground surface (0 cm) to 150 cm below the ground. Based on the data shown in **Figure 4-16** (a), the obtained average thickness of AC in the conventional pavement is approximately 150 mm, compared with the designed value of 148 mm. The thickness of UAB is approximately 270 mm, compared with the designed value of 267 mm. For the inverted section shown in **Figure 4-16** (b), the average measured thickness of the thin asphalt layer is approximately 60 mm, with only a 2 mm difference compared with the designed value of 58 mm. The average measured thickness of the

UAB is approximately 150 mm, only a 3 mm difference from the designed value of 153 mm. As for the CTB layer in the inverted pavement, the thickness shown in the GPR processor is about 200 mm, compared with the designed value of 204 mm. Based on these measurements, the GPR based layer thicknesses are validated and consistent with the designed thickness of the pavement layer well. **Figure 4-16** (c) shows the transition zone from the conventional pavement to the inverted pavement section. GPR analysis reveals that applications such as measuring the thicknesses of pavement layers can be determined if the design requirements are met or not in the framework of quality control/control-quality assurance (QA/QC) processes [31]. In this study, the design thicknesses of the investigated pavement layers were validated by the GPR data. And the measured pavement layer thicknesses will be used in the subsequent numerical analysis and simulation sections to build the investigated pavement geometry.

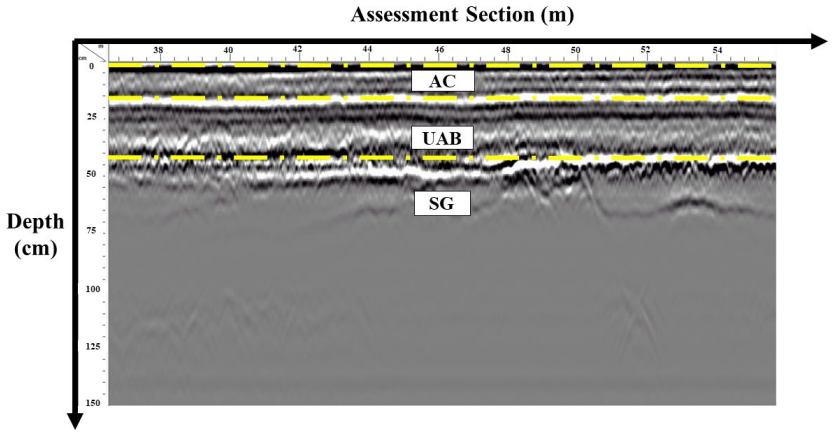

(a)

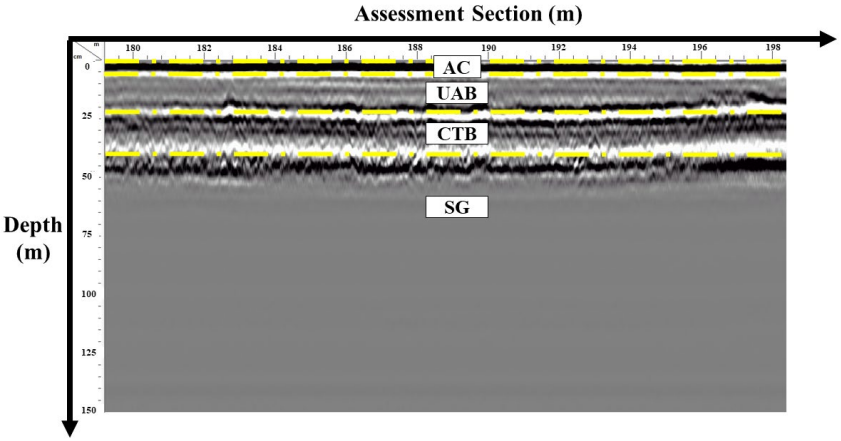

(b)

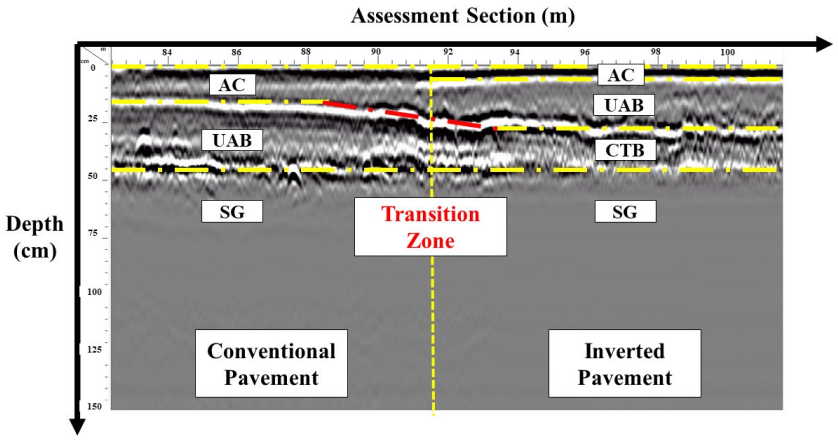

(c)

Figure 4-15. Results of GPR measurement of pavement layer thickness: (a) Conventional pavement section; (b) Inverted pavement section; (c) Transition zone between the inverted and the conventional pavement sections

4.2.2 Laboratory and field material characterization

During pavement construction, each layer of the pavement was carefully monitored. Extensive material sampling for characterization in the laboratory was done including the resilient modulus of unbound aggregates for the inverted section following the repeated load triaxial (RLT) test protocol (AASHTO T307). In addition, the field testing and evaluation methods such as the Benkelman beam test, 3D Road profiling test and FWD were conducted to further investigate the properties of pavements.

4.2.2.1 Lab testing - Repeated load triaxial test

The elastic modulus for unbound aggregate materials in pavement engineering is commonly characterized as the resilient modulus, M_R [49]. In the repeated load triaxial test (RLT), the resilient modulus is defined as the ratio of the applied cyclic stress to the recoverable strain after a hundred cycles of repeated load. In the inverted pavement system, the resilient modulus changes with the loading condition, which has significant effects on the structural response of the pavement. Thus, it is imperative to conduct the RLT to characterize the resilient modulus of the unbound materials. In this study, a repeated load triaxial was conducted to determine the modulus of the unbound aggregate materials for the inverted and conventional pavement sections. Based on the field record, the aggregates at optimum moisture content (OMC) and maximum dry density (MDD) were used to build the UAB layer. The aggregates under the same conditions were used to determine the resilient modulus of the materials using the RLT test. As shown in **Figure 4-17**, the Instron 8502 servo-hydraulic dynamic testing system was used to simulate traffic loads on the materials, which was following the AASHTO T307 standard test procedure. The capacity of the load cell is 25 kN (kilonewtons), and the axial displacement was measured as an average value from two linearly variable differential transducers (LVDT) placed between the top platen and the base of the load cell. A total of 15 loading sequences including different confining stresses and cyclic deviatoric stresses was put on the specimens. During the test, the repeated load cycles consist of a 0.1-second haversine-shaped loading pulse and a 0.9-

second resting period. During sample preparation, unbound materials were compacted in six layers at MDD and OMC.

(a) RLT test (b) Specimen preparation (c) Scaling materials

Figure 4-16. Preparation and testing of unbound materials in RLT test system

In this test, the variation of the resilient modulus was obtained by controlling the chamber confining pressure and the maximum axial stress. The increase of confining pressure and nominal maximum axial stress leads to the increase in resilient modulus of granular materials. Thus, UAB is regarded as a type of stress hardening material. It is known that the stiffness of inverted pavement has the property of stress-dependent due to the two stiffer layers—asphalt layer and cement-treated base. According to the Uzan' model [50], the resilient modulus can be estimated by **Equation (4-1)**:

$$M_R = K\theta^n \tau_{oct}^m \quad (4\text{-}1)$$

Where M_R is resilient modulus; θ is the bulk stress (sum of principle stresses) = $\sigma_1 + \sigma_2 + \sigma_3$, τ_{oct} is octahedral shear stress $= \sqrt{\frac{1}{3}[(\sigma_1 - \sigma_2)^2 + (\sigma_2 - \sigma_3)^2 + (\sigma_3 - \sigma_1)^2]}$ and K, n, m are materials constants.

The analysis of the resilient modulus data resulted in finding the material parameters as follows: $K = 6\times10^5$, n = 0.50 and m = 0. For the UAB of the conventional pavement section, the constants are $K = 5\times10^5$, n = 0.25 and m = 0.24, respectively. For this study, the resilient modulus of unbound aggregate materials will be used in the numerical analysis simulation to investigate the stress-dependent characteristic of UAB in the inverted pavement structure.

4.2.2.2 Field testing - Benkelman beam test

Benkelman beam test is commonly used to measure the pavement maximum surface deflection (AASHTO T 256). The test is considered as a non-continuous static loading method as described in the AASHTO standard. In this study, a HUMBOLDT H-3220A Benkelman beam was used to measure the deflection of both the inverted and the conventional pavement sections. The probe beam, with a length of 2.40 m, has a digital indicator with a resolution of 0.025 mm (0.001 in.), which is fixed on the main body to display the deflection measurements. As shown in **Figure 4-18**, a truck with 80 kN (18,000 lbf) load on the single rear axle was weighed on the scale. The beam was placed between the tires so that the probe was 1.37 m forward of and perpendicular

to the rear axle. Then, the digital dial gauge was reset to 0.000 mm (0.000 in.). The truck drove approximately 8 m forward at a creeping speed, and the maximum dial reading (D_m) was recorded. After the dial stabilized, the final reading (D_f) was recorded. The pavement surface deflection can be calculated by **Equation (4-2)**. The test was repeated at the measurement intervals similar to FWD test points shown in **Figure 4-19**. Six points with 20 m intervals were measured in both the left and the right sides of the conventional and the inverted pavement sections. The average deflection for each wheel track was reported as the final value.

$$D = 2 * (D_m - D_f) \quad (4\text{-}2)$$

(a) (b)

Figure 4-17. Overview of the Benkelman beam test

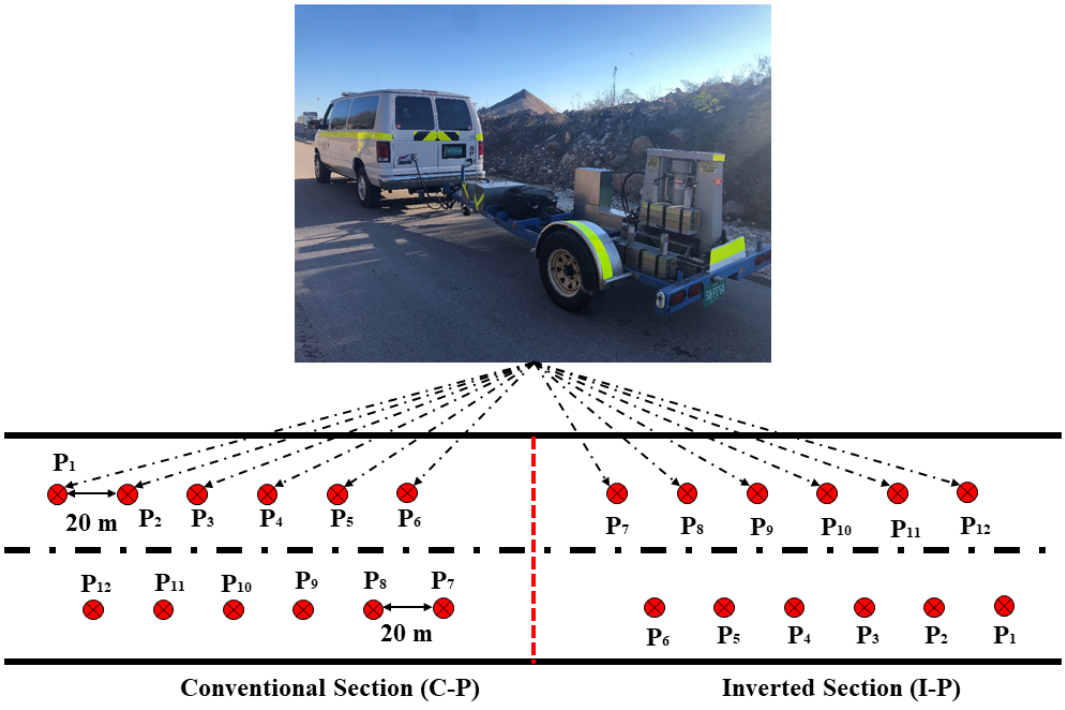

Figure 4-18. Overview of the FWD experimental framework (C-Conventional; I-Inverted)

Based on the collected data, when the test was conducted on the inverted pavement section, no deflection could be detected by the equipment. Therefore, the deformation of the inverted pavement surface was negligible and below the resolution of the dial gauge. However, an average deflection of 0.326 mm was measured for the conventional pavement section using the same dial gauge. The zero deflection measured in the inverted pavement reflected a negligible deformation of the whole pavement structure. Stiffer UAB in the inverted pavement might be the reason for the small deflection at the pavement surface.

After being subjected to the simulation of loaded truck traffic using the pavement for a long time, the UAB became stiffer under the repeated truck traffic loads and provided a good layer performance (cushion) between the asphalt and cement-treated base layers. And the "cushion" transferred the stress from the asphalt surface to the CTB layer, which resulted in negligible deflection on the pavement surface. In addition, the inverted structure contributed to the lower deformation. Nevertheless, whether the stiffer UAB could reduce the deflection of subgrade was not certain based on this test. Therefore, the FWD was used in this research to further investigate the pavement layers deflection.

4.2.2.3 Field testing - 3D Road profiling test by LCMS

A Laser Crack Measurement System (LCMS ®-2) was used to measure the longitudinal, transverse pavement surface profiles and macrotexture. The International Roughness Index (IRI) along the pavement surface is obtained from these measurements. This equipment system has many advantages such as a rapid roughness (ride quality) evaluation of pavement networks, real-time data collection, analysis and storage, operation at traffic speed so that no traffic control is required, and high quality of data from various sensors which are needed for a pavement management system (PMS). Therefore, LCMS is a suitable tool for project-level as well as network-level data collection and analysis. As shown in **Figure 4-20 (a)**, two high-speed scanning sensors and 3D cameras for real-time pavement information collection are mounted at the back of the testing vehicle. **Figure 4-20 (b)** shows the on-board data processing system during the operations. For accurate geographic location information, the GPS is equipped at the top of the vehicle shown in **Figure 4-20 (c)**. The LCMS testing vehicle is able to provide a complete 1 mm resolution automated pavement condition survey. The data received from the LCMS system were analyzed by the software Roadview Workstation, and the results are shown in **Table 4-3**. This test was conducted after a two-year service of the pavement.

(a)

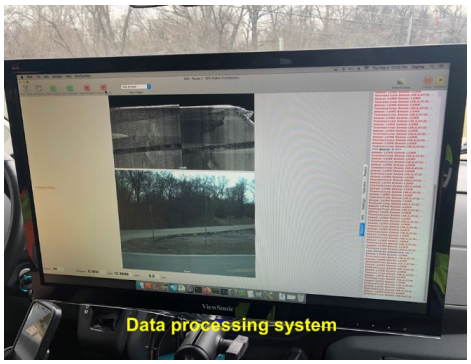

(b)

(c)

Figure 4-19. Pavement surface profile measurement system

Table 4-3 Road surface profile parameters and characteristics

Parameters and Characteristics	*Inverted Section*	*Conventional Section*
HPMS Average IRI (mm / km)*	1,196.3	1,963.4
Longitudinal Cracking Length- Low (mm / km)	3,450.8	3,704.9
Longitudinal Cracking Length- Medium (mm / km)	598.4	4,049.2
Longitudinal Cracking Length- High (mm / km)	0	0
Transverse Cracking Length - Low (mm / km)	0	0
Transverse Cracking Length - Medium (mm / km)	0	0
Transverse Cracking Length - High (mm / km)	0	0
Rutting Depth Average Left and Right (mm / km)	10.7	18.9

*: Federal Highway Performance Monitoring System

IRI is used to evaluate the ride quality of the pavement. A higher IRI value indicates a rougher pavement surface as described by the Federal Highway Administration (FHWA) standard [51]. Based on the pavement surface profile measurement, data demonstrated that the inverted pavement possessed better surface smoothness and ride quality. Longitudinal cracking describes a crack predominantly parallel to the pavement centerline, and its location is within the lane. There are three severity levels according to the crack width: low (≤ 6 mm), medium (6 to 19 mm) and high (≥ 19mm). As for the low severity longitudinal crack, the inverted section and conventional section had a comparative performance. However, the conventional section had a medium severity longitudinal crack of 4049.2 mm/km, almost seven times the length of that in the inverted section. No high severity longitudinal and no transverse cracking was found in both inverted and conventional sections. Based on the cracking survey, it can be found that the inverted structure could effectively delay and reduce the generation and propagation of reflection cracks. Rutting describes a longitudinal surface depression in the wheel paths, and it might also occur with transverse displacement. The average measured rutting depth in the inverted pavement section was 10.7 mm/km compared with 18.9 mm/km of the average rutting in the conventional pavement section (43.4% reduction). This indicates that the inverted pavement section outperformed the conventional pavement section in ride quality, cracking and rutting.

4.2.2.4 Field testing - Falling weight deflectometer measurement

A falling weight deflectometer is a testing system designed to simulate/measure the deflection of a pavement surface caused by an impact load. The FWD generates a load pulse by dropping a weight transmitted to the pavement through a 300 mm diameter circular load plate. The load pulse momentarily causes the pavement to deflect, and the shape of the deformed pavement surface is called a deflection basin. A typical FWD deflection basin used in this study is shown in **Figure 4-20**. Horak [34] investigated the individual layer's condition using Deflection Basin Parameters (DBPs) and evaluated the structural condition of flexible pavements based on the deflection basin and DBPs as shown in **Table 4-4** [34,35]. The only difference in this study is the name of each parameter. In this study, SCI, BDI and BCI are equal to BLI, MLI and LLI, respectively. Due to the same loading history and environmental condition of the conventional and inverted pavement sections, the same assessment method in Horak's study was used herein to evaluate the pavement's condition and conduct a comparative study between the two pavement sections. In this study, a 40 kN (9 kips) load was applied at 20 m intervals along the pavement. Deflections were recorded by seven sensors at radial distances of 0 mm (D_0), 305 mm (D_{300}), 457 mm, 610 mm (D_{600}), 914 mm (D_{900}), 1,219 mm and 1,524 mm (W_7) from the center of a loading plate with a 150 mm radius. **Figure 4-19** shows an overview of the FWD test framework. The collected test data is presented in **Table 4-5**. To maintain test result's repeatability and mitigate the effect of random errors, the arithmetic mean and coefficient of variance (COV) were calculated for each data group, as shown in **Table 4-5**. **Figure 4-22** shows the deflection basin curves for the inverted and conventional sections based on the FWD data.

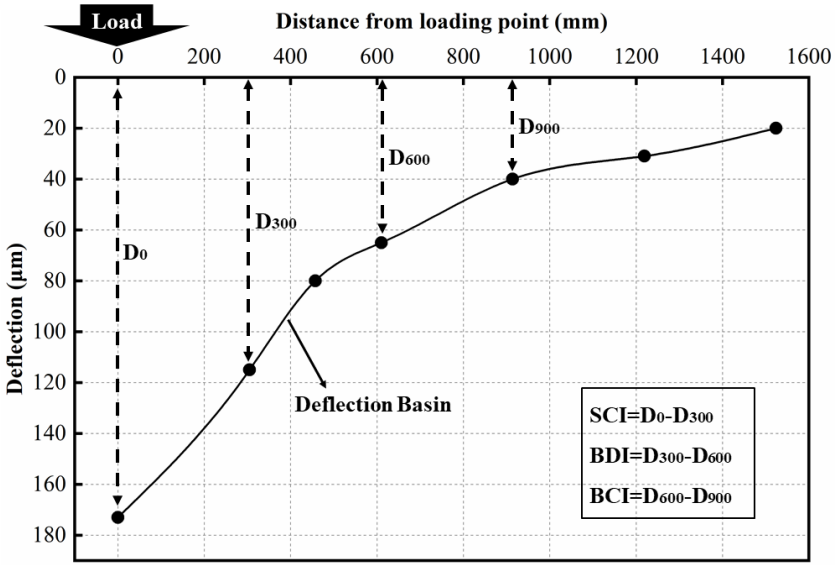

Figure 4-20. A typical FWD deflection basin and indexes

Table 4-4 Deflection Basin parameters (DBPs)

Parameter (μm)	***Calculation equation***	***Meaning***
D_0 – central deflection	n/a	n/a
Surface curvature index (SCI)	D_0-D_{300}	Surface layer condition
Base damage index (BDI)	D_{300}-D_{600}	Intermediate layer condition
Base curvature index (BCI)	D_{600}-D_{900}	Lower layer condition

n/a: not applicable

Table 4-5 Details of DBPs by FWD test in the inverted and conventional pavement section

Inverted Section	***D_0***	***D_{300}***	***D_{600}***	***D_{900}***	***W_7***	***SCI***	***BDI***	***BCI***
COV	3.03%	5.90%	7.03%	11.27%	9.23%	9.18%	5.85%	11.22%
Average (μm)	157.4	65.2	16.9	11.2	7.3	92.2	48.3	5.7
Conventional Section	***D_0***	***D_{300}***	***D_{600}***	***D_{900}***	***W_7***	***SCI***	***BDI***	***BCI***
COV	4.18%	7.79%	3.34%	5.56%	5.18%	25.36%	14.07%	4.86%
Average (μm)	148.8	101.5	48.9	20.5	11.6	47.3	52.6	28.4

COV: Coefficient of Variation

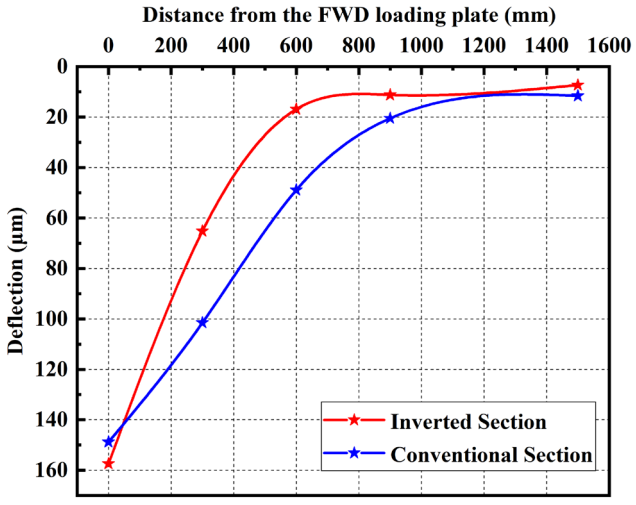

Figure 4-21. Deflection basins of inverted and conventional pavement sections

Based on the data in **Table 4-5**, the average value of SCI in the inverted pavement is 92.2 mm, which is larger than the SCI value of 47.3 mm in the conventional pavement. This value difference is due to the thickness of the asphalt layer. The AC layer of the inverted pavement has a thickness of 58 mm, which is just one third the thickness of the AC layer in the conventional pavement section. The same pulse load induced more deflection on the AC layer in the inverted pavement

section. As for the BDI value, the value of the inverted pavement section has almost the same value as the conventional section, which can reveal the function and benefit of the UAB. The UAB layer dispersed the stress and mitigated the stress dissipation from top to bottom. In addition, the stiffer layers of AC and CTB contribute to the denser UAB matrix, which improves the stiffness of UAB and leads to its better performance. The results of the BCI values could further confirm this explanation. The BCI values reflect the subgrade condition based on **Table 4-4** and research work by Horak et al. [35]. Based on the comparison of BCI values between the inverted and conventional pavement sections, the BCI value for the subgrade of the inverted pavement section was only 20.07% of that of the conventional pavement section. This confirms that the SG of the inverted pavement benefited from the UAB layer and also the inverted structure, which played an essential role in the stress distribution of the pavement structure. Chang et al. [52] also listed the DBPs and corresponding threshold ranges used in typical flexible pavements in Texas. They concluded that the smaller SCI, BDI, and W_7 values represent good structural condition of the asphalt layer, base layer and subgrade soil, respectively. The average W_7 of the inverted pavement section of this study was also only 37% of that of conventional pavement section, which indicates that the subgrade of inverted pavement section had lower deflections than that of conventional pavement section. However, DBP-based evaluation method could not present details such as stress and stiffness distributions for the assessment. Thus, this observational analysis is not enough to confirm an improved performance of inverted pavement compared with the conventional pavement. Therefore, a detailed quantitative analysis was accomplished by finite element method using a general-purpose FEM software ABAQUS.

4.2.3 Preliminary numerical analysis of the inverted pavement

In a study of inverted pavement, the authors conducted a comparative study to investigate the influence of linear and nonlinear stress dependent models on the conventional and inverted pavements [53]. The results show that the nonlinear model significantly affected the inverted pavement structure results but had little influence on conventional pavement results. Therefore, the nonlinear stress-dependent model is selected to model the inverted pavement during the analysis of structural response.

Thus, a preliminary numerical analysis was conducted to compare the impact of the FWD test on the inverted and conventional pavements. In a study by Rabbi and Mishra [54], they ignored the stress-dependent behavior of unbound base and assumed the characteristics of the asphalt layer was linear-elastic. Other studies [55–57] used linear-elastic models to simulate the FWD testing of traditional flexible pavements. The AC and unbound aggregate layers were assigned the linear-elastic property by Tarefder and Ahmed [56], which showed little effect on the simulation result. These studies mainly focused on the conventional flexible pavement structures. However, the nonlinear stress-dependent property of UAB should be accounted for due to its imperative influence on the inverted pavement. Otherwise, neglecting the nonlinear property in the inverted pavement analysis will put limitations on this research. Therefore, this study considers the nonlinear stress-dependent property for characterizing the unbound materials. The linear-elastic characteristic was assigned for the other layers of the inverted pavement. Furthermore, the temperature will also influence the properties of the pavement. The FWD test in this study was conducted in October in Knoxville, TN, where the test temperature was about 20 ℃ (68°F). The temperature correction process is needed for the FWD-based evaluation because AC layer is

sensitive to the temperature change. A temperature of 20℃ (68°F) is considered as the reference temperature since it is the standard reference temperature in the AASHTO 1993 Design Guide [58,59]. In this study, the correction process was omitted due to its reference test temperature.

4.2.3.1 Establishment of the constitutive model

To reflect the nonlinear characterization of the UAB layer when the FWD impulse load was applied on the pavement surface, a modified constitutive model is presented in **Equation (4-3)** [60].

$$M_r = (1+\nu)[\frac{K}{1+\nu}(\frac{\nu}{1-2\nu}+\frac{1}{3})^n]^\mu \rho^{\mu n}\gamma^{\mu m} \quad (4\text{-}3)$$

Where ν represents Poisson's ratio;$\mu = \frac{1}{1-n-m}$; ρ represents the bulk strain or sum of principal strains = $|\varepsilon_1+\varepsilon_2+\varepsilon_3|$; γ represents octahedral shear strain $= \sqrt{\frac{1}{3}[(\varepsilon_1-\varepsilon_2)^2+(\varepsilon_2-\varepsilon_3)^2+(\varepsilon_3-\varepsilon_1)^2]}$; and K, n, and m represent the material constants.

This equation is evolved from the original *k-θ* model and Uzan's model [61]. But it outperforms the previous models due to its advantages, such as 1) the process of incremental response in materials is included; 2) the shear-stress component is considered; 3) the dilation effect is considered; 4) it is easier to converge when the loads are too large.

4.2.3.2 Finite-element model generation and details

There are usually four methods to simulate the pavement under the FWD loading. The first one is a 2-Dimensional modeling method, mostly used in the early stages of pavement simulation. This method is more straightforward when compared with other methods, but the dimensional effect is not considered. The second method is the 3-Dimensional approach to model the pavement section, which can fully present the three directional structural conditions of the pavement structures. To reduce the analysis time, the axisymmetric (3rd method) and quarter-cube (4th method) methods are used to model the pavement structure. Accordingly, this study used a quarter cube 3-D FE model to simulate the FWD testing on the inverted pavement.

4.2.3.3 Geometry of the pavement structures

The GPR test confirmed the pavement layer thicknesses of both pavements as mentioned previously. The thickness of SG for both the conventional and the inverted pavement sections was selected as 1,585 mm and the rigid boundary at the bottom does not influence the simulation results. For the dimension of the model, a geometrical model size of 4 m × 4 m × 4 m cube quarter was created to simulate the pavement structure initially. However, the model's larger size resulted in a longer computing time and produced convergence problems [54]. Thus, the model dimensions were reduced until no boundary effect occurred. A 2m × 2m × 1m cuboid was modeled for both the inverted and the conventional pavement sections based on the dimensions of the actual pavement sections and adjustment results.

4.2.3.4 Mesh, loads and boundary conditions

A proper mesh can contribute to the accuracy of the simulation results and the computational time. The C3D8 type element (8-node linear brick element) was selected in this study to minimize the calculation time and improve accuracy. A finer mesh configuration was set for the upper layers and loading area at the AC surface. A finer mesh modeled the central zone of interest (loading zone) to improve the model efficiency. The dynamic load was applied in this study to

accurately predict the dynamic response of pavement under the FWD load. The actual amplitude pattern of the impulse load with a magnitude of 40 kN (9 kips) was applied on the circle loading plate with an area of $\pi D^2/4$, (D = 300 mm). Proper boundary constraints also improve the accuracy of the simulation. In this study, the bottom of the SG was constrained, and all types of movements were constrained (ENCASTRE). The roller support simulated the inside vertical surfaces, and the outside surfaces were modeled as free of movements. The interface between two adjacent layers is assumed to be fully bonded so that no slip occurs.

4.2.3.5 Layer properties

The layer properties are crucial to the accuracy of the simulation. Material properties of the different layers in inverted and conventional pavements are discussed below. Based on the back-calculation results of each layer and comparison with the field investigation, the modulus and other properties were determined in the numerical analysis. The asphalt material is usually regarded as a viscoelastic material during very high temperatures and at loads with slow rates. However, the FWD load is instantaneous and the strain is recoverable when the load disappears [56]. Also, this test was conducted at an intermediate temperature for the pavement. AC layer in inverted and conventional pavement sections was assumed as linear elastic with Young's modulus of 10,000 MPa and a Poisson's ratio of 0.35. For the unbound aggregate layer in the inverted pavement, the stress-dependent property was considered in this study. The nonlinear resilient modulus of the unbound aggregate materials was programmed in user-defined material subroutine (UMAT) of the ABAQUS software. The initial modulus for UAB was set as 100 MPa, and it was changed with the iteration calculation in the routine. Its Poisson's ratio was 0.35. For the CTB layer, it was also considered as linear elastic material with Young's modulus of 7,000 MPa and a Poisson's ratio of 0.25. For the subgrade at the bottom, it was considered to have the linear elastic property and it had Young's modulus of 150 MPa and a Poisson's ratio of 0.45. As for the conventional section, the AC, UAB and SG had the same properties as those of the inverted pavement section to provide a more reasonable comparison. The thickness of the pavement layers was based on the GPR assessment in the previous section.

4.2.3.6 Validation of the numerical model

In order to verify the reliability of the aforementioned model, the FWD data from the field investigation was compared with the results from the finite element simulation results done by ABAQUS software. As shown in **Figure 4-23** (a) & (b), the surface deflections in the AC layer of the inverted and conventional pavement sections are presented. For the inverted pavement section, it can be found that the maximum deflection at loading point D_0 is 0.1574 mm, which is 13.28% smaller than the simulation value of 0.1815 mm. For the conventional pavement section, the maximum deflection D_0 was 0.1488 mm, 0.2% larger than the prediction of 0.1485 mm. This indicates that the simulation model reasonably predicted the maximum deflections for both conventional and inverted pavement sections. Based on the comparison of the results in **Figure 4-23**, the error (%) between the prediction and field data for the inverted pavement section is within 14% and within 5% for the conventional pavement section. The simulation results are consistent with the field data for the conventional section when the radial distance ranges from 0.30 to 1.00 m, which shows a good correlation with the model. When the radial distance is larger than 0.20 m in the inverted section and larger than 1.00 m in the conventional section, the simulation results are larger than the FWD data. The error was within the error margin of 15% in

GTPAVE [39]. Therefore, it could be concluded that the simulation model used in this study was both satisfactory and robust to predict the response of the inverted and conventional pavements.

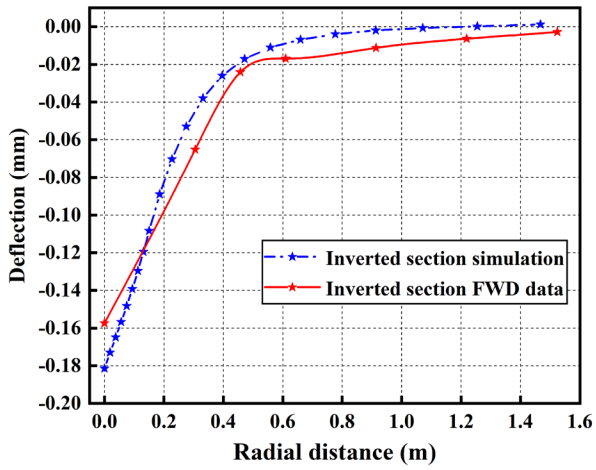

(a)

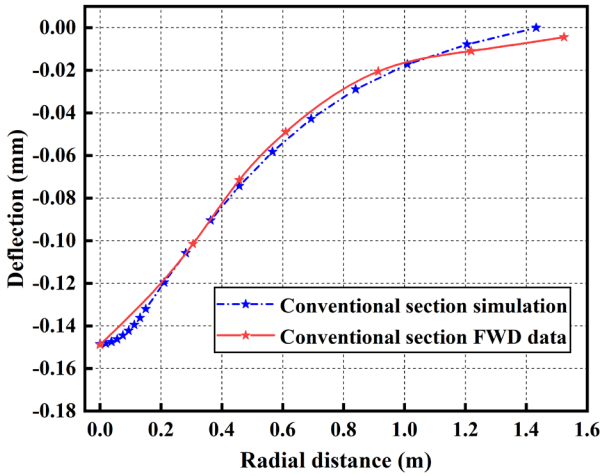

(b)

Figure 4-22. Comparison between the FE simulation and field data in (a) inverted and (b) conventional pavement sections.

4.2.3.7 Comparison of stress distribution between inverted and conventional pavements

The horizontal stress (S11) distribution is of great importance to pavement structures. Thus, the horizontal stress distribution between inverted and conventional pavements contributes to a better understanding of the inverted pavement structure. As shown in **Figure 4-24**, the stress distribution in the AC layer of inverted pavement was different from that of the conventional one. In the conventional pavement section, the stress changed from compression at the AC surface to tension at the bottom of the AC layer. On the contrary, only little tension stress due to the thin AC layer occurred at the AC surface in the inverted pavement section. Following the increase of depth, the stress changed into compressive stress at the middle of the AC and tensile stress at

the bottom of the AC. The tension at the bottom of the AC would initiate the bottom-up cracks and then impair the performance of the pavement surface. However, the tensile stress is 501.13 kPa at the bottom of the AC in the inverted pavement section, which is only 40.17% of that in the conventional pavement section. This indicated that the inverted structure had better performance based on evaluating stress distribution in the AC layer. The lower tension at the bottom of the AC layer was due to the relieving function of UAB. In addition, the thin thickness of AC was also the reason for the lower tensile stress. The horizontal stress in the UAB is compressive in the whole UAB layer and is larger than that in the conventional pavement section. However, the stress at the bottom of CTB is tensile. The change of the stress stage from compression at the surface of CTB to tension at the bottom of CTB is due to CTB acting like a kind of bound material in the inverted pavement. Furthermore, the stress change from CTB to AC showed that the inverted pavement structure could reduce the reflective cracks effectively, which was also confirmed by the crack results from the 3D road profiling test. The SG was little affected by the FWD load based on the simulation results. Whether the tension state would influence the SG will be discussed in the following part.

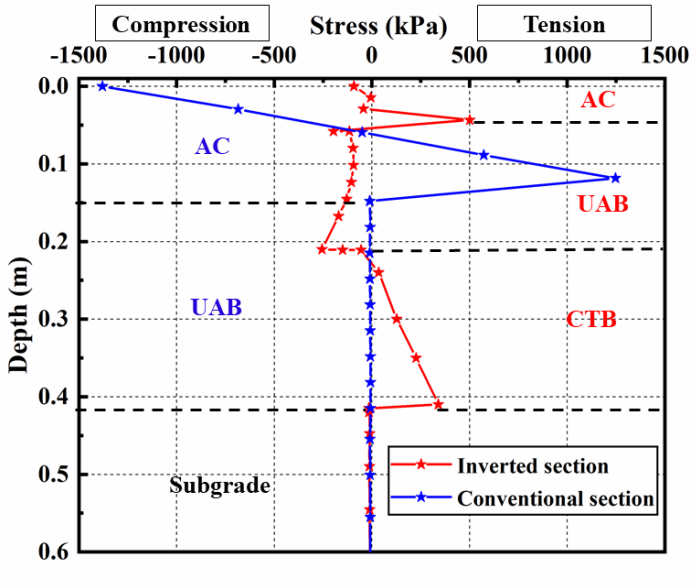

Figure 4-23. Comparison of horizontal stress (S11) distribution between inverted and conventional pavements

The calculated deflection at the surface of SG was presented in **Figure 4-25** and it can be found that the deflection of the SG surface in the inverted pavement section was smaller than that in the conventional pavement section. The deflection at the loading point in the inverted pavement section is 5.79×10^{-5} mm, which is 7.80% smaller than the 6.28×10^{-5} mm in the conventional pavement section. The deflection decreased with the radial distance and the gap between the inverted and conventional pavement sections increased first and decreased at last. The comparison shown in **Figure 4-25** reflects that the tension at the bottom of CTB did not affect SG. The inverted pavement had a lower deflection in SG, which contributed to the longevity of pavement structures. The better performance of SG in the inverted pavement section is also consistent with the smaller W_7 value in FWD data.

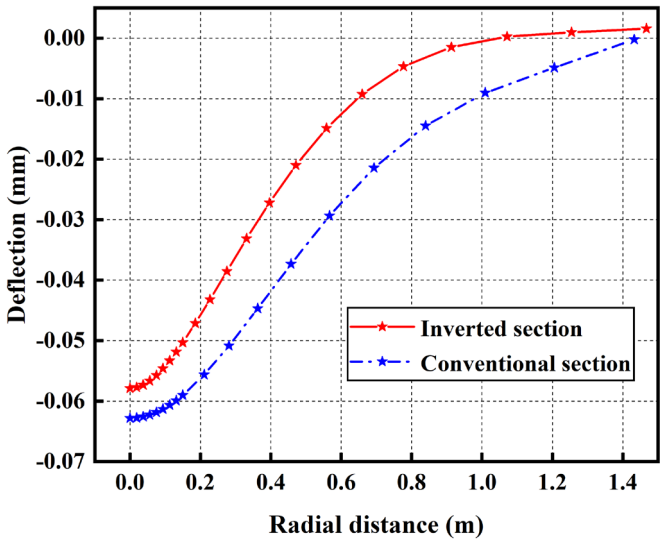

Figure 4-24. Calculated deflection of SG surface in inverted and conventional pavements

Figure 4-26 shows the comparison of vertical stress (S33) distribution between inverted and conventional pavements. It can be found that the vertical stress in the inverted pavement is larger than that of conventional pavement. To investigate the stress-dependent property of the UAB, the vertical stress in the UAB should be focused on. The vertical stress in the UAB of inverted pavement is much larger than that of the conventional pavement due to the support and constraint by the CTB. The maximum stress at the top of the UAB in inverted pavement section is 647.08 kPa, 13.52 times of 47.87 kPa in conventional pavement section. The minimum stress at the bottom of the UAB in inverted section is 286.96 kPa, which is 8.90 times of 32.23 kPa in the conventional pavement section. Larger vertical stress and support from the CTB led to a stiffer reaction in the UAB. Thus, the stiffness distribution is discussed in the following section.

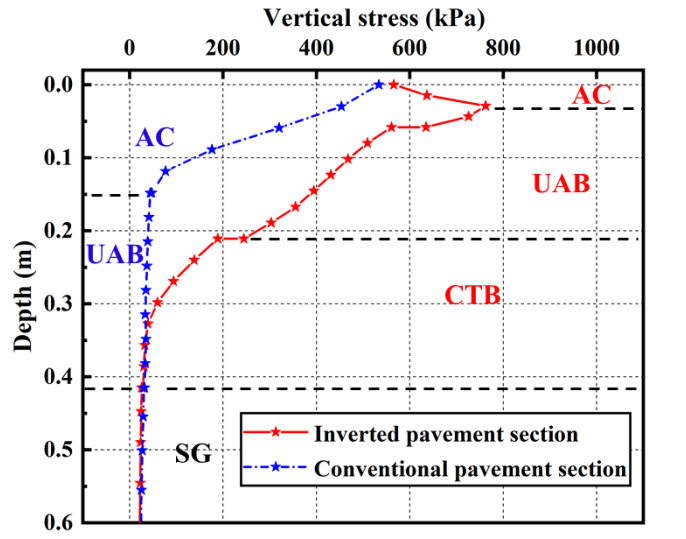

Figure 4-25. Comparison of vertical stress (S33) distribution between inverted and conventional pavements

Figure 4-27 shows the stiffness distribution in the UAB of inverted pavement. The aforementioned constitutive model computed the stiffness of the UAB. Based on the results, it can be found that the stiffness changes with the state of stress due to stress-dependent characteristic. And a higher stiffness occurred at the zone with a higher stress state and the stiffness decreased with increasing the distance from the loading point. The maximum stiffness of 597 MPa under the FWD load decreased to 108 MPa at the middle of the geometrical model. This stiff reaction is attributed to the much stiffer CTB, which created an effective base to promote the stiffness increase in the UAB. However, such a stiff reaction was not found in the conventional pavement model. Therefore, the stress-dependent property of the UAB is a key for inverted pavement structure to have a better performance compared to the conventional pavement.

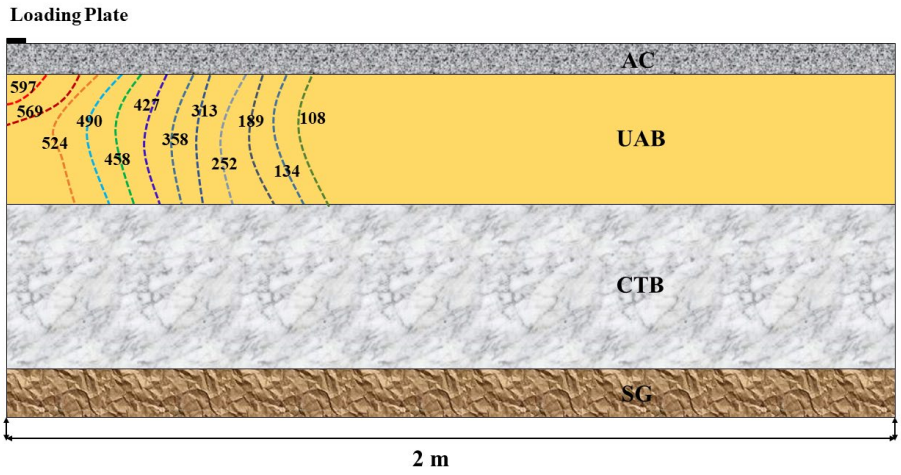

Figure 4-26. Stiffness distribution contours in the UAB of inverted pavement section (Unit: MPa)

4.2.4 Preliminary cost analysis

4.2.4.1 Pavement life prediction

Based on the average rutting depth of Vulcan testing pavements in **Table 4-3**, the pavement's service life can be predicted. The average rutting of the inverted pavement and conventional pavement in Vulcan is 1.32 mm and 2.16 mm, respectively. FHWA defines that pavement with rut depth larger than 10.2 mm (0.4 inch) is in poor condition. Therefore, 10.2 mm of rutting depth was considered the failure criteria in this study, as shown in **Figure 4-28**. When the testing pavement reached the AASHTOWare failure criteria, the predicted service year of inverted pavement and conventional pavement is about 11 years and 7 years, respectively.

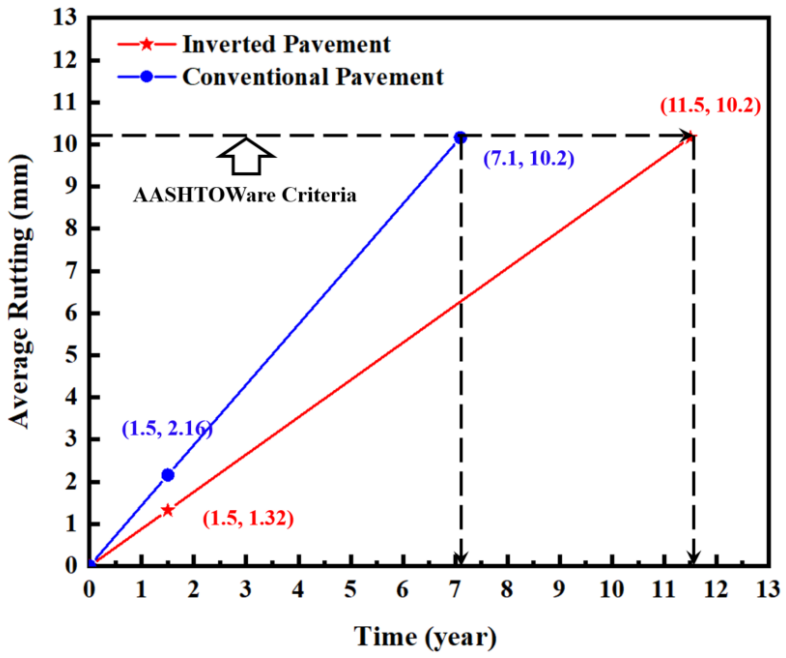

Figure 4-27. Pavement life prediction

4.2.4.2 Cost analysis

The Estimated Uniform Annual Cost (EUAC) method expresses life cycle costs as an annualized estimation of cash flow. The EUAC values of testing pavements could be calculated using the following equation:

$$EUAC = Cost \times \frac{i(1+i)^n}{(1+i)^n - 1} \quad (4\text{-}4)$$

where i is discount rate (%), and n = service life (year).

Unlike standard life cycle cost analysis, the EUAC method expresses life cycle costs as an annualized estimate of cash flow instead of a lump-sum estimate of present value. Because life cycle costs are calculated as an annualized amount, this method can be used to compare the economic value of different alternatives with different service lives. The discount rate i of 4% is applied according to the FHWA recommendation in this study.

In the calculation, the price of the materials was based on the local estimation. Based on the calculation results, the unit (per inch thickness) price of the AC layer is 18,562 dollars per lane mile. The unit (per inch thickness) price of UAB layer is 10,654 dollars per lane mile and the unit (per inch thickness) price of the CTB layer is 11,439 dollars per lane mile. The calculation is presented in **Table 4-6**. Therefore, the initial cost of the inverted and conventional pavements and corresponding EUAC were calculated in **Table 4-7**. This study just takes one life cycle into consideration and the future cost will take place every seven years for the conventional pavement and every eleven years for the inverted pavement. The value of EUAC can be used as the indicator of the economical comparison study between the inverted and conventional pavements. Based on the cost analysis results, it can be found that the EUAC for the inverted and conventional pavements is 22,510 dollars and 34,101 dollars, respectively. Therefore, the inverted pavement is more cost-effective than the conventional pavement.

Table 4-6 Layer cost of testing pavement

Layer	Materials	Weight (%)	Unit price $/kg	Price $ / lane mile	Total cost $ / lane mile
AC layer (per inch)	D rock	47.2 %	0.03	5369.8	18,562
	#10 rock	9.4 %	0.03	1074.0	
	Natural sand	23.4 %	0.01	831.4	
	RAP	15.0 %	0.02	852.3	
	Asphalt	5.0 %	0.56	10434.0	
UAB layer (per inch)	Aggregate	100.0 %	0.03	10653.8	10,654
CTB layer (per inch)	Cement	4.0 %	0.12	1634.2	11,439
	Aggregate	96.0 %	0.03	9805.1	

Table 4-7 Cost analysis of testing pavements

Pavements	AC	UAB	CTB	Total cost (dollar/lane mile)	EUAC
Inverted pavement thickness (inch)	2.25	6	8	197,201	22,510
Layer cost	41,765	63,924	91,512		
Conventional pavement thickness (inch)	5	10.5	0	204,677	34,101
Layer cost	92,810	111,867	0		

4.3 Evaluation of Inverted Pavement by Structural Condition Indicators from FWD

Horak et al. [35] proposed a detailed evaluation system that contained corresponding threshold values based on the DBPs in South Africa, as shown in **Table 4-6**. D_0 presents the maximum deflection at the loading point. Chang et al. [52] also proposed the structural condition indices in Texas, USA, based on FWD data and layer thickness to diagnose possible distressed layer, as shown in **Table 4-7**. The threshold values presented in **Tables 4-6** and **4-7** were based on a load of 40 kN or a contact pressure of 560 kPa by the FWD testing method. The difference between the two systems is the evaluation level. The assessment system in South Africa has three-level results in each parameter, and the system in the USA contains four evaluation results in each parameter. Also, these two systems were applied to only conventional pavement structures. This study applied both South African and USA evaluation systems to the inverted pavement system.

To properly use the FWD-based evaluation method, the temperature is of great importance because the AC layer is susceptible to the change of temperature [58,59]. Thus, the temperature correction of the FWD data is required before evaluating the pavement condition. In Tables 2 & 3, the pavement structural condition indices have been corrected to a reference temperature of

20 ℃ (68°F). The reason why 20℃ (68°F) is chosen is that this temperature is the standard reference temperature used in AASHTO 1993 Design Guide (AASHTO, 1993).

Table 4-8 Threshold values for 40 kN contact stress on a granular base pavement

Evaluation Results	***D_0***	***BLI***	***MLI***	***LLI***
Sound	＜500	＜200	＜100	＜50
Warning	500 – 750	200 - 400	100 - 200	50 – 100
Severe	＞750	＞400	＞200	＞100

Table 4-9 Structural condition indices for assessment of distressed layer

Index Parameters	***Asphalt Thickness (cm)* 2.54 – 6.35**	***Asphalt Thickness (cm)* 6.35 – 12.7**	***Evaluation Results***
SCI	＜30.48	＜15.24	Very Good AC
	30.48 – 45.72	15.24 – 25.4	Good AC
	48.72 – 60.96	25.4 – 38.1	Fair AC
	60.96 – 76.2	38.1 – 50.8	Poor AC
	＞ 76.2	＞50.8	Very Poor
BCI	＜10.16	＜7.62	Very Good base layer
	10.16 – 20.32	7.62 – 12.7	Good base layer
	20.32 – 30.48	12.7 – 20.32	Fair base layer
	30.48 – 40.64	20.32 – 25.4	Poor base layer
	＞40.64	＞25.4	Very Poor base layer
W_7	＜2.54		Very Good SG
	2.54 – 3.56		Good SG
	3.56 – 4.57		Fair SG
	4.57 – 5.59		Poor SG
	＞5.59		Very Poor SG

4.3.1 Simulation of FWD testing on inverted pavement

The feasibility of the DBP evaluation system on the inverted pavement was validated after the corresponding threshold values. The validation included the calculation of the DBPs for the pavement with different layer properties and evaluated the corresponding pavement section based on the evaluation parameters. To accomplish this, the relationship between the DBPs and pavement individual modulus must be established, which is able to provide a method to validate the suitability of the literature proposed DBPs threshold values in an inverted pavement system. The finite element method (FEM) through ABAQUS software was used in this study to simulate the surface deflection of inverted pavement under FWD impulse loading.

The dimensional model and materials properties are based on the typical inverted pavement in Morgan County [62]. This inverted pavement is a haul road for the Morgan County quarry (tested in September 2013). It contains four primary layers: a 75 mm AC as the surface, a 150 mm UAB as the base, a 200 mm CTB as a subbase and a subgrade soil layer [63]. Previous studies [55,56] used linear-elastic models to simulate FWD testing on the conventional flexible pavement. The

model limitations did not reflect the actual structural response of the pavement. In this study, the nonlinear stress-dependent property of UAB was considered by using the UMAT (user-defined material subroutine) input file in ABAQUS during the simulation analysis.

4.3.1.1 Development of FEM model

A quarter of the cube model was used to save time and storage capacity for a three-dimensional (3D) simulation [56,64]. To reduce the effect of boundary conditions on the simulation results, the domain size is supposed to be larger than 12-20 times the radius of the loading area in the horizontal direction and larger than 50 times the radius of the loading area in the vertical area [65,66]. For an optimum model geometry in this study, the final dimensions of the pavement model were selected to be 3000 mm in length, 3000 mm in width, and 6000 mm in depth.

4.3.1.2 Layer properties

The model in this study consists of four layers as mentioned before. The surface layer is the asphalt concrete layer (AC). The base layers contain the unbound aggregate layer (UAB) and the cement-treated base (CTB). The bottom layer is the natural soil subgrade (SG). The material properties of AC, CTB and SG for the 3D model are presented in **Table 4-8**. Due to the stress-dependent property of UAB, the user-defined material subroutine (UMAT) code was put into ABAQUS to simulate the stiffness change of aggregates by iteration. In addition, the initial modulus of UAB was set as 100 MPa since the initial stiffness had little effect on the final stress status of UAB during the calculation. The calculation process will be finished when the final iteration result of stiffness is equal to the last iteration.

Table 4-10 Material properties for the numerical study

Layer	**Thickness** (mm)	**Max. Dry Density** (kg/m^3)	**Poisson's Ratio**
AC	75	2400	0.35
UAB	1500	2193	0.35
CTB	200	2200	0.30
SG	infinite	1800	0.45

As for the properties of UAB, the details are based on the field data from Terrell et al. [63] and Papadopoulos et al. [62]. **Table 4-9** shows the properties of the unbound aggregate base from the Morgan County inverted pavement.

Table 4-11 Index properties for UAB tested in Morgan County inverted pavement

Indexes	**Values**
Maximum dry density (km/m^3)	2193
Optimum water content	6.7%
Mean grain size D50 (mm)	6.5
D_{10} (mm)	0.1
Uniformity coefficient C_u	100
Liquid limit	Non-plastic
Fines content	7%
Plastic limit	Non-plastic
USCS class	GP-GW

4.3.1.3 Boundary, loading condition, mesh and constitutive model

In the numerical model, interfaces between two adjacent layers are fully bonded, and slip is not considered to simplify the calculation process. Roller supports are assigned at the lateral faces of the model, which allows the vertical movement but constrains the horizontal direction. The bottom of the model is assigned with hinge supports, restraining its translation movement in all directions. The actual amplitude pattern was applied to simulate the structural response of the pavement under the impulse (dynamic) loading system by FWD. **Figure 4-28** shows the real-time load history collected from the FWD test, and its interval is 0.60 s. The impulse with a magnitude of 40 kN (9 kips) was utilized. A pressure of 560 kPa integrated with a field time-amplitude variation was applied on a circular area with a radius of 150 mm to match the load-time history in the field test. Mesh refinement is another key to make the simulation accurate and improve the calculation efficiency. In this model, the finer mesh was applied in the loading area. **Figure 4-29** shows the qualitative diagram of the pavement model and boundary conditions.

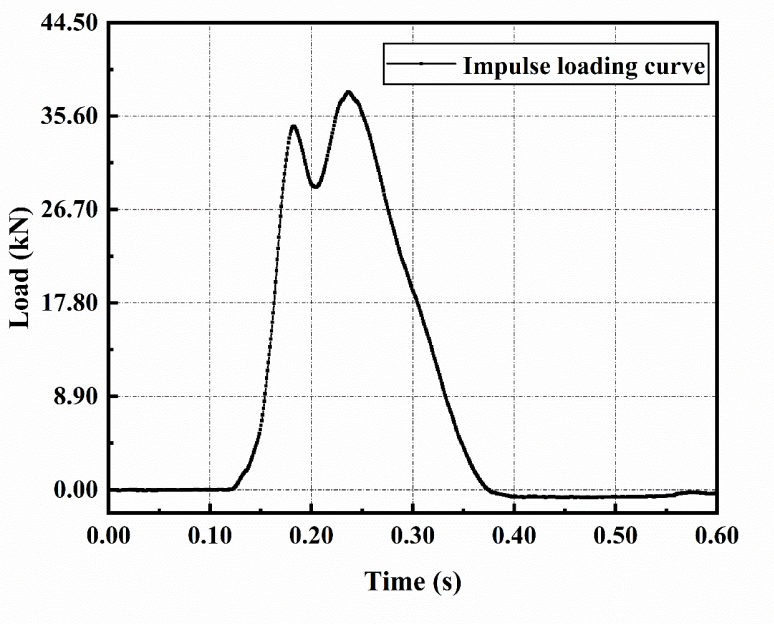

Figure 4-28. Amplitude pattern of the impulse in the FWD test

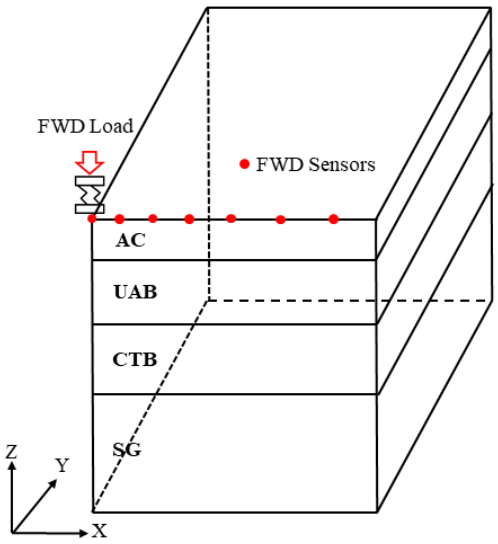

(a) 3D geometry of inverted pavement model

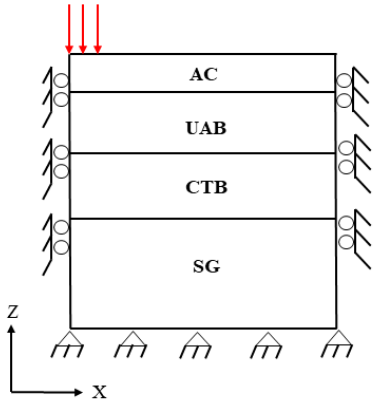

(b) X-Z plane

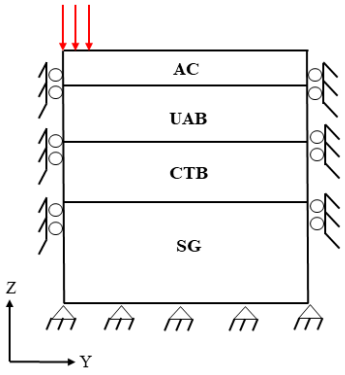

(c) X-Y plane

Figure 4-29. Qualitative diagram of the pavement model.

For the constitutive model to simulate the nonlinear stress-dependent property of UAB, the authors followed their previous publication [53]. The equation (4) in this study was utilized in the user-defined material subroutine (UMAT) codes. The codes were put into ABAQUS to conduct the repeated iteration process until the new modulus of UAB was equal to the last result in the software.

4.3.1.4 Determination of material elastic modulus and model verification

To verify the feasibility of the evaluation system, a range of possible elastic modulus were assigned to the AC layer, CTB layer and SG soil. The detailed elastic modulus for pavement layers was based on the research conducted by Rabbi and Mishra [54]. The maximum limit of the layer modulus represents a well-performing condition for this pavement layer, and the minimum limit indicates a poor condition for this pavement layer. Five different modulus values were assigned to AC, CTB, and SG to present a more comprehensive assessment of the inverted pavement. The

detailed modulus information is shown in **Table 4-10**. The third combination pavement type is considered as the benchmark (control case) for comparative study.

Table 4-12 Layer modulus variation

Combination Pavement Type	***AC (MPa)***	***CTB (MPa)***	***SG (MPa)***
1	4000	4000	100
2	3500	3400	80
3 (Control case)	3000	2800	60
4	2500	2200	40
5	2000	1600	20

For the UAB layer, the resilient modulus is changeable and the initial modulus of the UAB layer has little impact on the final pavement structural response. Thus, its modulus is fixed at 100 MPa for each assessment group. Considering the total 5×5×5=125 results of the pavement structural response, the pavement sections under FWD loading conditions are simulated. **Figure 4-30** shows the range of AC surface deflection of pavements with different layer modulus under FWD loads. The blue line presents the maximum deflection (493 μm) at the surface of the asphalt concrete layer when each layer has the lowest modulus in **Table 4-10**. And the red line presents the minimum deflection (298 μm) when each layer has the largest modulus. The surface deflections with all layer modulus combinations are between the red and blue solid lines.

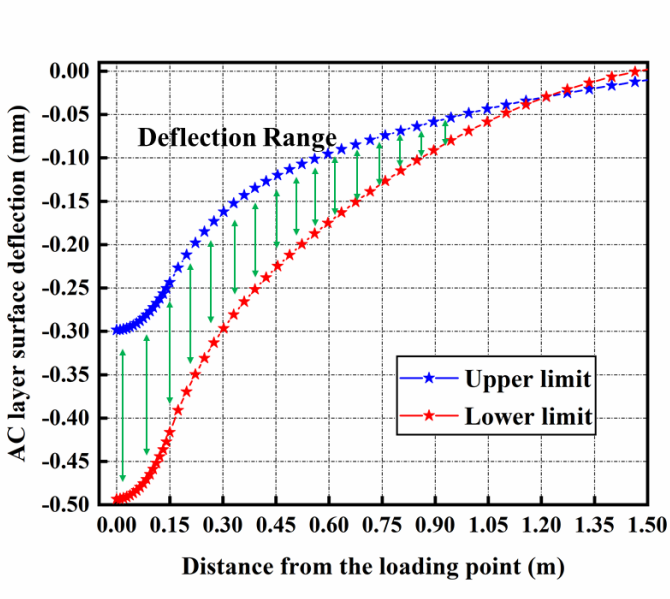

Figure 4-30. Range of AC surface deflection under FWD loads

To verify the constitutive model behind the ABAQUS calculation, the GTPAVE model was used to validate the model in this study [44]. The UMAT subroutine was utilized in the FEM software to present the nonlinear stress-dependent property of unbound aggregate materials. The predicted

vertical stress at the top of the SG layer was only 4.41% higher than the field data. The maximum deflection at the load center was 12.67% higher than the field measured data. As the error % between the prediction and field data is within 15%, the numerical model in this study can be validated based on the comparison results.

4.3.2 Investigation of DBPs evaluation system

After verifying the numerical simulation model, the feasibility of using the DBPs' system as indicators for individual layer condition of inverted pavement was investigated. DBP values are calculated for each layer of the inverted pavement with different moduli shown in **Table 4-10**. When the target layer is analyzed, the modulus of other layers keeps the same as the values in the control case. Thus, the modulus for the AC layer, CTB layer and SG was varied separately to investigate the influence of each layer on the DBPs' evaluation system of inverted pavement.

For the effect of the AC layer on DBPs, **Table 4-11** shows the evaluation groups. The elastic modulus of the AC layer decreased from 4000 MPa to 2000 MPa. The modulus of other layers was the same as the control group. **Figure 4-31** presents the influence of AC layer modulus variations on the DPBs values of the inverted pavement. Based on the results shown in **Figure 4-31**, it could be observed that the maximum deflection for each group occurred at the FWD loading point (0.00 mm), and the deflection decreased with the distance from the loading point. Meanwhile, the AC layer modulus significantly impacted the deflection curve, and the affected area was located at 0.00 m to 0.20 m from the loading point. Group five has the maximum surface deflection of 378 μm. And group one had the lowest surface deflection of 352 μm due to the highest AC layer stiffness, which was 6.9% less than group five. **Figure 4-32** shows the change of DBP values with the AC layer modulus. Based on the results, it can be found that the SCI values decreased with the increasing modulus of the AC layer. The minimum SCI value of 147 μm occurred when the AC layer had the maximum modulus. And the maximum SCI value of 172 μm was found in the AC layer with the minimum modulus. The negative correlation between the SCI value and AC layer stiffness validates the SCI value function to evaluate the surface layer condition. A smaller SCI value represents a better condition of the surface layer (AC). The BDI value increased a little from 82 μm to 84 μm (2.4%) with the increase of AC layer modulus. The BCI value kept constant at around 52 μm. Thus, the results indicate that the condition of the AC layer has little influence on the BDI and BCI values of the inverted pavement. In addition, BCI and BDI values are not able to reflect the condition of the surface layer of inverted pavement. The W_7 value also has a positive relationship with the stiffness of the AC layer. But the change is from 5.8 μm to 6.8 μm, which could not establish the relationship between W_7 and AC stiffness.

Table 4-13 Evaluation groups of AC layer

Group number	AC modulus (MPa)	CTB modulus (MPa)	SG modulus (MPa)
1	4000	2800	60
2	3500	2800	60
3	3000	2800	60
4	2500	2800	60
5	2000	2800	60

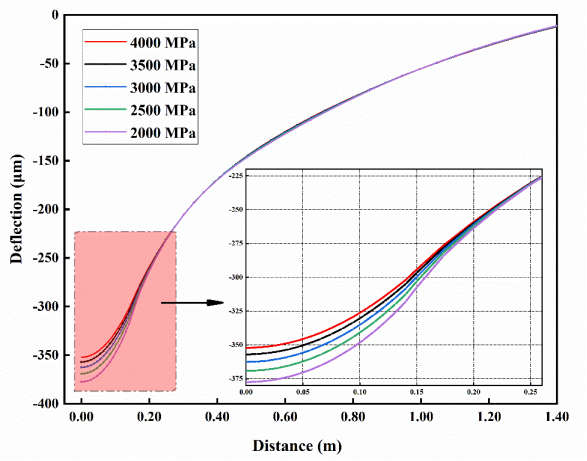

Figure 4-31. Change of surface deflection with the AC layer modulus (Made in OriginPro)

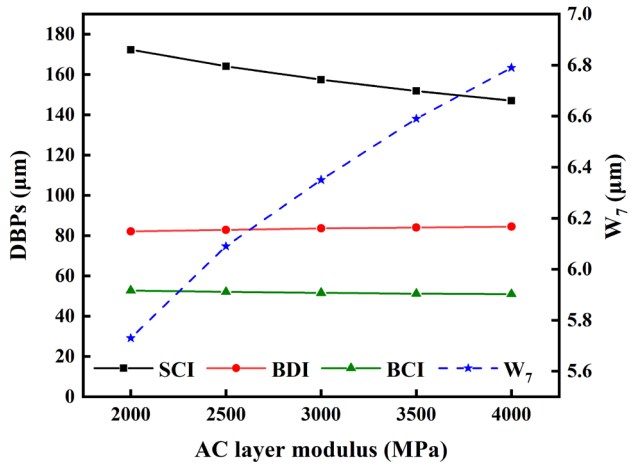

Figure 4-32. Change of DBP values with the AC layer modulus

For the effect of the CTB layer condition on the DBP system, **Table 4-12** shows the evaluation groups to investigate the influence of CTB stiffness on the DBPs values. The modulus of the CTB layer changed from 4000 MPa to 1600 MPa and other layers' stiffness keeps the same as that of the control group. **Figure 4-33** shows the change of surface deflection with CTB layer modulus. Based on the results in the deflection curve, it can be found that the affected area was located at 0.00 m to 1.00 m from the loading point, which was much larger than that in **Figure 4-31**. The maximum deflection for each group also occurred at the loading point. Group five had the maximum surface deflection of 402 μm, and group one had the minimum surface deflection of 339 μm, which indicated that the surface deflection also negatively correlated with the CTB layer stiffness. **Figure 4-34** shows the change of DBP values with the CTB layer modulus. Based on **Figure 4-34**, the SCI values decreased with the increasing CTB layer stiffness from 172 μm to 150 μm (12.8 %). The BDI value decreased from 100 μm to 74 μm (26.0%) with the modulus increase in the CTB layer. BCI value decreased from 59 μm to 47 μm (20.3%). The change of DBP values indicates that the BDI can fully reflect the condition of the interlayer or lower layer in the inverted pavement. Also, the BCI is suitable for evaluating the interlayer in the inverted pavement to a

certain extent. The SCI value cannot assess the interlayer condition well in the inverted pavement compared with BDI and BCI. For the W_7 value, it increased with the increasing modulus of the CTB layer from 0.34 μm to 10.4 μm, which had a much drastic change compared with that in **Figure 4-32**. This phenomenon indicates that the W_7 value is much more sensitive to stiffness of the CTB, and the stiffer CTB layer leads to a larger supporting area for the load, which results in a lower maximum deflection.

Table 4-14 Evaluation groups of CTB layer

Group number	AC modulus (MPa)	CTB modulus (MPa)	SG modulus (MPa)
1	3000	4000	60
2	3000	3400	60
3	3000	2800	60
4	3000	2200	60
5	3000	1600	60

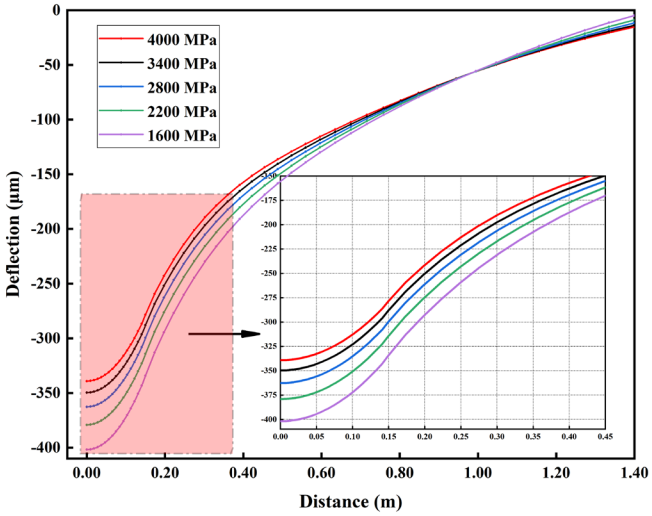

Figure 4-33. Change of surface deflection with the CTB layer modulus (Made in OriginPro)

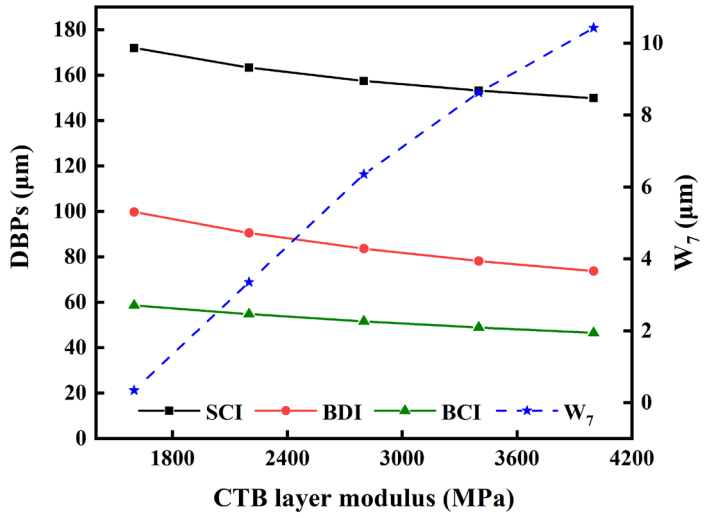

Figure 4-34. Change of DBP values with the CTB layer modulus

For the SG layer, **Table 4-13** shows the evaluation groups to investigate the effect of the SG layer on the DPBs system. The SG modulus changed from 50 MPa to 150 MPa. As shown in **Figure 4-35**, the surface deflection curve for each group is displayed. It can be found that the maximum deflection at the loading point of each group decreased with the increasing modulus of the SG layer from 436 μm for group five to 334 μm (23.4 %) for group one. Based on **Figure 4-35**, the affected area was located at a distance from 0.00 m to 1.40 m, which was larger than the AC and CTB affected areas. The most significant gaps among these curves occurred at the loading point and the distance of 0.50 m, which was also different from the AC or CTB affected deflection curves. **Figure 4-36** shows the change of DBP values with the SG layer modulus. The SCI value decreased a little from 168 μm to 156 μm (7.1 %). The BDI value decreased from 105 μm to 76 μm (27.6 %), which meant that BDI could reflect the base layer condition to a certain extent. The BCI value had the most significant reduction, from 72 μm to 42 μm (41.2 %), which indicated that BDI was able to evaluate the base layer condition well in the inverted pavement structure. The W_7 value decreased with the modulus of SG at first and then increased with SG modulus. The change that the W_7 decreased from 8.5 μm at 20 MPa to 3.7 μm at 40 MPa (56.5%) and increased to 8.4 μm at 100 MPa might be due to the optimum layers' combination of inverted structures among five groups.

Table 4-15 Evaluation groups of CTB layer

Group number	*AC modulus (MPa)*	*CTB modulus (MPa)*	*SG modulus (MPa)*
1	3000	2400	100
2	3000	2400	80
3	3000	2400	60
4	3000	2400	40
5	3000	2400	20

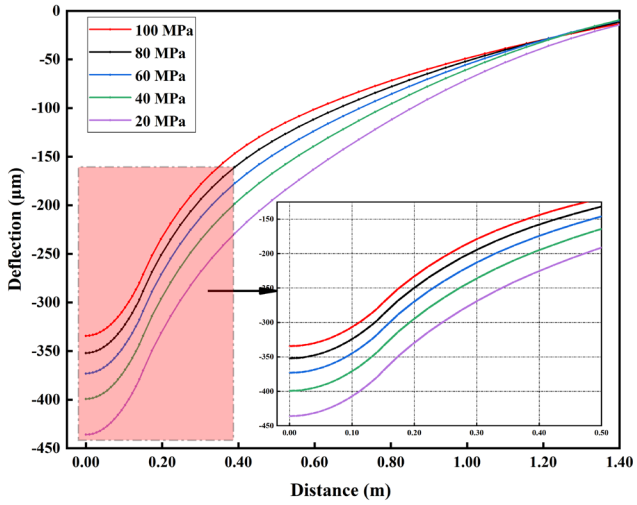

Figure 4-35. Change of surface deflection with the SG layer modulus (Made in OriginPro)

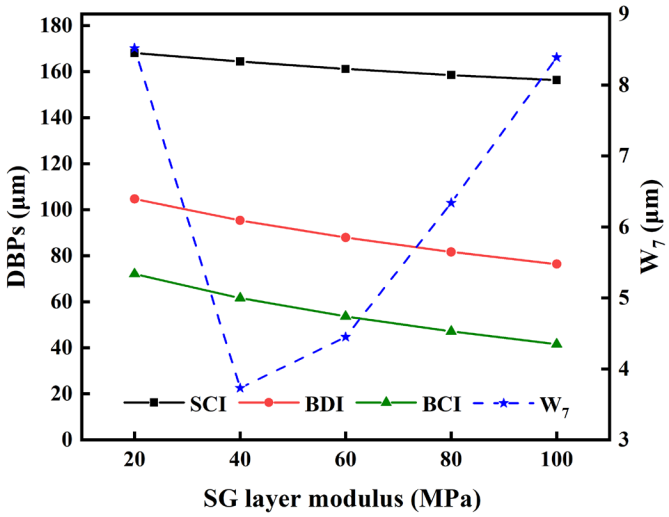

Figure 4-36. Change of DBPs values with the SG layer modulus

Based on the analysis results in this section, it can be found that the SCI value was governed by the surface layer (AC layer) stiffness and could reflect the condition of the surface layer. Rabbi and Mishra [54] thought that the SCI value was unsuitable for surface layer condition indicators because it could be influenced by other interlayers and the deflection in subgrade resulted in most surface deflection. However, they just used the elastic model for each layer, which could not reflect the realistic structural response of the inverted pavement. In this study, the nonlinear stress-dependent property was applied to the UAB material, which could reflect the actual layer condition. As for the BDI, it was little affected by the surface layer and changed a lot with the interlayer modulus, which indicated that the BDI value had the ability to evaluate the condition of interlayers or lower layer such as CTB in the inverted pavement system. As for the BCI value, it could be affected a lot when the modulus of the SG layer changed, which indicated that the BCI could be the indicator of the condition of the SG layer. For the W_7 value, it changed with the

modulus of each layer and the tendency was affected by the inverted pavement structures of different thicknesses. Thus, the W_7 value can only be used as a rough evaluation reference rather than a reliable parameter. In **Figure 4-30**, the SCI, BDI and BCI value for the best combination (blue line) is 136 μm, 67 μm and 37 μm, respectively. The DBPs for the worst combination (red line) are 197 μm, 109 μm and 84 μm. According to the South African evaluation system shown in **Table 4-6**, the worst-case belongs to sound condition, which is unreasonable. In contrast, the US evaluation system shown in **Table 4-7** can assess the extreme cases well, and it can also evaluate the inverted pavement structures with different layer conditions.

4.3.3 Field investigation and assessment using DBPs system

After figuring out the effect of individual layers on the DBP evaluation method in the inverted pavement system, the field investigation is supposed to be conducted to explore its practical value in the pavement industry. Thus, the pavement condition assessment based on the deflection basin parameters was applied to the field project, which could validate the adequacy of DBPs as structural conditions of the inverted pavement.

The inverted pavement studied in this study is located in Knoxville, TN. Its construction started in November 2018 and was completed in April 2019. This inverted pavement contains an AC layer, UAB layer, CTB layer and SG layer. The thickness of each layer is 63 mm, 153 mm, 204 mm for AC, UAB and CTB, respectively. In order to evaluate the pavement quickly, the FWD test was conducted one-and-a-half-years after traffic opened. The test time was in October and the testing temperature was about 20 ℃ (68°F). Thus, the temperature correction process was omitted. In this test, a 40 kN (9kips) load mode was applied, and the deflections were recorded by sensors at radial distances of 0 mm, 305 mm, 457 mm, 610 mm, 914 mm, 1219 mm and 1524 mm (W_7) from the center of loading plate. Twelve points with a 20-m interval were measured at both the left and right lanes of the inverted pavement. The final deflection data was based on the arithmetic mean of all the testing data, giving an overall assessment of this inverted pavement. **Figure 4-37** presents the FWD deflection basin of the testing inverted pavement.

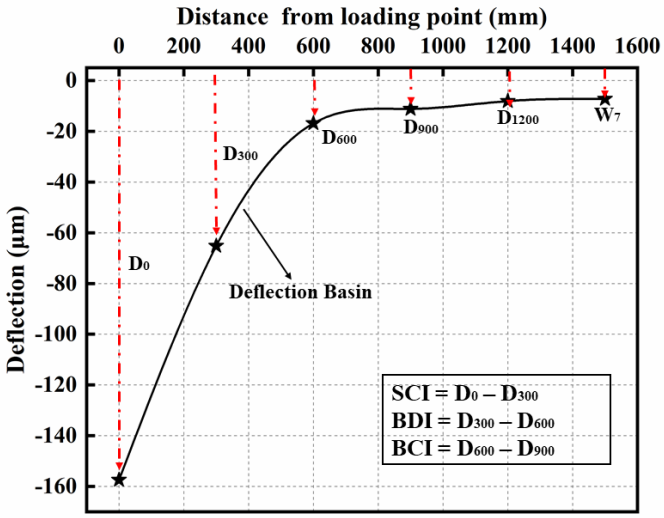

Figure 4-37. FWD deflection basin in testing inverted pavement

Based on the results from **Figure 4-37**, it can be found that the value of SCI, BDI, BCI and W_7 is 92.2 μm, 48.3 μm, 5.7 μm and 2.8 μm, respectively. Based on the evaluation indices in **Tables 4-6 & 4-7**, its SCI, BDI, BCI (LLI) and W_7 values are smaller than the thresholds. Therefore, it can be concluded that the AC layer, CTB layer and SG layer of this inverted pavement are in very good condition after one-and-a-half years of service for the heavy trucks. In order to have a more comprehensive investigation of this pavement, **Figure 4-38 (a-d)** displays all the measuring points over all of the inverted pavement section, which shows the change of DBPs. Based on the results in **Figure 4-38**, the overall condition of the testing inverted pavement can be investigated. Although the data fluctuates with the road, the changes are within a reasonable and acceptable range.

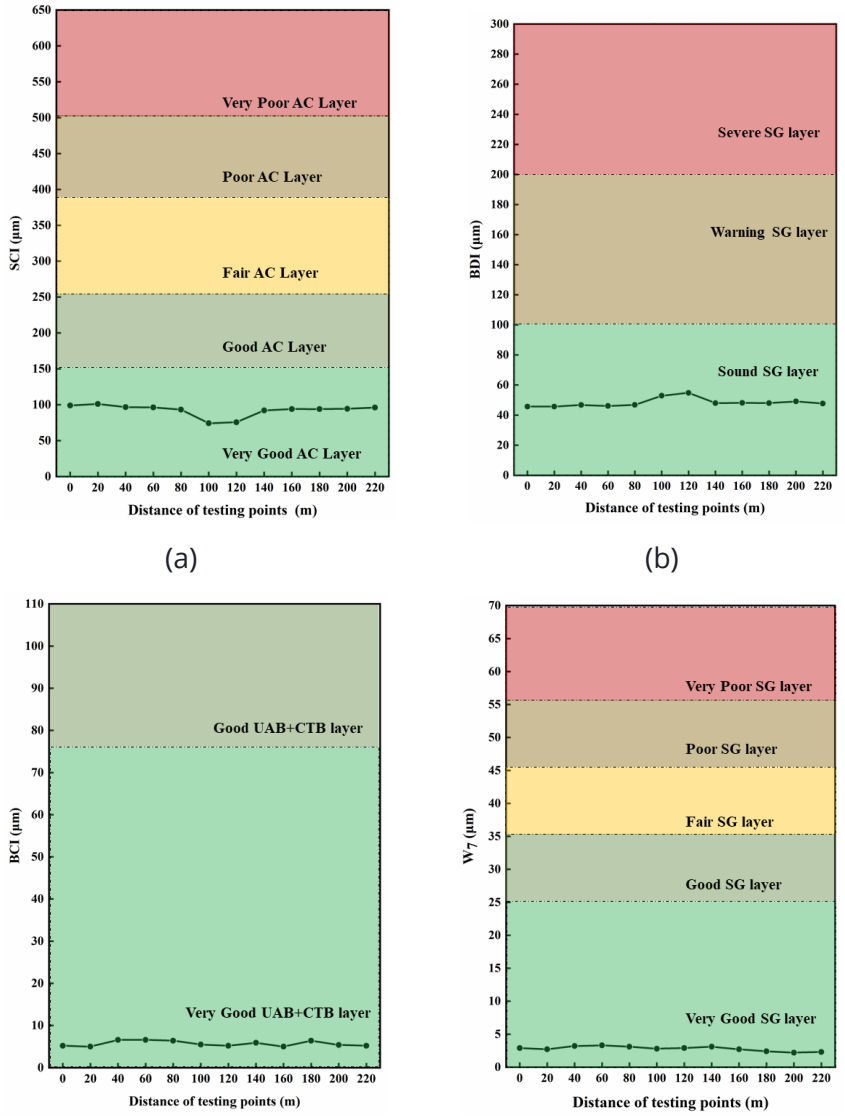

Figure 4-38. Change of DBPs along the testing inverted pavement section

It is commonly understood that better structural capacity typically leads to better pavement performance. To improve the reliability of assessment in the inverted pavement test section, a testing vehicle equipped with a laser crack measurement system (LSCM) was used to measure the longitudinal profile, International Roughness Index (IRI), transverse profile and macrotexture. Meanwhile, the estimated annual traffic for this inverted pavement was approximately 33,000 equivalent single-axle loads (ESALs). This road is not public, and the annual traffic was estimated based on the number of trucks from the aggregate company. After analyzing the data from the testing vehicle, it was found that the Federal Highway Performance Monitoring System (HPMS) average IRI was only 124.0 cm per km, which indicates that the smoothness of the pavement was in good condition. The low and medium longitudinal cracking length of 49.4 cm also reflected the good condition in the AC surface layer. The average rutting depth of left and right lanes was only 0.13 cm, which means that the inverted pavement would perform well in the base layer and subgrade. The above testing results are consistent with the evaluation results based on the DBP system. Therefore, the DBP-based inverted pavement evaluation method is suitable for the inverted pavement structure and contributes to the inverted pavement management system (IPMS). Meanwhile, the testing and assessment results indicate the good performance of the inverted pavement structure.

4.4 Evaluating the Performance of Inverted Pavement Using APT at UT Campus

4.4.1 Construction of test sections

The testing sections were located at the University of Tennessee, Knoxville. As shown in **Figure 4-39** (a & b), the thicknesses and layout of the layers are presented. The inverted pavement lanes (I) and (II) are constructed at the right and left sides to keep the same boundary condition. The conventional pavement section was paved at the middle lane as the benchmark for comparison. In addition, the wooden slabs were inserted at the boundaries of middle lane to separate the lanes and keep the same boundary conditions. The thickness of the AC layer, UAB layer, and subgrade was 127 mm (5 inches), 254 mm (10 inches) and, 534 mm (21 inches), respectively. The thickness of the AC layer was 63.5 mm (2.5 inches) in the two inverted pavement lanes and 127 mm (5 inches) in the conventional pavement lane.

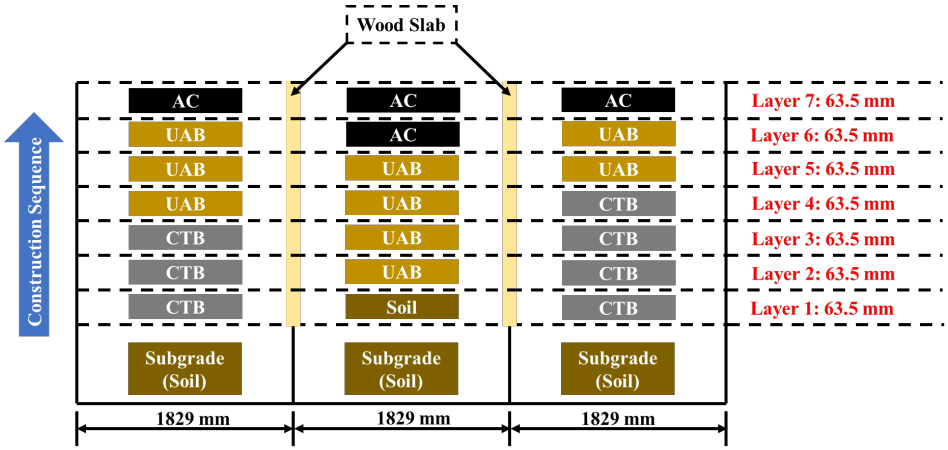

(a)

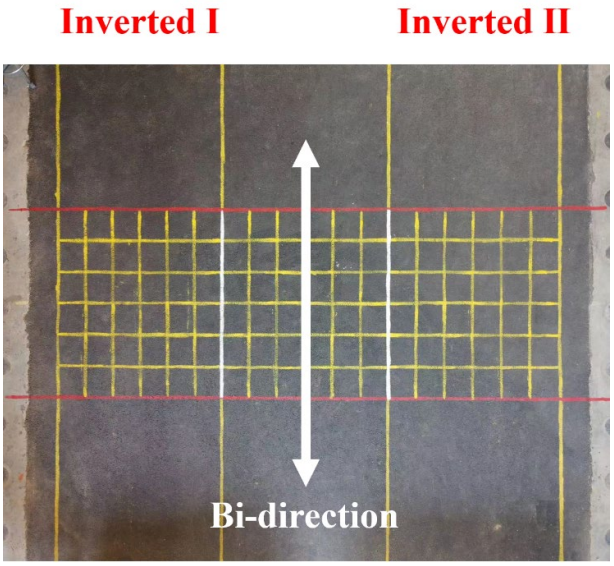

(b)

Figure 4-39. (a) The schematic design of testing pavement; (b) Testing pavement lanes for APT

Figure 4-40 shows the construction processes of the testing pavement. The filling and compaction processes of subgrade soil for inverted and conventional pavement sections are shown in **Figure 4-40** (a & b). The wooden slabs were set up to separate pavement lanes in the pit, as shown in **Figure 4-40** (c). During the construction of the CTB, 6 % (by weight) of ordinary Portland cement was added to the soil, and a tiller mixed them. During the one-week curing, the moisture was kept by spraying water on the CTB and then a plastic sheet was used to cover the pit. After 7-days if curing, the UAB was placed above the CTB. After compaction of the UAB for each pavement lane, the AC was paved as the surface.

(a)

(b)

(c)

(d)

(e)

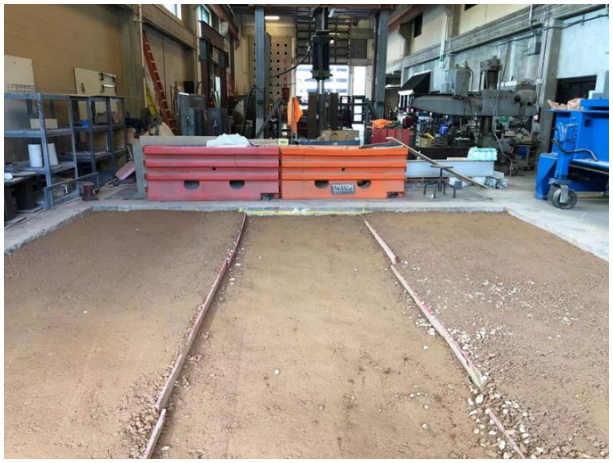

(f)

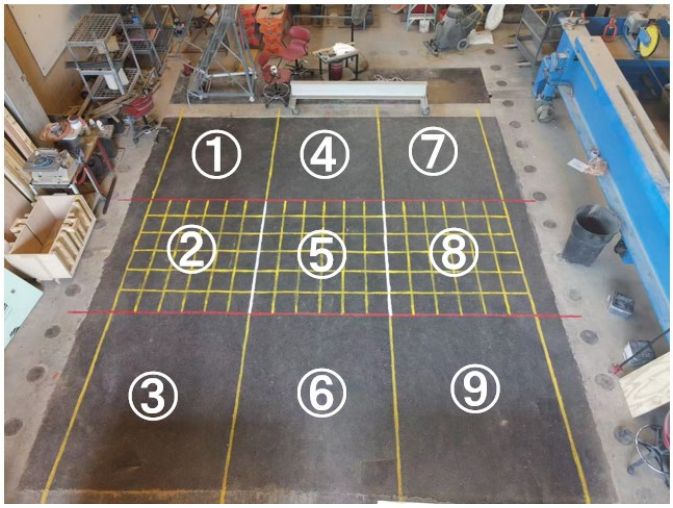

(g)

Figure 4-40. (a-f) Construction processes of the testing pavement; (g) Top view of the testing pavement

4.4.2 Materials selection and properties

4.4.2.1 Subgrade soil

In this full-scale test of inverted and conventional pavement sections, the subgrade soil was collected from Knoxville, TN. The optimum moisture content (OMC) is 9.6%, and the maximum dry density (MDD) is 19.6 kN/m^3 (125.9 pcf) tested by the standard compaction method according to Standard AASHTO T 99-15. According to the laboratory tests, the subgrade soil was categorized as clayey silt (CL-ML) according to the standard ASTM D2487. **Figure 4-41** shows the gradation of the subgrade soil and unbound aggregates for UAB.

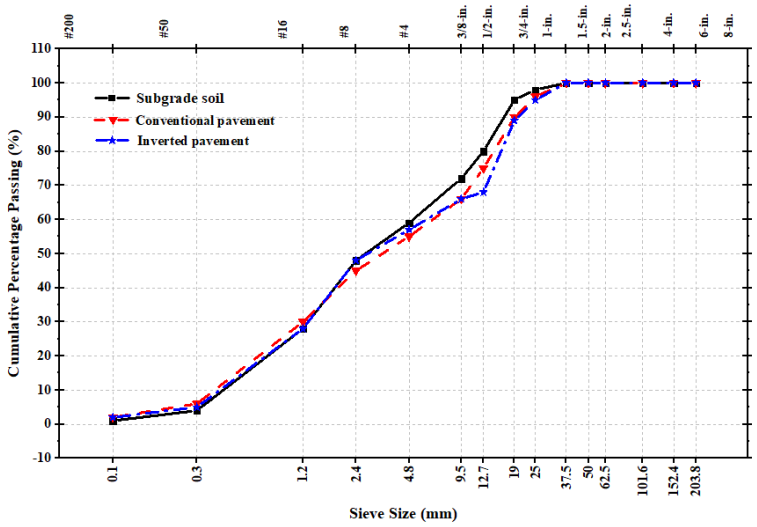

Figure 4-41. Gradation of the subgrade soil and unbound aggregates for UAB

4.4.2.2 Unbound aggregate materials

The unbound aggregate materials used for the UAB are from Vulcan Quarry, Knoxville, TN. The particle size distribution of unbound aggregate materials is also shown in **Figure 4-41**, and it can be classified into Grade D aggregate [47]. The OMC and MDD obtained from laboratory test was 6.9% and 22.1 kN/m^3 (140.5 pcf). There was a difference in the aggregate between the conventional and inverted sections. Fewer finer aggregates were used for the inverted section, and the aggregates on the 1/2 inch-sieve were removed in this study. Based on the gradation of aggregates used in the UAB, the difference of the aggregates between the inverted and conventional pavements was insignificant and can, therefore, be neglected.

4.4.2.3 Cement-treated materials

In this study, the method to build the CTB followed the approach by the Louisiana Department of Transportation (LDOT) to mix subgrade soil with 6% (by weight) ordinary Portland cement [1,67]. The compression test was conducted according to the standard ASTM D 1633, the compressive strength of cement-treated materials for seven days in the laboratory was 2.2 MPa (321 psi) and the test specimen moisture content was 7.5%.

4.4.2.4 Asphalt concrete materials

The asphalt mix used in this study was 411-D with the asphalt binder PG 64-22 from the Tennessee Department of Transportation (TDOT) with a density of 1040 kg/m^3, and the bulk

density of the aggregate was 2510 kg/m^3. The AC (ACS-HM) in this study had a theoretical density of 2470 kg/m^3 and optimum asphalt content of 5.70%.

4.4.3 Construction quality control

To control the construction quality of the pavement, the nuclear gauge test, as shown in **Figure 4-42** (b), was conducted on each layer of the testing pavement to verify the compaction. A total of nine testing points were chosen, as shown in **Figure 4-40**, to ensure the compaction quality of the whole testing pavement. The compaction and moisture content of the SG and UAB are presented in **Table 4-14**. To achieve suitable compaction, the subgrade layer was compacted using three layer-iterative procedures. Based on the data in **Table 4-14**, the SG and UAB were in good compaction.

Table 4-16 Moisture content and compaction degree of SG and UAB

Section	**Compaction (%)**		**Moisture content (%)**	
Layer	SG	UAB	SG	UAB
1	94.6	96.7	14.9	5.3
2	95.7	97.5	14.3	5.2
3	92.4	98.1	15.1	5.4
4	93.5	97.7	14.2	5.6
5	94.3	96.4	13.8	5.6
6	95.6	97.1	13.6	5.8
7	94.7	95.3	13.4	5.5
8	92.9	98.1	14.5	5.7
9	93.8	97.5	14.3	5.4
Average Value	94.2	97.1	14.2	5.7
Standard Deviation	0.53	0.18	1.06	0.85

A dynamic cone penetration (DCP) test was also used to evaluate the strength of the underlying SG and UAB by measuring the penetration of the device into the soil after each hammer blow. In addition, the penetration results were used to predict the modulus of individual layer in pavement sections based on standard ASTM D6951, as shown in **Figure 4-42**. The penetration rate of DCP is related to the California Bearing Ratio (CBR), which can predict the strength of the SG and UAB layers based on the tabulated correlation of the CBR versus DCP index. CBR profiles are related to the penetration rate of the DCP in mm/blow according to ASTM 6951. **Figure 4-43** presents the predicted CBR of the SG, UAB, and CTB layers based on the penetration depth from the DCP test and standard ASTM D6591. The SG had the minimum strength with an average CBR of 15%, and the CTB had the largest strength with an average CBR of 86%. The achieved CBR is larger than the laboratory value due to the higher compaction levels from the heavy roller compared with the standard Proctor test [68]. Based on the DCP data, it was found that the strength of the UAB was a little larger than SG, reflecting that the UAB without loading had a small initial strength.

(a)

(b)

Figure 4 42. (a) Process of DCP test; (b) Process of nuclear gauge test

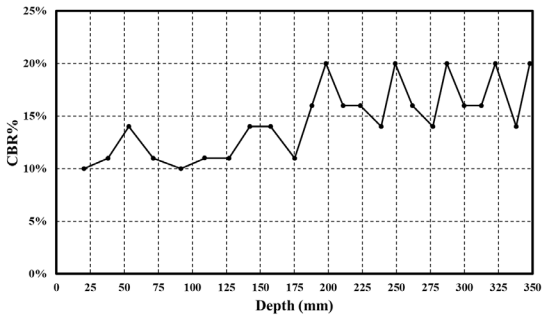

(a)

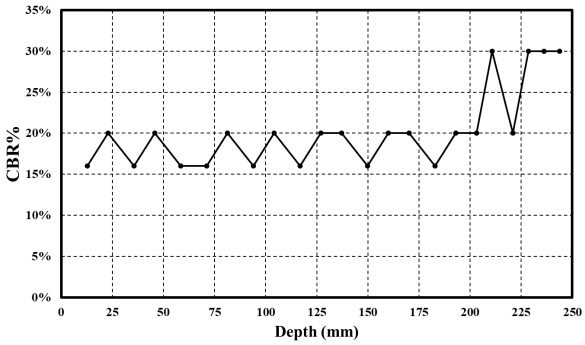

(b)

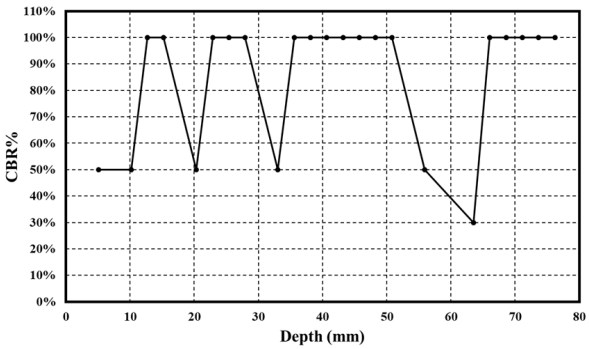

(c)

Figure 4-42. Relationship between penetration depth and CBR: (a) SG; (b) UAB; (c) CTB

For the construction of the AC layer, the plant asphalt mix was delivered by dump truck 30 minutes before the surface construction. The target air void % (Va %) was set at 8%. To ensure the consistency of compaction, a handheld compactor was used to compact the edge areas of the testing pavement. For the thickness validation, the individual thickness for each pavement lane was confirmed by digging transverse trenches after completing all APT testing.

4.4.4 Measurement of permanent surface deformation

A digital measuring instrument was used to measure the rutting depth and deformation of the testing pavement lanes with the loading passes, as shown in **Figure 4-44 (a)**. The measurement results were based on the reference outside the testing pit. A total of 100,000 repetitious loading passes were applied to the testing pavements. The permanent surface deformation in this study was defined as the accumulating elevation difference of the measuring points on the pavement surface., The elevation difference at fixed loading passes of 2k, 4k, 6k,8k 10k, 15k, 20k, 25k, 30k, 40k, 50k, 60k, 70k, 80k, 90k, and 100k were recorded to investigate the change in the pavement profile. As shown in **Figure 4-44 (b)**, each testing pavement lane was painted with lines for deformation measurement, and more measuring points were added near the wheel loading area to exclude the influence of boundary effects, as shown in **Figure 4-44 (c)**. Each testing pavement lane was divided into 13 rows for the transverse profile and 13 columns for the longitudinal profile. In addition, the corresponding points were marked with numbers for easier and more convenient calculation purposes.

(a)

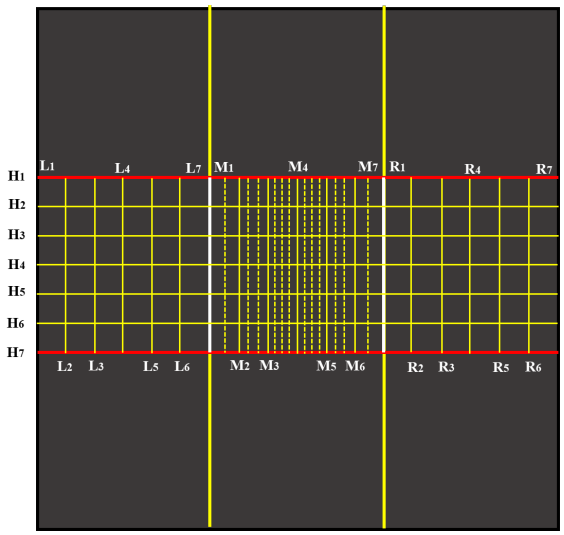

(b)

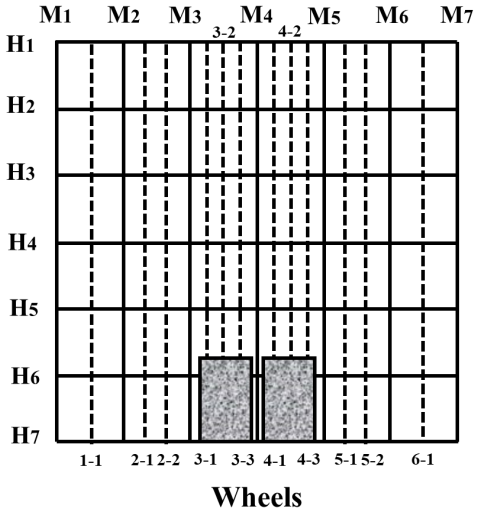

(c)

Figure 4-43. (a) Measurement of deformation of testing pavement; (b) Measuring point on testing pavements; (c) Detailed measuring points on the middle lane

4.4.5 Performance evaluation

4..4.5.1 Surface deformation with passing times

After different loading passes by the APT facility, surface deformation was detected and measured in each pavement lane. **Figure 4-45** shows each testing pavement lane's final surface deformation contours along the longitudinal wheel path after finishing the wheel-loading process. Based on the presented data, it can be found that the influencing area for each lane was within the central 100.0 cm. The area of the outer 30.0 cm at either side of each lane was not affected by the moving wheels. Therefore, the boundary effect of the two adjacent lanes could be neglected in this test, which provided comparable deformation results for this study. The black points in **Figure 4-45** represent the measuring points to detect the pavement deformation. Based

on the deformation data in **Figure 4-45**, the maximum deformation area is located between 600 mm and 1200 mm from the origin point in all three pavement lanes because this area is along the wheel path. The largest deformation of 26.7 mm was found in the conventional pavement (middle) lane. And the largest surface deformation of inverted pavement (I) was 24.4 mm, which was worse than 19.9 mm of deformation in inverted pavement (II). Furthermore, the general condition of surface deformation in the conventional lane was more severe than the inverted structure. Inverted pavement (II), with a thicker CTB, had better performance than inverted lane (I) with a thicker UAB.

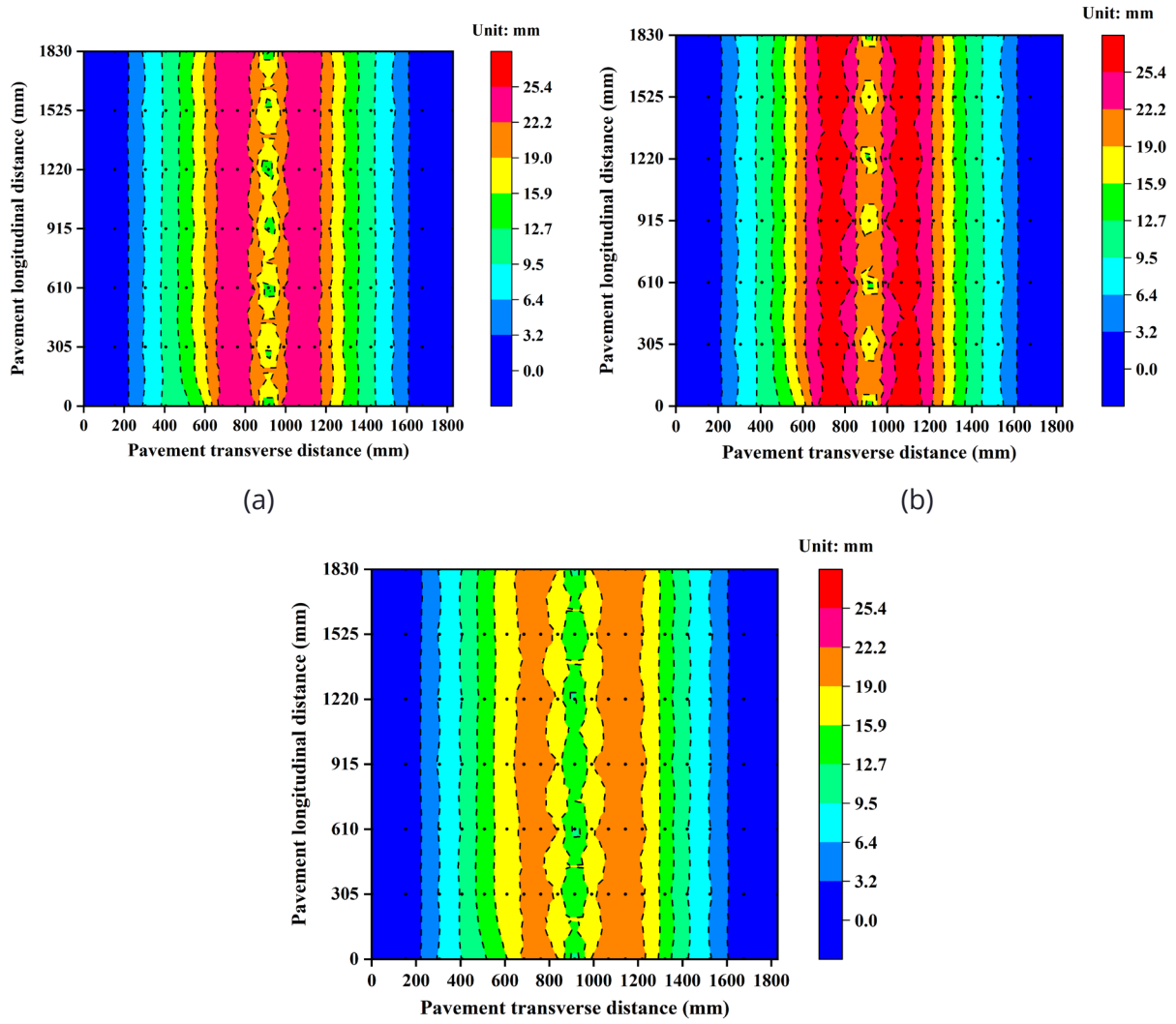

Figure 4-44. Final surface deformation contours of each testing pavement lane (a) Inverted pavement (I); (b) Conventional pavement; (c) Inverted pavement (II)

Figure 4-46 exhibits the surface profiles in transverse direction due to bi-directional accelerated pavement loading passes. After completing the measurements for each lane, all the data were calibrated based on the initial pavement profile. Thus, the initial profile elevation at the beginning is 0 mm. The rutting failure criterion was set as 25.4 mm (1 inch), considering the APT facility's

experimental time and stroke limitation. The rutting failure criterion of 25.4 mm was chosen based on the past experimental experience [69]. Based on **Figure 4-46**, the non-uniform W-shaped deformation with double peaks was observed in the dual-wheel rutting profiles, and an uplift was found between the dual wheels for three lanes. As for the final deformation, the conventional lane and inverted pavement (I) had a comparative performance on the maximum profile elevation, and both of them exceeded the failure criterion. But inverted pavement (I) had a smaller failure area than the conventional lane. For the two inverted pavement lanes, the profile elevation of inverted pavement Ⅱ was within the failure criterion, indicating its better performance than the other two lanes. There is an interesting phenomenon to be noticed in **Figure 4-46**. The shape of curves of inverted pavement has a wider breadth compared with the conventional structures, which indicates that a larger area was affected due to the surface loading in the inverted pavement structure. And the affected area of inverted lane Ⅱ is also wider than that of inverted lane (I), which might be due to the thicker CTB layer. The larger affected area having lower permanent deformation in the inverted structure might be due to the function of the CTB layer. And the thicker CTB coupled with UAB re-distributed the stress in the pavement and resulted in a larger affected area, which has been validated in the numerical simulation by Jiang et al. [53].

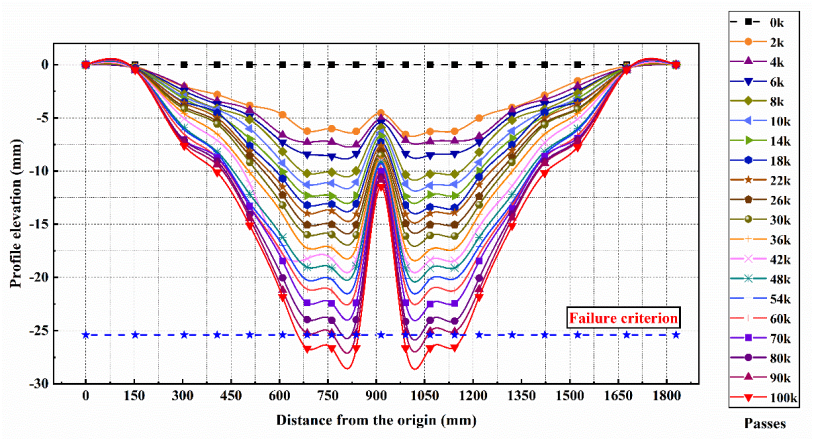

(a)

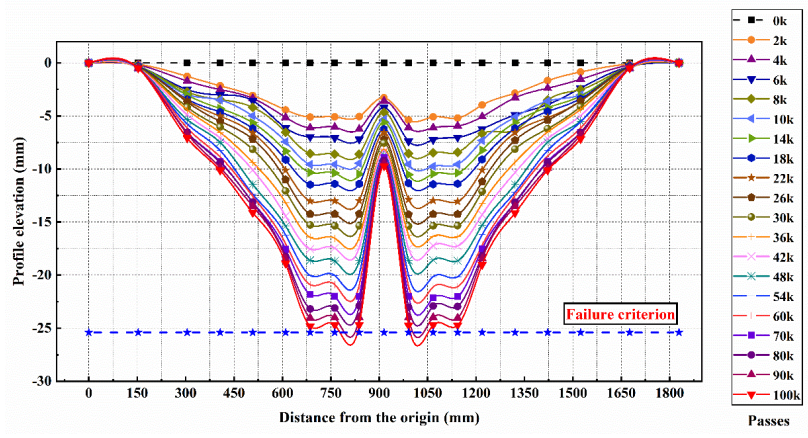

(b)

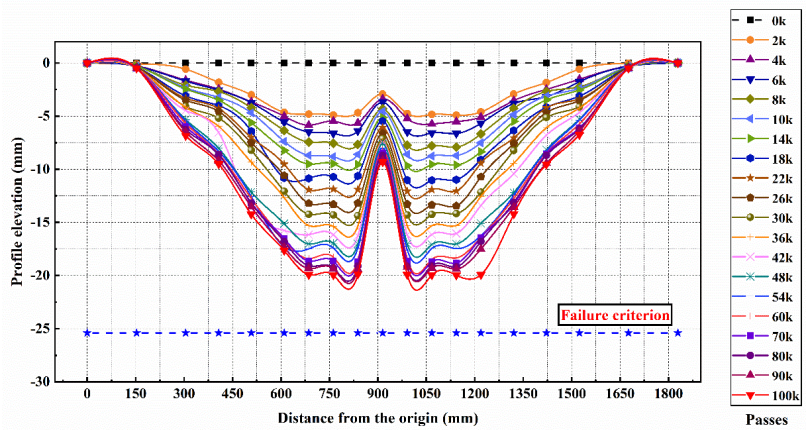

(c)

Figure 4-45. Pavement profile of (a) Conventional lane, (b) Inverted (I), (c) Inverted (II) with loading passes

Figure 4-47 shows the accumulating permanent deformation concentrated on the wheel-loading areas. The average value of measuring points $M_{3\text{-}1}$, $M_{3\text{-}2}$, $M_{3\text{-}3}$, $M_{4\text{-}1}$, $M_{4\text{-}2}$ and $M_{4\text{-}3}$ were plotted in **Figure 4-47**. Based on the data curve, the entire deformation process of pavements could be divided into three phases. In phase one, all three pavement lanes experienced an accelerating increase in surface deformation. This change was mainly due to the rapid densification from the loading wheel. The conventional pavement contains a thicker UAB layer than the inverted structures, thus, a steeper curve could be observed for the conventional lane. And the phase two with a stable and gentle curve occurred next. In this phase, the permanent surface deformation increased slowly in all three lanes, and the permanent deformation came to the same value when the number of passes reached 60k. The deformation of inverted pavement (I) in this phase contributed 32.4% to the final deformation. The reason why the deformation of inverted lane (I) increased a lot during this phase is the relatively thin AC layer and greater compaction in the UAB layer. After 60k passes, the deformation gradually slowed down in the inverted pavement lanes, but the conventional lane's deformation rate remained constant. Based on the condition in phase three, it can be seen that the fatigue of conventional pavement further deepened but the inverted pavement lanes presented a better performance. The deformation of the SG and UAB led to the larger profile elevation in the conventional pavement structure.

On the contrary, the stiffness of the UAB layer in the inverted pavement structure increased a lot with the loading passes. Therefore, the stiffer UAB could provide a cushion for the thin AC layer. The reflective cracks generated from the lower part of the pavement could be prevented by the UAB, which may result in lower rutting and longer service life of the pavement. Thus, the inverted pavement (I) had a smaller permanent deformation than that of the conventional lane when 100k loading passes were reached. Based on the overall performance, inverted pavement (II) had the best condition after 100k passes of loading, and the conventional pavement had a comparative performance with inverted pavement (I) based on the final value of deformation.

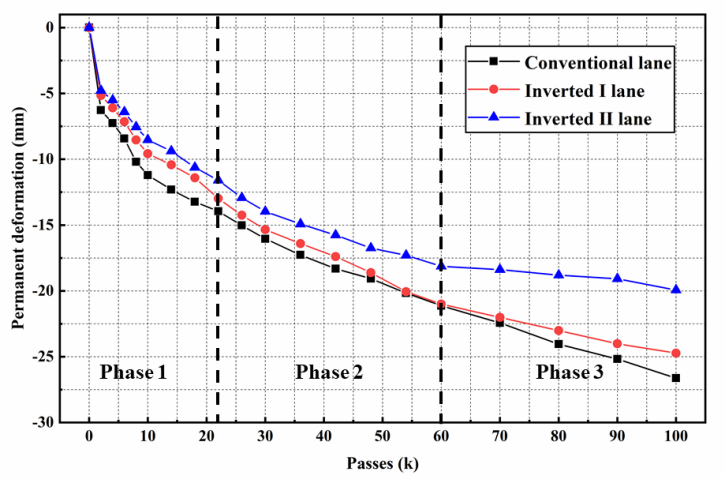

Figure 4-46. Accumulating permanent surface deformation for three lanes

4.4.6 Pavement trenches investigation

To investigate the deformation in individual pavement layers in detail, the testing pavement was trenched at the middle section after finishing the entirety of APT tests, as shown in **Figure 4-48**. The permanent deformation could be measured easily at the pavement section, which could also be used to validate the measurement on the surface. According to Han et al. [70], the total permanent surface deformation was calculated by adding the deformations of surface, base, and subgrade. But, for our study, the deformations below the CTB layer were hard to measure from the cross-section because the CTB layer had much higher stiffness, and little deformation could be found. Based on the cross-sections, it can be easily observed that the AC surface in conventional and inverted pavement (I) lanes had greater deformation, and the top of the UAB in these two lanes also had larger deformations. The results from the pavement trenches verified the measurements discussed in earlier sections of this study. The lessened deformation at the top of the UAB layer in the inverted pavement structures indicated that lower tension could lead to cracking of the AC layer, which was generated at the bottom of AC layer. Another reason for this phenomenon was because the UAB layer in the inverted pavement was stiffer than that in the conventional pavement. In addition, a thicker CTB layer in inverted pavement (I) had a better performance than inverted pavement (I), which means a thicker CTB, coupled with a UAB layer, contributed to the rutting performance and mitigated the potential reflective cracks generated from the CTB in the inverted pavement. Therefore, the trench results showed that the inverted pavement structures outperformed the conventional flexible pavement structure or had a comparative performance compared with the traditional pavement structures.

(a)

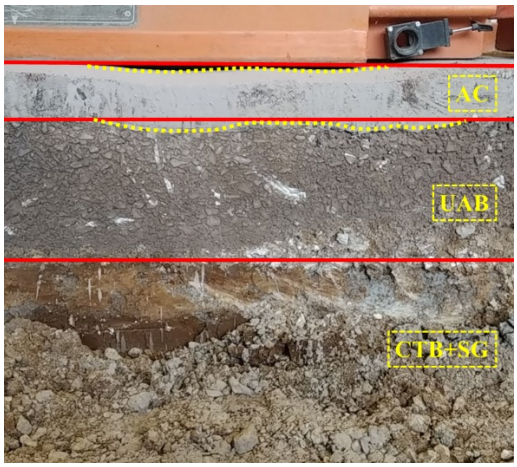

(b)

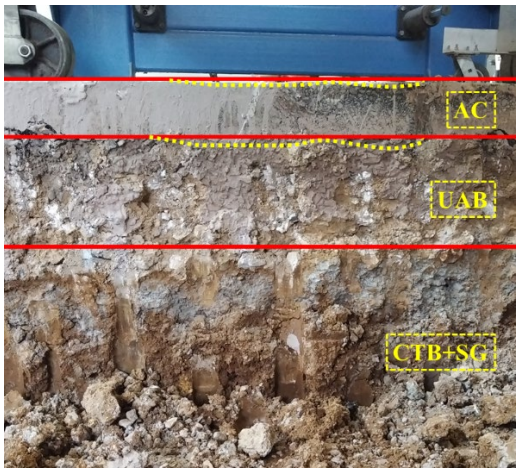

(c)

Figure 4-47. Trench sections at the middle of (a) conventional pavement, (b) inverted pavement (I), (c) inverted pavement (II)

Chapter 5 Conclusion

This study aimed to conduct long-term evaluation of the performance, longevity and cost-effectiveness of inverted pavements as an alternative pavement structure in the state of Tennessee for State Industrial Access projects. To this end, the research team first investigated the effects of nonlinear stress-dependency of the UAB layer on the structural responses of inverted and conventional pavements through numerical simulation. A commonly used stress-dependent resilient modulus model was programmed into a user-defined material subroutine (UMAT) of the ABAQUS finite element program. The published data from GTPAVE were utilized to validate the program developed by the research team. Then, the linear and nonlinear models were utilized to analyze conventional and inverted pavements. Meanwhile, the stress distribution, stiffness contours within the UAB, and deflection of both the inverted pavement and conventional pavement structures were investigated using the program developed in this study.

Second, a full-scale inverted and conventional pavement section were constructed in Knoxville, TN, and a comprehensive field study was conducted in collaboration with Vulcan Materials Company and the Tennessee Department of Transportation. To systematically investigate the inverted pavement structure with respect to the conventional pavement structure, a non-destructive testing method-ground penetrating radar was used to evaluate and confirm the design thickness of pavement layers on both pavement types. In addition, the Benkelman beam test was used to measure the rebound deflection of the pavement surface for both the inverted and conventional pavements. Moreover, a 3-D road profiling system coupled with a Laser Crack Measurement System was utilized to assess/evaluate the pavement surface conditions. Falling weight deflectometer measurements were also conducted to evaluate the structural capacity and layer moduli of both the inverted and conventional pavement sections. Meanwhile, the FWD data was used to validate and verify the numerical simulation work conducted using the finite element method. The numerical analysis and simulation study was conducted to compare the performance of the inverted pavement and the conventional pavement using the model that was validated in a more quantitative analysis approach.

Third, a comprehensive literature review concerning DBP evaluation and its corresponding applications by other researchers were presented. Then, numerical analysis to simulate realistic FWD test and calculations of representative DBPs under simulated loading was conducted. After establishing the DBP assessment system for the inverted pavement conditions, the system was applied to a inverted pavement test section in Tennessee, USA. The field investigation results validated the industrial benefit for the inverted pavement management system (ISMS), which contributed to its future maintenance and rehabilitation measures. Finally, the performance of a full-scale inverted pavement was investigated using APT method, and a conventional flexible pavement under the same environmental and loading conditions were studied and compared. In addition, a comparison study between the inverted pavements with different thicknesses of UAB and CTB was also conducted to investigate the optimum structural design for inverted pavement. Through the full-scale test coupled with APT, the detailed construction experience of the full-scale inverted pavement structure was provided, and the testing results could also extend the understanding of the difference in structural responses between the inverted and conventional pavement structures.

The key findings and recommendations are summarized as follows.

► Numerical differences between the linear and nonlinear models were much smaller in the conventional pavement. Thus, the structural response of the inverted pavement was much more sensitive to the nonlinear stress-dependent characteristic of the UAB layer due to the compaction effect from two stiffer layers of an upper, thin AC layer and a lower CTB layer. Therefore, it is necessary to apply nonlinear stress-dependent resilient modulus for the UAB layer during numerical analyses of inverted pavements.

The stress history and current stress state made the stiffness of the UAB layer changeable, and the larger stress induced higher stiffness within the UAB layer. The inverted pavement had a different stress distribution from the conventional pavement. The smaller tensile stress at the bottom of the AC layer in the inverted pavement indicated that the UAB layer could mitigate the tension of the AC layer that transferred from the CTB layer to reduce the reflective cracks in the inverted pavement. In addition, the smaller tensile stress at the top of the SG in the inverted pavement indicated that the UAB layer could reduce the deformation of the pavement structure and improve its bearing capacity. The maximum deflection of the AC surface was much less than that of the conventional pavement, which could result in longer service life.

► Ground-coupled GPR is a reliable approach to estimate thicknesses of pavement structures. Using a combination of GPR thickness data and designed thickness values can determine, with high-accuracy, the thickness of different pavement layers without structural destruction, with time savings and without traffic disruption. Meanwhile, the accurate characterization of pavement layer thicknesses contributes to the better analysis of pavement structures and to the reliability of numerical simulation work.

The deformation of the inverted pavement surface could not be detected by the Benkelman beam test, which meant that the deflection was negligible and below the resolution of the dial. However, the average deflection of 0.326 mm was reported for the conventional pavement. The much smaller deflection in the inverted pavement was due to the higher stiffness of UAB. After being subjected to the traffic of loaded trucks using the pavement for a long time, the UAB became stiffer under such repeated truck traffic loads and provided a good cushion between the asphalt and cement-treated base layers. And the “cushion” resulted in less deflection on the pavement surface.

In addition, the inverted structure also contributed to the less deformation. The stiffness distribution in the UAB of the inverted section revealed the stress-dependent property of the UAB. The higher stiffness occurred at the zone with a higher stress state and stiffness decreased with the increase in distance from the loading point, which is attributed to the properties of a much stiffer CTB. The CTB created an effective base to promote the stiffness increase in the UAB. The much higher vertical compressive stress in the inverted pavement section also confirms the stiffer reaction of the UAB.

► Limited scale cost analysis was conducted in this study. Based on the profile data of Vulcan Materials Quarry Entrance testing pavements at 1.5 service years, the pavement service life was predicted. According to economic analyses, the inverted pavement structure for that specific pavement section is significantly more cost-effective than the conventional pavement.

► The DBP-based method by FWD test can evaluate the structural conditions of the individual layer in the inverted pavement. Due the advantages of high-efficiency and no damage of DBP-based method by FWD, this evaluation method contributes to the maintenance and rehabilitation of inverted pavement. The individual layer's modulus of the inverted pavement had a different influence on the deflection basin curve. The influencing zone in the deflection curve affected by the AC layer's modulus is smaller than the CTB layer and the SG layer. And the modulus of the SG layer had the most significant affecting area on the deflection curve, which proved that the deflection on the SG layer contributed to most of the pavement deflection on the surface. The individual layer's modulus of the inverted pavement affected the DBPs differently. The modulus of the AC layer had little influence on the BDI and BCI values. Nevertheless, the stiffer AC layer had an obvious negative relationship with the SCI value, which showed that the SCI value could reflect the pavement surface condition. The modulus of the CTB layer also had a negative relationship with the BDI value. It influenced the SCI & BCI values, which indicated that the BDI value was able to reflect the condition of the base layer like the CTB layer in the inverted system. Lastly, the modulus of the SG layer had a significant influence on the BCI and BDI values but little effect on the SCI value. This phenomenon indicated that the BCI value could evaluate the subgrade condition.

► The inverted pavement structure differed from the conventional pavement structure in the accumulating permanent surface deformation with APT passes. For the inverted pavement, three phases could be observed. When the loading passes reached a certain number (60k in this case), the UAB layer in the inverted pavement became much stiffer due to its stress-dependent property. Thus, the permanent deformation in the inverted pavement slowed down and the deformation curve became gentle. However, the rutting in the conventional pavement became more severe with the increasing loading passes because the stress-dependent property of the UAB did not take effect in the conventional pavement due to its lack of a rigid CTB layer. The CTB layer contributed more to the performance of the inverted pavement compared with the UAB layer. Based on the rutting performance between the inverted pavements with different thicknesses of CTB and UAB layers, the inverted pavement with a thicker CTB layer had a better performance than the inverted pavement with a thicker UAB layer. Based on the cross-sections of pavements, more deformation was observed at the top of the UAB layer in the conventional pavement, which meant less tension was generated at the bottom of the AC layer. In addition, the stiffer UAB layer in the inverted pavement contributed to the rutting performance and reducing the reflective cracks.

Based on the final results and conclusions from this project, the inverted pavement is recommended for future research. The inverted pavement structure displays different structural responses from the conventional flexible pavement structures under the same loading conditions. The stress-dependent property of the unbound aggregate layer in the inverted pavement is obvious, leading to the unconventional stress and stiffness distributions within the pavement layers. In addition, this study shows that the inverted pavement structure outperformed conventional flexible pavement structure in rutting, cracking and roughness.

However, more field projects of inverted pavements should be investigated to verify the conclusions of this study. Despite the demonstrated potential, future studies are needed to facilitate the application of inverted pavement in the USA. And since the Volkswagen inverted

pavement in Chattanooga, Tennessee has not been finished due to the COVID-19 pandemic, the preliminary cost-benefit analysis was conducted based on the data in Vulcan testing pavements in this study. Therefore, the future research is suggested to be conducted in the following aspects:

(1) More research is suggested to be conducted in the full-scale inverted pavements to accumulate construction experience and have a better understanding of inverted pavement structures;

(2) Based on the results from the DOT survey, the drainage issue of the inverted pavement structure should be focused on due to the impermeable cement-treated base. In the rich-rainfall areas like southeast Tennessee, this issue would be imperative for the durability of the inverted pavement structure.

(3) The cost-analysis of the inverted pavement should be conducted based on the Volkswagen inverted pavement in Chattanooga, Tennessee. In addition, the design methodology of the inverted pavement under the pavement ME framework should be proposed in future.

References

[1] H. Titi, M. Rasoulian, M. Martinez, B. Becnel, G. Keel, Long-term performance of stone interlayer pavement, J. Transp. Eng. 129 (2003) 118–126. doi:10.1061/(ASCE)0733-947X(2003)129:2(118).

[2] R.L. Lytton, J. Uzan, E.G. Fernando, R. Roque, D. Hiltunen, S.M. Stoffels, Development and validation of performance prediction models and specifications for asphalt binders and paving mixes. SHRP-A-357, 1993.

[3] J.M. Vandenbossche, A.J. Fagerness, Performance, analysis, and repair of ultrathin and thin whitetopping at Minnesota Road Research facility, Transp. Res. Rec. (2002) 191–198. doi:10.3141/1809-21.

[4] E. Tutumluer, R.D. Barksdale, Inverted flexible pavement response and performance, Transp. Res. Rec. (1995) 102–110. http://onlinepubs.trb.org/Onlinepubs/trr/1995/1482/1482-013.pdf (accessed December 4, 2019).

[5] Richard D. Barksdale, A Study of Factors Affecting Crushed Stone Base Course Performance: Final Report, 1983.

[6] M. Rasoulian, B. Becnel, G. Keel, Stone Interlayer Pavement Design, Transp. Res. Rec. J. Transp. Res. Board. 1709 (2000) 60–68. doi:10.3141/1709-08.

[7] R.G. Terrell, B.R. Cox, K.H. Stokoe, J.J. Allen, D. Lewis, Field Evaluation of the Stiffness of Unbound Aggregate Base Layers in Inverted Flexible Pavements, in: Transp. Res. Rec., 2003: pp. 50–60. doi:10.3141/1837-06.

[8] F.C. Barker, W R ; Brabston, W N ; Townsend, An Investigation of the Structural Properties of Stabilized Layers in Flexible Pavement Systems, 1973. https://apps.dtic.mil/dtic/tr/fulltext/u2/769292.pdf.

[9] M. Kim, E. Tutumluer, J. Kwon, Nonlinear pavement foundation modeling for three-dimensional finite-element analysis of flexible pavements, Int. J. Geomech. 9 (2009) 195–208. doi:10.1061/(ASCE)1532-3641(2009)9:5(195).

[10] P. Cao, F. Jin, D. Feng, C. Zhou, W. Hu, Prediction on dynamic modulus of asphalt concrete with random aggregate modeling methods and virtual physics engine, Constr. Build. Mater. 125 (2016) 987–997. doi:10.1016/j.conbuildmat.2016.08.121.

[11] J. Han, S.K. Pokharel, X. Yang, C. Manandhar, D. Leshchinsky, I. Halahmi, R.L. Parsons, Performance of geocell-reinforced rap bases over weak subgrade under full-scale moving wheel loads, J. Mater. Civ. Eng. 23 (2011) 1525–1534. doi:10.1061/(ASCE)MT.1943-5533.0000286.

[12] P. Cao, F. Jin, C. Zhou, D. Feng, W. Song, Steady-state dynamic method: An efficient and effective way to predict dynamic modulus of asphalt concrete, Constr. Build. Mater. 111 (2016) 54–62. doi:10.1016/j.conbuildmat.2016.02.071.

[13] Z. Han, A. Sha, L. Hu, R. Wu, H. Li, Full-scale investigation on the traffic load influence zone and its dimension for HMA layer in inverted pavement, Constr. Build. Mater. 219 (2019) 19–30. doi:10.1016/j.conbuildmat.2019.05.110.

[14] E. Papadopoulos, J.C. Santamarina, Inverted base pavements: construction and performance, Int. J. Pavement Eng. 20 (2019) 697–703. doi:10.1080/10298436.2017.1326237.

[15] C.W. Johnson, COMPARATIVE STUDIES OF COMBINATIONS OF TREATED AND UNTREATED BASES AND SUBBASES FOR FLEXIBLE PAVEMENTS, Highw. Res. Board. (1961). http://onlinepubs.trb.org/Onlinepubs/hrbbulletin/289/289-003.pdf.

[16] W. Song, B. Huang, M. Asce, ; Xiang Shu, A.M. Asce, J. Stránský, H. Wu, Interaction between Railroad Ballast and Sleeper: A DEM-FEM Approach, (2019). doi:10.1061/(ASCE)GM.1943-5622.0001388.

[17] S.W. Park, R.L. Lytton, Effect of stress-dependent modulus and poisson's ratio on structural responses in thin asphalt pavements, J. Transp. Eng. 130 (2004) 387–394. doi:10.1061/(ASCE)0733-947X(2004)130:3(387).

[18] Y. Li, J.B. Metcalf, S.A. Romanoschi, M. Rasoulian, Performance and failure modes of Louisiana asphalt pavements with soil-cement bases under full-scale accelerated loading, Transp. Res. Rec. 1673 (1999) 9–15. doi:10.3141/1673-02.

[19] I. Al-Qadi, H. Wang, E. Tutumluer, Dynamic analysis of thin asphalt pavements by using cross-anisotropic stress-dependent properties for granular layer, Transp. Res. Rec. 2154 (2010) 156–163. doi:10.3141/2154-16.

[20] A. Abu-Osei, D.N. Little, R.L. Lytton, International Center for Aggregates Research (ICAR) Report 502-1: Structural Characteristics of Unbound Aggregate Bases to Meet AASHTO 2002 Design Requirements, 2001. http://aftre.nssga.org/Reports/Project-502-2.pdf (accessed February 1, 2020).

[21] E. Tutumluer, M.R. Thompson, Anisotropic modeling of granular bases in flexible pavements, Transp. Res. Rec. (1997) 18–26. doi:10.3141/1577-03.

[22] E. Papadopoulos, J.C. Santamarina, Analysis of inverted base pavements with thin-asphalt layers, Int. J. Pavement Eng. 17 (2016) 590–601. doi:10.1080/10298436.2015.1007232.

[23] D.D. Cortes, J.C. Santamarina, The LaGrange case history: Inverted pavement system characterisation and preliminary numerical analyses, Int. J. Pavement Eng. 14 (2013) 463–471. doi:10.1080/10298436.2012.742192.

[24] P.J. Yoo, I.L. Al-Qadi, M.A. Elseifi, I. Janajreh, Flexible pavement responses to different loading amplitudes considering layer interface condition and lateral shear forces, Int. J. Pavement Eng. 7 (2006) 73–86. doi:10.1080/10298430500516074.

[25] HICKS RG, MONISMITH CL, Factors influencing the resilient response of granular materials, Highw Res Rec. (1971) 15–31.

[26] K.D. Hjelmstad, E. Taciroglu, Analysis and Implementation of Resilient Modulus Models for Granular Solids, J. Eng. Mech. 126 (2000) 821–830. doi:10.1061/(asce)0733-9399(2000)126:8(821).

[27] G.W. Allison, G.C. Whited, A.S. Hanna, H.G. Nasief, Evaluation of probing versus coring for determination of portland cement concrete pavement thickness, Transp. Res. Rec. 2152 (2010) 3–10. doi:10.3141/2152-01.

[28] K. Mu, Z. Gao, X. Shi, Y. Li, Interface behavior of asphalt pavements constructed by conventional and double-decked paving methods, Materials (Basel). 13 (2020) 1351. doi:10.3390/ma13061351.

[29] C. Plati, A. Loizos, K. Gkyrtis, Integration of non-destructive testing methods to assess asphalt

pavement thickness, NDT E Int. (2020) 102292. doi:10.1016/j.ndteint.2020.102292.

[30] P. Shangguan, I.L. Al-Qadi, Z. Leng, R.L. Schmitt, A. Faheem, Innovative approach for asphalt pavement compaction monitoring with ground-penetrating radar, Transp. Res. Rec. 2347 (2013) 79–87. doi:10.3141/2347-09.

[31] C. Plati, A. Loizos, K. Gkyrtis, Assessment of Modern Roadways Using Non-destructive Geophysical Surveying Techniques, Springer Netherlands, 2020. doi:10.1007/s10712-019-09518-y.

[32] K.R. Maser, T. Scullion, Automated Pavement Subsurface Profiling Using Radar: Case Studies of Four Experimental Field Sites, Transp. Res. Rec. 1344 (1992) 148–154.

[33] C. Plati, A. Loizos, Using ground-penetrating radar for assessing the structural needs of asphalt pavements, Nondestruct. Test. Eval. 27 (2012) 273–284. doi:10.1080/10589759.2012.695784.

[34] E. Horak, Benchmarking the structural condition of flexible pavements with deflection bowl parameters, J. South African Inst. Civ. Eng. 50 (2008) 2–9.

[35] J. Horak, E., Emery, S., and Maina, Review of Falling Weight Deflectometer Deflection Benchmark Analysis on Roads and Airfields, in: Conf. Asph. Pavement South Africa, Sun City, South Africa, 2015.

[36] O. Talvik, A. Aavik, Use of FWD deflection basin parameters (SCI, BDI, BCI) for pavement condition assessment, Balt. J. Road Bridg. Eng. 4 (2009) 196–202. doi:10.3846/1822-427X.2009.4.196-202.

[37] A. Vargas-nordcbeck, The Roles of Accelerated Pavement Testing in Pavement Sustainability, 2016. doi:10.1007/978-3-319-42797-3.

[38] W.J. Steyn, Significant Findings from Full-Scale Accelerated Pavement Testing, 2012. doi:10.17226/22699.

[39] D.R. Biswal, U. Chandra Sahoo, S. Ranjan Dash, Structural response of an inverted pavement with stabilised base by numerical approach considering isotropic and anisotropic properties of unbound layers, Road Mater. Pavement Des. (2019). doi:10.1080/14680629.2019.1595701.

[40] D.D. Cortes, J.C. Santamarina, The LaGrange case history: Inverted pavement system characterisation and preliminary numerical analyses, Int. J. Pavement Eng. 14 (2013) 463–471. doi:10.1080/10298436.2012.742192.

[41] D.D. Cortes, H. Shin, J.C. Santamarina, Numerical simulation of inverted pavement systems, J. Transp. Eng. 138 (2012) 1507–1519. doi:10.1061/(ASCE)TE.1943-5436.0000472.

[42] U.C. Sahoo, K.S. Reddy, Effect of nonlinearity in granular layer on critical pavement responses of low volume roads, Int. J. Pavement Res. Technol. 3 (2010) 320–325. doi:10.6135/ijprt.org.tw/2010.3(6).320.

[43] B. Saad, H. Mitri, H. Poorooshasb, Three-dimensional dynamic analysis of flexible conventional pavement foundation, J. Transp. Eng. 131 (2005) 460–469. doi:10.1061/(ASCE)0733-947X(2005)131:6(460).

[44] E. Tutumluer, D.N. Little, S.H. Kim, Validated Model for Predicting Field Performance of Aggregate Base Courses, in: Transp. Res. Rec., 2003: pp. 41–49. doi:10.3141/1837-05.

[45] I. Ahmed, N. Thom, S. Bilal Ahmed Zaidi, J.S. Carvajal-Munoz, T. Rahman, A. Dawson, Application

of a novel linear-viscous approach to predict permanent deformation in simulative inverted pavements, Constr. Build. Mater. 267 (2020) 120681. doi:10.1016/j.conbuildmat.2020.120681.

[46] E. Papadopoulos, J.C. Santamarina, Optimization of inverted base pavement designs with thin asphalt surfacing, in: Geotech. Spec. Publ., American Society of Civil Engineers, Reston, VA, 2014: pp. 2996–3004. doi:10.1061/9780784413272.291.

[47] Tennessee Department of Transportation, Tennessee Department of Transportation Standard Specifications for Road and Bridge, 2015. https://www.tn.gov/content/dam/tn/tdot/construction/old_web_page/TDOT_2015_Spec_Book_FINAL_pdf.pdf.

[48] E. Kleyn, Successful G1 Crushed Stone Basecourse Construction, Abstr. 31st South. African Transp. Conf. (SATC 2012) Proc. (2012) 110–118.

[49] B. Han, J. Ling, X. Shu, W. Song, R.L. Boudreau, W. Hu, B. Huang, Quantifying the effects of geogrid reinforcement in unbound granular base, Geotext. Geomembranes. 47 (2019) 369–376. doi:10.1016/j.geotexmem.2019.01.009.

[50] J. Uzan, CHARACTERIZATION OF GRANULAR MATERIAL., Transp. Res. Rec. (1985) 52–59. doi:10.1016/0148-9062(86)91013-2.

[51] FHWA - 2015 - The Long-Term Pavement Performance Program.pdf, (n.d.).

[52] C. Chang, D. Saenz, S. Nazarian, I.N. Abdallah, A. Wimsatt, T. Freeman, E.G. Fernando, TxDOT Guidelines to Assign PMIS Treatment Levels, 2014.

[53] X. Jiang, M. Zhang, R. Xiao, P. Polaczyk, Y. Bai, B. Huang, An investigation of structural responses of inverted pavements by numerical approaches considering nonlinear stress-dependent properties of unbound aggregate layer, Constr. Build. Mater. 303 (2021) 124505. doi:10.1016/j.conbuildmat.2021.124505.

[54] M.F. Rabbi, D. Mishra, Using FWD deflection basin parameters for network-level assessment of flexible pavements, Int. J. Pavement Eng. (2019) 1–15. doi:10.1080/10298436.2019.1580366.

[55] Z. Xie, J. Shen, Z. Guo, L. Cong, Effect of distresses on deflection basins and backcalculation modulus of asphalt pavement with cement-treated base, Int. J. Pavement Res. Technol. 8 (2015) 283–288. doi:10.6135/ijprt.org.tw/2015.8(4).283.

[56] R.A. Tarefder, M.U. Ahmed, Modeling of the FWD Deflection Basin to Evaluate Airport Pavements, Int. J. Geomech. 14 (2014) 205–213. doi:10.1061/(asce)gm.1943-5622.0000305.

[57] L. Li, H. Chen, J. Li, D. Sun, An elastoplastic solution to undrained expansion of a cylindrical cavity in SANICLAY under plane stress condition, Comput. Geotech. 132 (2021) 103990. doi:10.1016/j.compgeo.2020.103990.

[58] M.C. Vrtis, Investigation of Deflection Basins to Identify Structural Distress Within Flexible Pavements, Auburn University, 2017. https://connect.ncdot.gov/projects/research/RNAProjDocs/2000-04FinalReport.pdf.

[59] D. Jansen, E. Straube, Temperature correction of falling weight deflectometer measurements, in: Bear. Capacit. Roads, Railw. Airfields, CRC Press, 2009: pp. 789–798. doi:10.1201/9780203865286.ch84.

[60] G. Zuo, Impacts of Environmental Factors on Flexible Pavements, University of Tennessee,

2003. https://trace.tennessee.edu/utk_graddiss/2349.

[61] K.D. Hjelmstad, E. Taciroglu, Analysis and implementation of resilient modulus models for granular solids, J. Eng. Mech. 126 (2000) 821–830. doi:10.1061/(ASCE)0733-9399(2000)126:8(821).

[62] E. Papadopoulos, D.D. Cortes, J. Carlos Santamarina, In-situ assessment of the stress-dependent stiffness of unbound aggregate bases: application in inverted base pavements, Int. J. Pavement Eng. 17 (2016) 870–877. doi:10.1080/10298436.2015.1022779.

[63] R.G. Terrell, B.R. Cox, K.H. Stokoe, J.J. Allen, D. Lewis, Field Evaluation of the Stiffness of Unbound Aggregate Base Layers in Inverted Flexible Pavements, Transp. Res. Rec. (2003) 50–60. doi:10.3141/1837-06.

[64] X. Wang, W. Wu, H. Zhu, F. Liu, H. Zhang, J.S. Lin, Three-dimensional discontinuous deformation analysis with explicit contact formulation and block-wise multicore CPU acceleration, Comput. Geotech. 139 (2021) 104410. doi:10.1016/j.compgeo.2021.104410.

[65] J.M. Duncan, C.L. Monismith, E.L. Wilson, Finite Element Analyses of Pavements, Highw. Res. Board. 38 (1968) 18–33.

[66] R.A. Tarefder, M.U. Ahmed, A. Rahman, Effects of cross-anisotropy and stress-dependency of pavement layers on pavement responses under dynamic truck loading, J. Rock Mech. Geotech. Eng. 8 (2016) 366–377. doi:10.1016/j.jrmge.2016.01.001.

[67] U.S. Department of Transportation, LOUISIANA EXPERIENCE WITH INVERTED PAVEMENT SYSTEMS LOUISIANA EXPERIENCE WITH FHWA-HIF-19-082, 2017. https://www.fhwa.dot.gov/pavement/sustainability/case_studies/hif19082.pdf.

[68] I.I.A. Qamhia, E. Tutumluer, H. Ozer, H. Shoup, S. Beshears, J. Trepanier, Evaluation of Chemically Stabilized Quarry Byproduct Applications in Base and Subbase Layers through Accelerated Pavement Testing, Transp. Res. Rec. 2673 (2019) 259–270. doi:10.1177/0361198118821099.

[69] B. Han, P. Polaczyk, H. Gong, R. Ma, Y. Ma, F. Wei, B. Huang, Accelerated Pavement Testing to Evaluate the Reinforcement Effect of Geogrids in Flexible Pavements, Transp. Res. Rec. J. Transp. Res. Board. (2020) 036119812093512. doi:10.1177/0361198120935120.

[70] B. Han, P. Polaczyk, H. Gong, R. Ma, Y. Ma, F. Wei, B. Huang, Accelerated Pavement Testing to Evaluate the Reinforcement Effect of Geogrids in Flexible Pavements, Transp. Res. Rec. 2674 (2020) 134–145. doi:10.1177/0361198120935120.

Appendices

Survey

The University of Tennessee

Evaluating the Performance of Inverted Pavements

The concept of inverted pavement was developed in South Africa, and many successful applications have been reported in Georgia, Louisiana, and other states. In the inverted pavement design, an unbound aggregate layer, which is usually used as a subbase beneath the stabilized base, is sandwiched between the asphalt surface layer and the cement stabilized base. The reason for the unique location of the unbound base in an inverted pavement is that the unbound aggregate is a type of highly stress-dependent materials. When unbound base is placed closer to the pavement surface, the unbound aggregates will be subjected to a higher stress state, resulting in a higher stiffness of the unbound aggregate layer and thus a better pavement performance.

This questionnaire from the University of Tennessee is to collect practical experience and lessons on the inverted pavement based on your expertise. Your response to this questionnaire will be beneficial to this study and is highly appreciated. **This questionnaire will take you around 5 mins.**

Email address:

Name:

State:

1. Is there any inverted pavement in your state?

a. Yes b. No

2. Have you ever heard about any inverted pavement built in the USA?

a. Yes b. No

If “yes”, where? _____

3. Do you have any experience (design, construction, etc) with inverted pavement?

a. Yes b. No

If “yes” in which state(s)

_____

4. Why do you choose (not choose) to build the inverted pavement instead of the conventional pavement?

a. Rutting (Better or Worse)

b. Crack (Better or Worse)

c. Roughness (Better or Worse)

c. Cost (More or Less)

d. Other

5. Do you think inverted pavement can replace conventional flexible pavement?

a. Yes b. No

Why?

6. Based on your experience, what is the best thickness range of the asphalt concrete layer for inverted pavement that?

a. Less than 2 inches

b. 2-3 inches

c. 3-5 inches

d. 5-8 inches

e. More than 8 inches

7. What is the percentage of cement in the cement-treated base layer?

a. 1-3 %

b. 4 %

c. 5-6 %

d. 7-8%

e. More than 8%

8. Based on your knowledge, how many days should the cement-treated base (for inverted pavement) be cured?

a. less than 7 days

b. 7 days

c. 10 days

d. 14 days

e. more than 14 days

9. What type of aggregate and properties will you choose to build the unbound aggregate base in the inverted pavement?

a.

b.

c.

d.

10. The inverted pavement was introduced in 1950s but it is not widely used. Do you have any thoughts on why inverted pavement is not popular nowadays?

11. Does the inverted pavement contribute to the environmental issue? Why?

a. yes

Reason:_____

b. no

Reason:_____

12. Do you have any suggestions on how to improve the inverted pavement?

13. Do you think the inverted pavement is suitable for nationwide utilization?

a. yes

b. no

14. Would you like to get a copy of the final report of this research project?

a. yes

b. no